UNIVERSITY OF OKLAHOMA

GRADUATE COLLEGE

CONTROLLED STRUCTURES AND PROPERTIES OF SINGLE WALLED CARBON

NANOTUBES CUSTOM-PRODUCED BY CHEMICAL VAPOR DEPOSITION METHOD

A DISSERTATION

SUBMITTED TO THE GRADUATE FACULTY

in partial fulfillment of the requirements for the

degree of

Doctor of Philosophy

By

LIANG ZHANG
Norman, Oklahoma
2006

UMI Number: 3238431

UMI®

CONTROLLED STRUCTURES AND PROPERTIES OF SINGLE WALLED CARBON
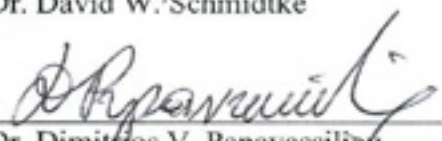NANOTUBES CUSTOM-PRODUCED BY CHEMICAL VAPOR DEPOSITION METHOD

A DISSERTATION APPROVED FOR THE
SCHOOL OF CHEMICAL, BIOLOGICAL AND MATERIALS ENGINEERING

BY

_____
Dr. Daniel E. Resasco

_____
Dr. John F. Scamehorn

_____
Dr. David W. Schmidtke

_____
Dr. Dimitrios V. Papavassiliou

_____
Dr. Zhisheng Shi

ACKNOWLEDGEMENTS

This book emblematizes an end of four-year challenging but fruitful academic experience and a start of new exploration. Looking back into those unforgettable days of combination of exciting discovery and discouraging failure, I can't believe I can go through it to be here without indebtedness to a long list of people whose names are haunting in my mind. The first one on the "thank you" list is my advisor Dr. Daniel E. Resasco for his continuous and generous support all the way through the Ph.D program. It is him who introduced me into a brand new world of nanomaterials which I never stepped in before. It is his encouragement and guidance that leads me to where I am now. As a mentor and also a friend, he taught me not only a wealth of knowledge but the character and spirit essential to a scientific researcher.

Innumerous thanks also go to all the members in our research group: Leandro Balzano, Jose E. Herrera, Walter E. Alvarez, Olga Matarredona, Olga L. Rueda, Nataphan (Mai) Sakulchaicharoen, Yongqian Tan, Giulio Lolli, Zhongrui Li, Federico Scodelaro, Stefano Cosma, David Martyn, Veronica Irurzun, Siriporn Jongpatiwut, Andrea R. Beltramone, Malee (Jeab) Santikunaporn, Robert C. Santana, Phuong T. DO, Stephon P. Crossley, and other exchanging students and visiting scholars. Working with those colleagues and friends is my luck in the life. I can't

help repeatedly playing the scenes in my mind: collaboration on the experiments, designing and building reaction systems, discussion on the problems, casual chattering at the coffee corner, enjoyment in parties. I own them for the intellectual sparkles excited during our communications and lifer experience sharing.

I would also like to acknowledge Department of Energy and National Science Foundation for the financial support in the project. In addition to financial support from Federal organizations, the collaboration with national laboratories under Federal organizations, such as Oak Ridge National Laboratory and Lawrence Berkeley National Laboratory, is gratefully acknowledged.

Thanks are also due to the faculty at the University of Oklahoma (OU) for the knowledge that they have passed along during my studies in Norman, including the members of my doctoral committee. Here I'd like to acknowledge Dr. Richard G. Mallinson, Dr. Matthias Nollert, and Dr. Lloyd L. Lee at CBME for teaching me thinking as a chemical engineer, Dr. Randall L. Kolar at CE for knowledge on mathematical treatment of engineering process, Dr. Patrick McCann and Dr. Zhisheng Shi at ECE for expanding my scientific view to semiconductor and optoelectronics.

I can't leave OU without mentioning Greg Strout, Preston Larson, Bill Chissoe at Samuel Roberts Noble Electron Microscopy Laboratory of OU. Those beautiful

and insightful pictures in this book and other publications of mine are crystallite of their effort. I gratefully acknowledge their kind and professional help in electron microscopic imaging for my research. In addition, they have taught me to become a microscopist with mastery of this very powerful tool for characterization of nanostructures.

This dissertation is dedicated to my family for their love and constant selfless support of my career. I'd like to thank my parents who are far away on the other end of this Planet for their encouraging my interest in science when I was a child and for many sacrifices they have made for my studies all these years. I would like to thank my wife Qin Yang, a soul mate in my life who understands me more than anyone else in the world and always stands in my back whenever whatever happens. I can't be luckier to have her accompany me through the road we have walked and keep fulfilling goals we have pictured.

TABLE OF CONTENTS

LISTS OF TABLES

LIST OF FIGURES

ABSTRACT

Single walled carbon nanotubes (SWNT) are considered as one of the most promising nanomaterials for a large variety of applications such as composites, solar cells, field emission displays, nanosensors, and integrated circuits. In all of these applications, SWNTs are required to be supplied with controlled structures and properties, which is the main focus of this dissertation. The first approach to tackle this problem is to develop appropriate methods to synthesize SWNTs of controlled structure. To achieve this goal, a number of techniques have been developed in our research group to selectively grow SWNTs on different support from porous silica to flat substrates. It is demonstrated that a precise control over chirality, diameter and bundle size can be obtained by tuning the reaction temperature in the growth of SWNT over Co-Mo/silica powder by CO disproportionation, the so-called CoMoCAT® process. In addition, a novel method for selective growth of SWNT on flat substrates has been developed. In this method, SWNTs can be grown either in random direction or vertical alignment on the surface under standard CoMoCAT® reaction conditions. However, on these flat surfaces, the SWNTs produced have larger tubes than those produced on porous silica and are extremely clean and pure. One of the great advantages of these materials is that they do not require any purification after growth. In addition, by carefully patterning the catalyst over the surface, vertically aligned SWNTs (VSWNT) in different forms has been fabricated.

The second trust of this dissertation is to investigate the properties of as-produced SWNTS with their controlled structural parameters (i.e., diameter, bundle size, chirality, and alignment). Field emission measurements have been conducted to evaluate the dependence of the emission characteristics on the SWNT structure, as characterized by electron microscopy (TEM and SEM), resonance Raman spectroscopy, and optical absorption (NIR and UV-Visible). Experimental and calculated field emission curves indicate that the bundle size, rather than the nanotube diameter or differences in work function are more important in determining the field emission properties of SWNT/silica composites. For the nanotubes grown on flat substrates, the response of the vertically aligned SWNT to polarization of both X-rays (in X-ray absorption near edge spectroscopy, XANES) and visible light (in Raman spectroscopy) clearly revealed the anisotropic optical properties of V-SWNT. These studies also gave evidence for the existence of a top layer of misaligned nanotubes.

Finally, efforts have been made to explore the growth mechanism of VSWNT on flat substrate. First, X-ray photoelectron spectroscopy and atomic force microscopy conducted on the flat surface with deposited catalyst gave detailed information about the chemical status of Co-Mo catalyst and their morphological distribution. Second, the evolution of the growth of VSWNT with time was visualized by scanning electron microscopy and clearly demonstrated a two-step

process involving the formation of a crust layer followed by a concerted growth constrained by crust, that resulted on the vertical alignment. Third, a kinetic study with fitted growth data has been derived and the maximum growth rate estimated (i.e. 12.5 nm/sec). Several examples of patterned VSWNT have been given to illustrate the effect of crust. In addition to the growth of VSWNT, oxidation and transferring of VSWNT has been investigated for future applications. It was observed that oxidation of VSWNT can remove smaller tubes and leave behind only the larger tubes. Transferring of VSWNT to a conducting surface has been realized by a couple of methods which may have an important impact in the fabrication of SWNT-based nanoelectronic devices (sensors, electrodes, etc.).

CHAPTER 1

FUNDAMENTALS OF SINGLE-WALLED CARBON NANOTUBES

1.1 INTRODUCTION

With one hundred times the tensile strength of steel, thermal conductivity better than all but the purest diamond[1-3], and electrical conductivity similar to copper[4, 5], but with the ability to carry much higher currents[6-8], carbon nanotubes are one of the most commonly mentioned building blocks of nanotechnology. The first conception of this extremely small diameter carbon filament was brought out by Smalley at a workshop in December 1990. These conjectures were later followed up in August 1991 by an oral presentation at a fullerence workshop in Philadelphia by Dresselhaus. However, the real breakthrough on carbon nanotube research came with Iijima's report of experimental observation of carbon nanotubes using transmission electron microscope[9]. Since then, the study of carbon nanotubes has progressed rapidly. Among all kinds of carbon nanotubes, single-walled carbon nanotubes (SWNT) are most intriguing. Since their discovery and structure determination by Iijima and Ichihashi in 1993[10], numerous theoretical studies on SWNT have been done[11-19] and showed that the physical properties of SWNTs differs greatly by their helical structures. But the experimental studies on SWNTs had little progress until various production methods were established in the late 1990s, such as laser-furnace (1996)[20],

arc-discharge (1997)[21], catalytic CVD with supported catalysts (1996)[22]. Along with these advances, many creative applications have been proposed. Included in the long list are one-dimentional quantum wire[23, 24], field effect transistor[25-29], electron emitters[30-35], chemical sensors[36-40], probe tips for scanning probe microscopes[41-46]. Obviously, specific application requires specific flavors of SWNTs: long, short, individual, bundled, small diameter, large diameter, metallic, semiconducting, and even the chiral angle. Therefore, in order to fully achieve these applications by employing specific physical/chemical properties of SWNT, custom growth of SWNT of controlled structures is needed and is attracting more and more interest, which is also the motivation of our work.

1.2 SWNT'S MOLECULAR AND ELECTRONIC STRUCTURES

A single-wall carbon nanotube (SWNT) can be described as a single layer of a graphite crystal that is rolled up into a seamless cylinder, one atom thick, a few nanometers in diameter and a long length (microns) along the cylinder axis. By this definition, construction of a SWNT needs conceptual specification of a rectangular region on a graphene sheet. As shown in Figure 1.1, the region can be defined by Translational vector $\mathbf{T}$, which is parallel to nanotube axis, and chiral vector $\mathbf{C_h}$, that is in the circumferential direction of a nanotube. The vector $\mathbf{C_h}$ connects two crystallographically equivalent sites on a two-dimensional (2D) graphene sheet where a carbon atom is located at each vertex of the honeycomb structure[47] and can be expressed by

$$\mathbf{C_h} = n\mathbf{a}_1 + m\mathbf{a}_2 \qquad (1)$$

where the pair of indices (n,m) denote the number of unit vectors $\mathbf{a_1}$ and $\mathbf{a_2}$ in the hexagonal honeycomb lattice contained in the vector $\mathbf{C_h}$. The chiral vector $\mathbf{C_h}$ makes an angle $\mathbf{\theta}$, called the chiral angle, with the zigzag or $\mathbf{a_1}$ direction. The axis of the zigzag nanotube corresponds to $\theta = 0^o$, while the armchair nanotube axis corresponds to $\theta = 30^o$, and the general nanotube axis corresponds to $0 < \theta < 30^o$. In terms of the integers (n,m), the nanotube diameter d_t is given by

$$d_t = \mathbf{C_h}/\pi = 3^{1/2}a_{C\text{-}C}(m^2+mn+n^2)^{1/2}/\pi \qquad (2)$$
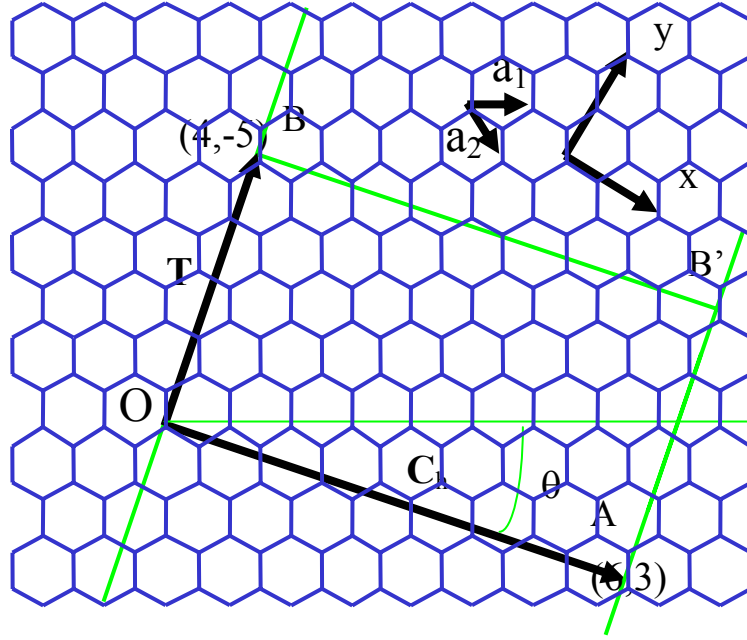
Figure 1.1: *The unrolled honeycomb lattice of a nanotube.*

where $a_{C\text{-}C}$ is the nearest-neighbour C-C distance (1.421 Å in graphite), C_h is the length of the chiral vector C_h and the chiral angle θ is given by

$$\theta = \tan^{-1}s \qquad\qquad (3)$$

Thus, a nanotube can be specified by either its (n,m) indices or equivalently by d_t And θ.
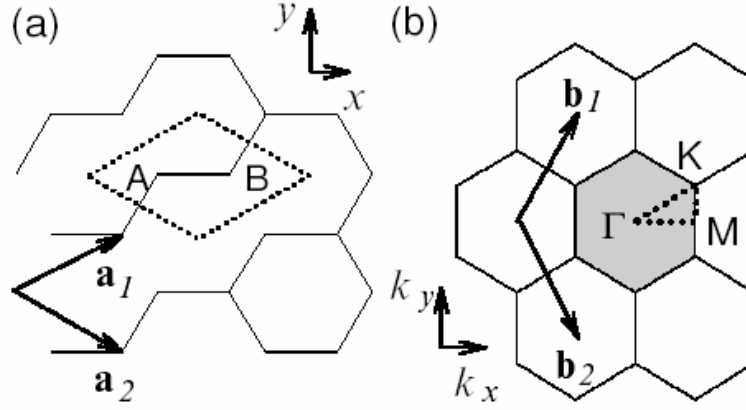
Figure 1.2: (a) The unit cell and (b) Brillouin zone of two-dimensional graphite are shown as the dotted rhombus and the shaded hexagon, respectively. a_i, and b_i, (i=1,2) are basis vectors and reciprocal lattice vectors, respectively. Energy dispersion relations are obtained along the perimeter of the dotted triangle connecting the high symmetry points, G, K and M

48

In figure 1.2, (a) the unit cell and (b) the Brillouin zone of two-dimensional graphite are shown as a dotted rhombus and shaded hexagon, respectively, where **a₁** and **a₂** are basis vectors in real space, and **b₁** and **b₂** are reciprocal lattice basis vectors. In the *x,y* coordinates shown in figure 2, the real space basis vectors **a₁** and **a₂** of the hexagonal lattice are expressed as

$$a_1 = \left(\frac{3^{1/2}}{2}a, \frac{a}{2}\right), \quad a_2 = \left(\frac{3^{1/2}}{2}a, -\frac{a}{2}\right) \tag{4}$$

where $a = |a_1| = |a_2| = 1.42 \times 3^{1/2} = 2.46$ Å is the lattice constant of two-dimensional graphite. Correspondingly the basis vectors $\mathbf{b}_1$ and $\mathbf{b}_2$ of the reciprocal lattice are given by:

$$b_1 = \left(\frac{2\pi}{3^{1/2}a}, \frac{2\pi}{a}\right), \quad b_2 = \left(\frac{2\pi}{3^{1/2}a}, -\frac{2\pi}{a}\right) \tag{5}$$

corresponding to a lattice constant of $4\pi/3^{1/2}a$ in reciprocal space. The direction of the basis vectors $\boldsymbol{b_1}$ and $\boldsymbol{b_2}$ of the reciprocal hexagonal lattice are rotated by 30° from the basis vectors $\boldsymbol{a}_1$ and $\boldsymbol{a}_2$ of the hexagonal lattice in real space, as shown in figure 1.2. By selecting the first Brillouin zone as the shaded hexagon shown in figure 1.2 (*b*), the highest symmetry is obtained for the Brillouin zone of 2D graphite. Here we define the three high symmetry points, Γ, K and M as the centre, the corner, and the centre of the edge, respectively. The energy dispersion relations are calculated for the triangle ΓMK shown by the dotted lines in figure 1.2 (*b*).

The translation vector $\mathbf{T}$ is the shortest repeat distance along the nanotube axis and therefore defines the unit cell for the 1D nanotube with $\mathbf{C_h}$. The translation vector $\mathbf{T}$ can be expressed as

$$\mathbf{T} = t_1\mathbf{a}_1 + t_2\mathbf{a}_2 \equiv (t_1, t_2) \tag{6}$$

where the coefficients t_1 and t_2 are related to (n,m) by

$$t_1 = (2m+n)/d_R \tag{7}$$

$$t_2 = -(2n+m)/d_R \tag{7}$$

where d_R is the greatest common divisor of (2m+n,2n+m) and is given by

$$d_R = \begin{cases} d, & \text{if } n-m \text{ is not a multiple of } 3d \\ 3d, & \text{if } n-m \text{ is a multiple of } 3d \end{cases} \tag{8}$$

in which d is the greatest common divisor of (n,m). The magnitude of the translation vector T is

$$T = |\mathbf{T}| = 3^{1/2} L / d_R \tag{9}$$

where L is the length of the chiral vector $Ch=\pi/d_t$ and d_t is the nanotube diameter. The unit cell of the nanotube is defined as the area delineated by the vectors $\mathbf{T}$ and C_h. The number of hexagons, N, contained within the 1D unit cell of a nanotube is determined by the integers (n,m) and is given by

$$N = \frac{2(m^2 + n^2 + nm)}{d_R} \tag{10}$$

The addition of a single hexagon to the honeycomb structure in figure 1.2 corresponds to the addition of two carbon atoms. Assuming a value $a_{C\text{-}C} = 0.142$ nm on a carbon nanotube, we obtain $d_t = 1.36$ nm and $N = 20$ for a (10,10) nanotube. Since the real space unit cell is much larger than that for a 2D graphene sheet, the 1D Brillouin zone (BZ) for the nanotube is much smaller than the BZ for a single two atom graphene 2D unit cell. Because the local crystal structure of the nanotube is so close to that of a graphene sheet, and because the Brillouin zone is small, Brillouin

7

zone-folding techniques have been commonly used to obtain approximate electron and phonon dispersion relations for carbon nanotubes (n,m) with specific symmetry.

Whereas the translational vector $\mathbf{T}$, given by equation (6), and the chiral vector $\mathbf{C_h}$, given by equation (1), both determine the unit cell of the carbon nanotube in real space, the corresponding vectors in reciprocal space are the reciprocal lattice vectors $\mathbf{K_2}$ along the nanotube axis and $\mathbf{K_1}$ in the circumferential direction, which gives discrete k values in the direction of the chiral vector $\mathbf{Ch}$. The vectors $\mathbf{K_1}$ and $\mathbf{K_2}$ are obtained from the relations

$$C_h \cdot K_1 = 2\pi, \quad T \cdot K_1 = 0$$
$$C_h \cdot K_1 = 0, \quad T \cdot K_1 = 2\pi$$

(11)

From equations (11) it follows that $\mathbf{K_1}$ and $\mathbf{K_2}$ can be written as:

$$K_1 = \frac{1}{N}(-t_2 b_1 + t_1 b_2), \quad K_2 = \frac{1}{N}(m b_1 - n b_2)$$

(12)

where $\mathbf{b_1}$ and $\mathbf{b_2}$ are the reciprocal lattice vectors of a two-dimensional grapheme sheet given by equation (5). The N wave vectors $\mu\mathbf{K_1}$ ($\mu = 0,...,N-1$) give rise to N discrete k vectors in the circumferential direction. For each of the μ discrete values of the circumferential wave vectors, a one-dimensional electronic energy band appears. Because of the translational symmetry of $\mathbf{T}$, we have continuous wave vectors in the direction of $\mathbf{K_2}$ for a carbon nanotube of infinite length. However, for a nanotube of finite length L_t, the spacing between wave vectors is $2\pi/L_t$.

The 1D electronic energy band structure for carbon nanotubes is related to the energy band structure calculated for the 2D graphene honeycomb sheet used to form the nanotube.[49] These calculations for the electronic structure of SWNTs show that about 1/3 of the nanotubes are metallic and 2/3 are semiconducting,[50] depending on the nanotube diameter d_t and chiral angle θ. It can be shown that metallic conduction in (n,m) carbon nanotube is achieved when

$$2n+m = 3q \ \text{ or } \ n-m = 3q \tag{13}$$

where q is an integer. All armchair carbon nanotubes ($\theta = 30^\circ$) are metallic and satisfy the general equation (13). The unique features of the electronic structure of SWNTs can be understood on the basis of the electronic structure of a graphene sheet which is a zero gap semiconductor with bonding and antibonding π bands that are degenerate at the K-point (zone corner) of the hexagonal 2D Brillouin zone. The periodic boundary conditions for the 1D carbon nanotubes of small diameter permit only a few wave vectors to exist in the circumferential direction, and these wave vectors k satisfy the relation $n\lambda = \pi d_t$, where $\lambda = 2\pi/k$ is the deBroglie wavelength. Metallic conduction occurs when one of these allowed wave vectors k passes through the K-point of the 2D Brillouin zone, where the 2D valence and conduction bands are degenerate because of the special symmetry of the 2D graphene lattice. As the nanotube diameter increases, more wave vectors become allowed for the circumferential direction, so that the nanotubes become more two dimensional and the semiconducting band gap disappears. The band gap for isolated semiconducting

carbon nanotubes is proportional to the reciprocal nanotube diameter $1/d$t. At a nanotube diameter of $d_t \sim 3$ nm, the bandgap becomes comparable to thermal energies at room temperature, showing that small diameter nanotubes are needed to observe 1D quantum effects.

The electronic density of states plots in figure 1.3 show that the metallic nanotubes have a small, but non-vanishing 1D density of states at the Fermi level, and this non-vanishing density of states is independent of energy until the energies of the first subband edges of the valence and conduction bands are reached.
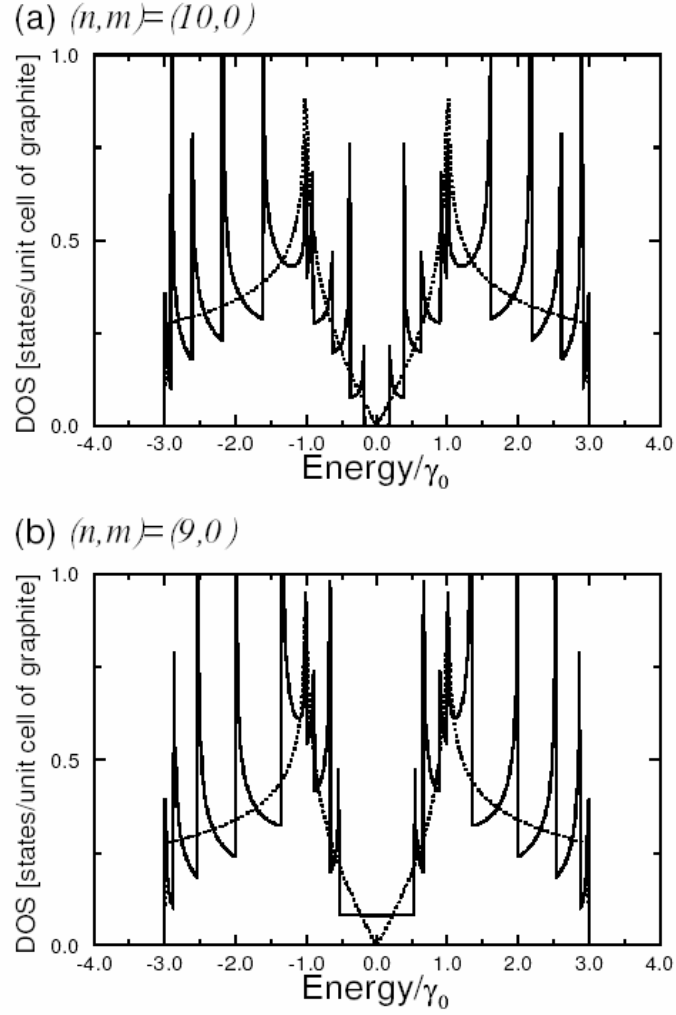
Figure 1.3: *Electronic 1D density of states per unit cell of a 2D graphene sheet for two zigzag nanotubes: (a) the (10,0) nanotube which has semiconducting behaviour, (b) the (9,0) nanotube which has metallic behaviour. Also shown in the figure is the density of states for the 2D graphene sheet (dotted line)[51]*

In contrast, for a 2D graphene sheet (dashed curve), the 2D density of states is zero at the Fermi level, and varies linearly with energy, as we move away from the Fermi level. Furthermore, the density of states for the semiconducting 1D nanotubes is zero throughout the bandgap, as shown in figure 1.3 (*a*), and their bandgap energy *E*g is equal to the energy difference $E_{11}(d_t)$ between the two van Hove singularities in the 1D density of states that span the Fermi level, where it is noted that *E*g is proportional to the reciprocal nanotube diameter. Because of these singularities in the density of states, high optical absorption is expected when the photon energy matches the energy separation between an occupied peak in the electron density of states and one that is empty. This situation occurs at the band gap for the semiconducting nanotubes, but also at higher energies for transitions from an occupied subband edge state to the corresponding unoccupied subband edge state. Such transitions between subband edge states can occur for both semiconducting ad metallic nanotubes.

1.3 IDENTIFICATION OF SWNT'S STRUCTURES

1.3.1 STRUCTURE PROBED BY ELECTRON-SWNT INTERACTION

1.3.1.1 Scanning Electron Microscopy

In a typical SEM electrons are thermionically emitted from a tungsten or lanthanum hexaboride (LaB6) cathode and are accelerated towards an anode; alternatively electrons can be emitted via field emission (FE). Tungsten is used because it has the highest melting point and lowest vapour pressure of all metals, thereby allowing it to be heated for electron emission. The electron beam, which typically has an energy ranging from a few hundred eV to 50 keV, is focused by one or two condenser lenses into a beam with a very fine focal spot sized 1 nm to 5 nm. The beam passes through pairs of scanning coils in the objective lens, which deflect the beam in a raster fashion over a rectangular area of the sample surface. Through these scattering events, the primary electron beam effectively spreads and fills a teardrop-shaped volume, known as the interaction volume, extending from less than 100 nm to around 5 μm into the surface. Interactions in this region lead to the subsequent emission of electrons which are then detected to produce an image. X-rays, which are also produced by the interaction of electrons with the sample, may also be detected in an SEM equipped for energy-dispersive X-ray spectroscopy or

wavelength dispersive X-ray spectroscopy. With its powerful surface detecting capability, SEM allows one to image the ropes of SWNT or even a single SWNT with up-to-date high resoltion SEM as shown in figure 1.4. This technique can also used to determine the existence of amorphous or catalyst particles (with backscattered electron detector).
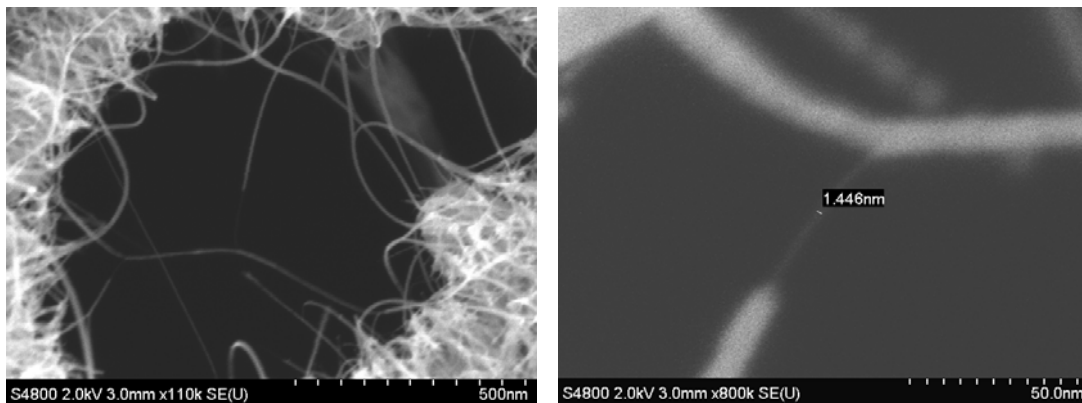
Figure 1.4: *SEM images of vertically aligned single walled carbon nanotubes from the top*

1.3.1.2 *Transmission Electron Microscopy*

Transmission electron microscopy (TEM) is an imaging technique whereby a beam of electrons is focused onto a specimen causing an enlarged version to appear on a fluorescent screen or layer of photographic film (see electron microscope), or to be detected by a CCD camera. The first practical transmission electron microscope

was built by Albert Prebus and James Hillier at the University of Toronto in 1938 using concepts developed earlier by Max Knoll and Ernst Ruska.
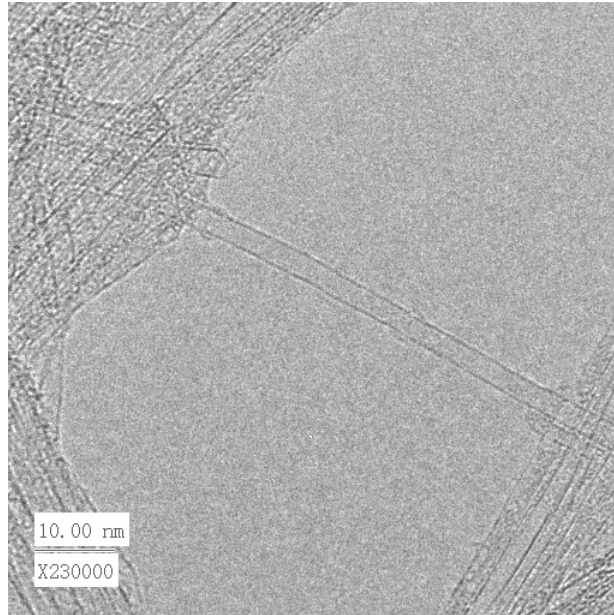
Figure 1.5: *TEM image of vertically aligned single walled carbon nanotubes mounted on TEM grid.*

Although SEM is useful in imaging the 1-D structure of carbon nanotubes, it is not able to determine the in depth molecular structure such as number of walls, crystal structure of SWNT, or structure of impurity or dopent in carbon nanotubes. However, TEM is able to perform these functions.[52-55] Figure 1.5 shows the clear structure of single walled carbon nanotubes: diameter and abnormous structure can be carefully determined.

1.3.1.3 Electron Diffraction

Electron diffraction is a technique used to study matter by firing electrons at a sample and observing the resulting interference pattern. This phenomenon occurs due to the wave-particle duality, which states that a particle of matter (in this case the incident electron) can be described as a wave. For this reason, an electron can be regarded as a wave much like sound or water waves. This technique is similar to X-ray diffraction and neutron diffraction. Electron diffraction is most frequently used in solid state physics and chemistry to study the crystal structure of solids. These experiments are usually performed in a Transmission Electron Microscope (TEM), or a Scanning Electron Microscope (SEM) as electron backscatter diffraction.
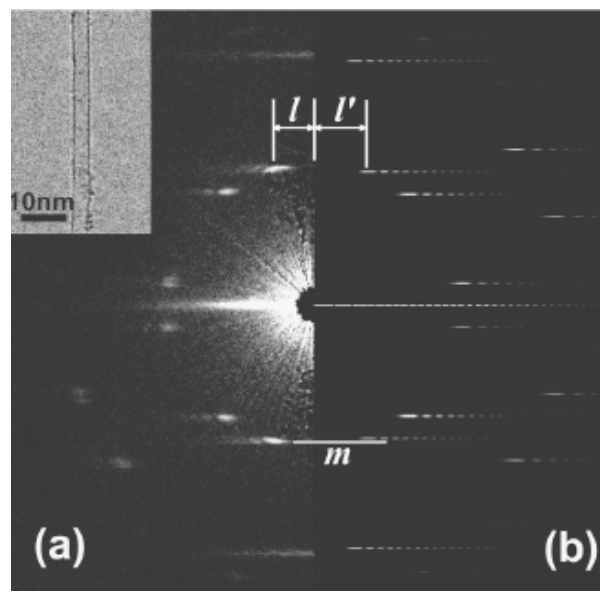
Figure 1.6: Eletron diffraction from one single walled carbon nanotube. (adapted from Gao, M.; Zuo, J. M.; Twesten, R. D.; Petrov,

I.; Nagahara, L. A.; Zhang, R., Structure determination of individual single-wall carbon nanotubes by nanoarea electron diffraction. *Applied Physics Letters* **2003,** 82, (16), 2703-2705. copyright (2003) with permission from AIP)

The periodic structure of a crystalline solid acts as a diffraction grating, scattering the electrons in a predictable manner. Working back from the observed diffraction pattern, it may be possible to deduce the structure of the crystal producing the diffraction pattern. According to this principle, crystal structure (chirality) of SWNT can be determined by the technique[56-60] as shown in figure 1.6.[61]

1.3.1.4   Electron Energy Microanalysis

Energy dispersive X-ray spectroscopy (EDX or EDS) is a method used to determine the energy spectrum of X-ray radiation. It is mainly used in chemical analysis, in an X-ray fluorescence spectrometer (especially portable devices), or in an electron microprobe (e.g. inside an scanning electron microscope). The detector is a semiconductor detector, usually a Silicon Drift Detector or a silicon crystal doped with lithium (Si(Li) detector). The semiconductor is polarized with a high voltage; when an X-ray photon hits the detector, it creates electron-hole pairs that drift due to the high voltage. The electric charge is collected, it is like charging a capacitor; the increment of voltage of the condensator is proportional to the energy of the photon, it

is thus possible to determine the energy spectrum. The condensator voltage is reset regularly to avoid saturation. By using this method, elemental composition of carbon nanotubes and related materials can be determined.

1.3.2   STRUCTURE IDENTIFIED BY PROBE-SWNT
INTERACTION

1.3.2.1   Atomic Force Microscopy

The atomic force microscope (AFM) is a very high-resolution type of scanning probe microscope, with a maximum magnification power of 5,000,000 times the regular size of an image. The AFM was invented by Binnig, Quate and Gerber in 1986, and is one of the foremost tools for imaging, measuring and manipulating matter at the nanoscale. The AFM consists of a microscale cantilever with a sharp tip (probe) at its end that is used to scan the specimen surface. The cantilever is typically silicon or silicon nitride with a tip radius of curvature on the order of nanometers. When the tip is brought into proximity of a sample surface, forces between the tip and the sample lead to a deflection of the cantilever according to Hooke's law. Depending on the situation, forces that are measured in AFM include mechanical contact force, Van der Waals forces, capillary forces, chemical bonding, electrostatic forces, magnetic forces (see Magnetic force microscope (MFM)), Casimir forces, solvation forces etc. Typically, the deflection is measured using a laser spot reflected from the top of the cantilever into an array of photodiodes. Other methods that are

used include optical interferometry, capacitive sensing or piezoresistive AFM probes. These probes are fabricated with piezoresistive elements that act as a strain gage. Using a Wheatstone bridge, strain in the AFM probe due to deflection can be measured, but this method is not as sensitive as laser deflection or interferometry. With this surface sensitive technique, diameter (measured by height of SWNT) and length can be measured.[62-64] Figure 1.7 shows single SWNT grown from Co nanoparticles deposited on Si substrate in our group.
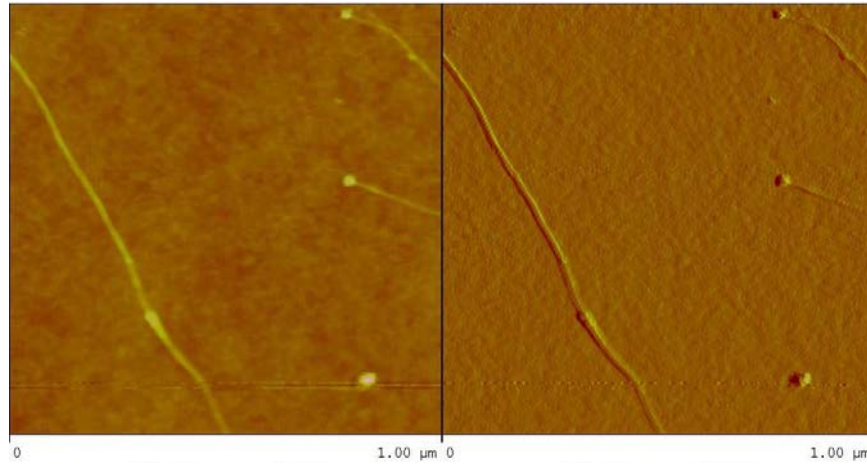
Figure 1.7: AFM images of SWNT grown from Co nanopartiles on Si substrate.

1.3.2.2 Scanning Tunneling Microscopy

The STM is a non-optical microscope which employs principles of quantum mechanics. An atomically sharp probe (the tip) is moved over the surface of the material under study, and a voltage is applied between probe and the surface.

19

Depending on the voltage electrons will "tunnel" (this is a quantum-mechanical effect) or jump from the tip to the surface (or vice-versa depending on the polarity), resulting in a weak electric current. The size of this current is exponentially dependent on the distance between probe and the surface. For a current to occur the substrate being scanned must be conductive (or semiconductive). Insulators cannot be scanned through the STM, as the electron has no available energy state to tunnel into or out of due to the band gap structure in insulators. The beauty of this technique is it can be used to determined carbon lattice or electronic structure of SWNT.[59, 65-71] Figure 1.8 shows STM image of CoMoCAT® nanotubes.
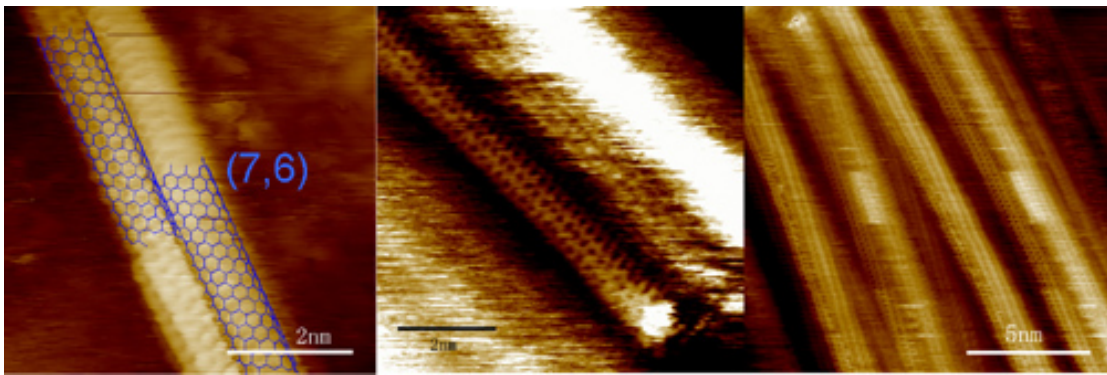
Figure 1.8: *STM images of* CoMoCAT® *SWNT. (courtesy of Prof. C. Lieber at Harvard)*

1.3.3 STRUCTURE PROBED BY PHOTON-SWNT INTERACTION

1.3.3.1   Resonant Raman Scattering

Raman spectroscopy is a spectroscopic technique used in condensed matter physics and chemistry to study vibrational, rotational, and other low-frequency modes in a system. It relies on inelastic scattering, or Raman scattering of monochromatic light, usually from a laser in the visible, near infrared, or near ultraviolet range. Phonons or other excitations in the system are absorbed or emitted by the laser light, resulting in the energy of the laser photons being shifted up or down. The shift in energy gives information about the phonon modes in the system. Raman has been used extensively to study the bonding and properties of pristine, metallic, and superconducting phases of graphite intercalation compounds and fullenrene-based solids.[72-77] It is natural to extend this technique to characterize carbon nanotubes. Raman scattering in carbon nanotubes involves strong resonances of the incoming and outgoing light and the vibrational states with the electronic energy levels of a tube. The Raman spectra therefore carry a wealth of information about the electronic states and the phonon dispersion of carbon nanotubes. Each part of the Raman spectrum, the radial breathing mode (RBM), the disorder induces mode (D mode) and the high-energy mode (HEM), can be used to access different properties of single-walled carbon nanotubes. Out of all Raman modes the radial breathing mode is unique to single-walled carbon nanotubes. In the high energy range around 1600 cm-1 single-walled nanotube show a characteristic double-peak structure. Here are some examples for what can be told from a nanotube Raman spectrum: presence of nanotubes, orientation of isolated tubes[78] or aligned samples[79,]

21

[80], diameter and chirality of carbon nanotubes,[81-83] metallic character of a tube,[84, 85] energies of the excited electronic states, dependence of the phonon frequencies on the strain,[86] defect concentration in nanotube samples,[87] temperature,[88] doping levels,[87] and etc.

1.3.3.2   Optical Absorption and Fluorescence Spectroscopy

The optical absorption and luminescence process has enormous scientific value because of the detailed information that spectral positions and intensities can reveal about a sample's electronic structure and permit the sensitive qualitative and quantitative analysis. A key feature of carbon nanotubes is the strong dependence of their electronic properties on physical tube structure. Because SWNT are formed in a variety of discrete structures having distinct diameters and chiralities, a corresponding variety of pi-electron band structures and excitations are found in mixtures of nanotubes. Each possible SWNT structure is uniquely described by a pair of integers (n,m) that describe the length and orientation of the tube's circumference vector when projected onto a grapheme sheet. An important feature of SWNT electronic structure is sets of sharp maxima, called van Hove singularities. Nanotube optical spectra are dominated by strong dipole allowed transitions, polarized along the tube axis, between van Hove singularities in matching valence and conduction sub-bands. These are referred to as E_{ii} transitions, with $i = 1, 2, 3$, etc.

The absorption or fluorescence spectra are obtained in normally aqueous surfactant suspension of SWNT that has been enriched in individual, disbundled nanotubes. Careful analysis allowed each of peaks in spectra to be assigned to a specific (n,m) species.[89-96] Figure 1.8 illustrates specified (n,m) structure of CoMoCAT [®] SWNT determined by optical absorption and fluorescence. This spectral assignment provided a large body of precise optical transition energies for a significant range of tube diameters and chiralities. However, it should be careful when analyzing specta because the optical absorption or fluorescence of SWNT is affected by aggregation,[93] chemical derivatization,[97] interaction between nanotube and surfactant.[98]
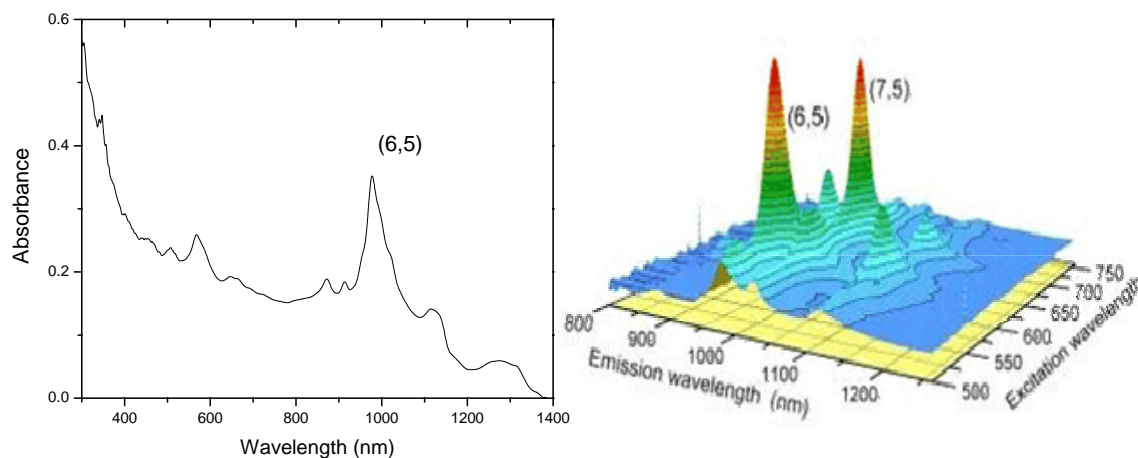
Figure 1.9: *Optical absorption and fluorescence spectra of* *CoMoCAT[®] SWNT.*

1.3.3.3   *X-ray Absorption Fine Structure*

X-ray absorption fine structure (XAFS) is a specific structure observed in X-ray absorption spectroscopy (XAS). By analyzing the XAFS, information can be acquired on the local structure and on the unoccupied electronic states. The X-ray absorption spectra show a steep rise at the core-level binding energy of X-ray-absorbing atoms and attenuates gradually with the X-ray energy. The XAS spectra are usually divided in three energy regions: 1) the edge region, 2) the X-ray Absorption Near Edge Structure (XANES); 3) the extended X-ray absorption fine structure (EXAFS). The absorption peaks at the absorption edges in a range of about 5 eV were first explained by Walther Kossel as due to electronic transitions to first unoccupied molecular levels above the chemical potential, and for many years was referred to as the "Kossel structure" now it is known as absorption edge region. The oscillatory structure extending for hundreds of electron volts past the edges was called the "Kronig structure" after the scientist, Ralph Kronig, who assigned this structure to the single scattering of the excited photoelectron by neighbouring atoms.

The peak positions and spectral line shape in a XANES spectrum are directly associated with the nature of these unoccupied electronic states. Accordingly XANES can be used to obtain qualitative bonding information for a full range of the sp^2/sp^3 bonding ratios. It can be used to identify specific bonds in molecules (*e.g.* C=C, C-C, and C-O bonds) as well as the presence of chemisorbed species. Of

greater importance for this study, by using linearly polarized X-ray beam, angle-dependent XANES can be used to investigate the angular dependence of the specific orbitals involved in the transition $1s \rightarrow \pi^*$ and $1s \rightarrow \sigma^*$.

1.4 PROPERTIES AND APPLICATIONS OF SWNT

1.4.1 COMPOSITE MATERIALS

Because of the stiffness of carbon nanotubes, they are ideal candidates for structural applications. For example, they may be used as reinforcements in high strength, low weight, and high performance composites.

Theoretically, SWNTs could have a Young's Modulus of 1 TPa.[99, 100] MWNTs are weaker because the individual cylinders slide with respect to each other. Ropes of SWNTs are also less strong. The individual tubes can pull out by shearing and at last the whole rope will break. This happens at stresses far below the tensile strength of individual nanotubes. Nanotubes also sustain large strains in tension without showing signs of fracture. In other directions, nanotubes are highly flexible.[10]

One of the most important applications of nanotubes based on their properties will be as reinforcements in composite materials.[99-109] However, there have not been many successful experiments that show that nanotubes are better fillers than the traditionally used carbon fibres. The main problem is to create a good interface between nanotubes and the polymer matrix, as nanotubes are very smooth and have a small diameter, which is nearly the same as that of a polymer chain. Secondly, nanotube aggregates, which are very common, behave different to loads than individual nanotubes do. Limiting factors for good load transfer could be sliding of cylinders in MWNTs and shearing of tubes in SWNT ropes. To solve this problem

the aggregates need to be broken up and dispersed or cross-linked to prevent slippage. A main advantage of using nanotubes for structural polymer composites is that nanotube reinforcements will increase the toughness of the composites by absorbing energy during their highly flexible elastic behaviour. Other advantages are the low density of the nanotubes, an increased electrical conduction and better performance during compressive load.

Another possibility, which is an example of a non-structural application, is filling of photoactive polymers with nanotubes. PPV (Poly-p-phenylenevinylene) filled with MWNTs and SWNTs is a composite,[110] which has been used for several experiments. These composites show a large increase in conductivity with only a little loss in photoluminescence and electro-luminescence yields. Another benefit is that the composite is more robust than the pure polymer.

Of course, nanotube-polymer composites could be used also in other areas. For instance, they could be used in the biochemical field as membranes for molecular separations or for osteointegration (growth of bone cells). However, these areas are less explored. The most important thing we have to know about nanotubes for efficient use of them as reinforcing fibres is knowledge on how to manipulate the surfaces chemically to enhance interfacial behaviour between the individual nanotubes and the matrix material.

1.4.2 MOLECULAR ELECTRONICS WITH CNTS

1.4.2.1 Field Emitting Devices

If a solid is subjected to a sufficiently high electric field, electrons near the Fermi level can be extracted from the solid by tunnelling through the surface potential barrier. This emission current depends on the strength of the local electric field at the emission surface and its work function (which denotes the energy necessary to extract an electron from its highest bounded state into the vacuum level). The applied electric field must be very high in order to extract an electron. This condition is fulfilled for carbon nanotubes, because their elongated shape ensures a very large field amplification.[111-113]

For technological applications, the emissive material should have a low threshold emission field and large stability at high current density. Furthermore, an ideal emitter is required to have a nanometre size diameter, a structural integrity, a high electrical conductivity, a small energy spread and a large chemical stability. Carbon nanotubes possess all these properties. However, a bottleneck in the use of nanotubes for applications is the dependence of the conductivity and emission stability of the nanotubes on the fabrication process and synthesis conditions.

Examples of potential applications for nanotubes as field emitting devices are flat panel displays,[114-116] gas-discharge tubes in telecom networks,[114] electron guns for electron microscopes,[117] AFM tips and microwave amplifiers.[118-121]

1.4.2.2 Transistors

The field-effect transistor − a three-terminal switching device − can be constructed of only one semi-conducting SWNT.[25, 122] By applying a voltage to a gate electrode, the nanotube can be switched from a conducting to an insulating state. Figure 1.9 illustrate a transistor based on carbon nanotube. Such carbon nanotube transistors can be coupled together, working as a logical switch, which is the basic component of computers.
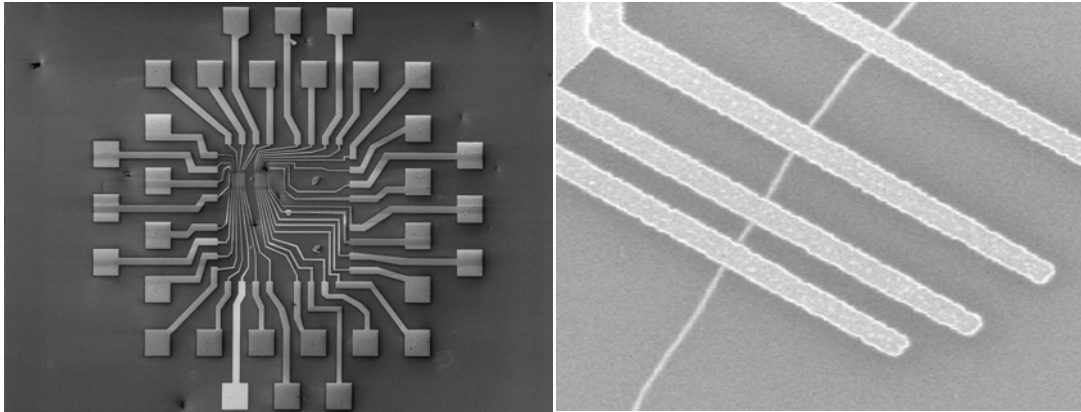
Figure 1.10: *Carbon nanotube-based field emission transistor (from*

open source http://hone.mech.columbia.edu/fet.htm)

1.4.2.3 Nanoprobes and Sensors

Because of their flexibility, nanotubes can also be used in scanning probe instruments.[43, 44, 46] Since MWNT-tips are conducting, they can be used in STM and AFM instruments (Figure 1.10). Advantages are the improved resolution in

29

comparison with conventional Si or metal tips and the tips do not suffer from crashes with the surfaces because of their high elasticity. However, nanotube vibration, due to their large length, will remain an important issue until shorter nanotubes can be grown controllably.
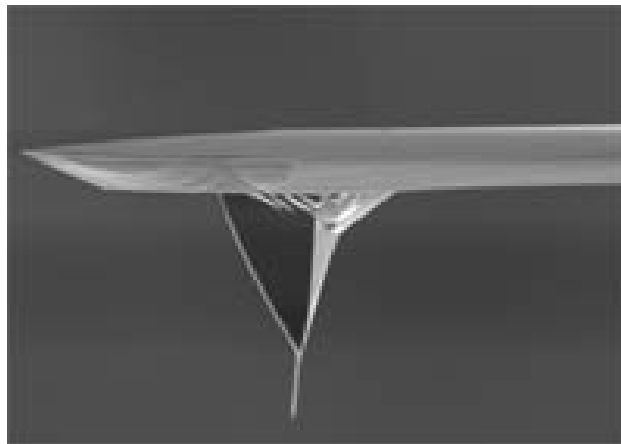
Figure 1.11: MWNT-based AFM tip (from open source http://www.nanoscience.com/products/carbon_nanotube_probes.html)

Nanotube tips can be modified chemically by attachment of functional groups. Because of this, nanotubes can be used as molecular probes, with potential applications in chemistry and biology.

Other applications are the following: A pair of nanotubes can be used as tweezers to move nanoscale structures on surfaces.73 Sheets of SWNTs can be used as electromechanical actuators, mimicking the actuator mechanism present in natural muscles. SWNTs may be used as miniaturised chemical sensors. On exposure to

environments, which contain NO2, NH3 or O2, the electrical resistance changes.

1.4.3 ENERGY STORAGE

Graphite, carbonaceous materials and carbon fibre electrodes are commonly used in fuel cells, batteries and other electrochemical applications. Advantages of considering nanotubes for energy storage are their small dimensions, smooth surface topology and perfect surface specificity. The efficiency of fuel cells is determined by the electron transfer rate at the carbon electrodes, which is the fastest on nanotubes following ideal Nernstian behaviour. Electrochemical energy storage and gas phase intercalation will be described more thoroughly in the following chapters of the report.

1.4.3.1 Hydrogen Storage

The advantage of hydrogen as energy source is that its combustion product is water. In addition, hydrogen can be easily regenerated. For this reason, a suitable hydrogen storage system is necessary, satisfying a combination of both volume and weight limitations. The two commonly used means to store hydrogen are gas phase and electrochemical adsorption.

Because of their cylindrical and hollow geometry, and nanometre-scale diameters, it has been predicted that carbon nanotubes can store a liquid or a gas in

the inner cores through a capillary effect.[123, 124] As a threshold for economical storage, the Department of Energy has set storage requirements of 6.5 % by weight as the minimum level for hydrogen fuel cells. It is reported that SWNTs were able to meet and sometimes exceed this level by using gas phase adsorption (physisorption). Yet, most experimental reports of high storage capacities are rather controversial so that it is difficult to assess the applications potential. What lacks, is a detailed understanding of the hydrogen storage mechanism and the effect of materials processing on this mechanism. Another possibility for hydrogen storage is electrochemical storage. In this case not a hydrogen molecule but an H atom is adsorbed. This is called chemisorption.

1.4.3.2 Lithium Intercalation

The basic principle of rechargeable lithium batteries is electrochemical intercalation and de-intercalation of lithium in both electrodes. An ideal battery has a high-energy capacity, fast charging time and a long cycle time. The capacity is determined by the lithium saturation concentration of the electrode materials. For Li, this is the highest in nanotubes if all the interstitial sites (inter-shell van der Waals spaces, inter-tube channels and inner cores) are accessible for Li intercalation. SWNTs have shown to possess both highly reversible and irreversible capacities. [125] Because of the large observed voltage hysteresis, Li-intercalation in nanotubes is still unsuitable for battery application. This feature can potentially be reduced or

eliminated by processing, i.e. cutting, the nanotubes to short segments.

1.4.3.3 Electrochemical Supercapacitors

Supercapacitors have a high capacitance and potentially applicable in electronic devices. Typically, they are comprised two electrodes separated by an insulating material that is ionically conducting in electrochemical devices. The capacity of an electrochemical supercap inversely depends on the separation between the charge on the electrode and the counter charge in the electrolyte. Because this separation is about a nanometer for nanotubes in electrodes, very large capacities result from the high nanotube surface area accessible to the electrolyte. In this way, a large amount of charge injection occurs if only a small voltage is applied. This charge injection is used for energy storage in nanotube supercapacitors.[126] Generally speaking, there is most interest in the double-layer supercapacitors and redox supercapacitors with different charge-storage modes.

1.5 SYNTHESIS OF SWNT

Researchers dedicated to nanomaterials synthesis have achieved great success in synthesizing SWNT by a large variety of techniques since SWNT was first produced by Dr. Iijima's group at NEC. Those techniques differ in nature of carbon source, energy input, and catalyst preparation. As the seed for carbon nucleation, catalyst preparation is of greatest importance in SWNT growth. Consequently, methods for SWNT synthesis can be categorized in terms of preparation of catalyst nanoparticles: dispersed in gas phase, supported by porous media, and deposited on flat substrate.

1.5.1 SWNT GROWN FROM CATALYST NANOPARTICLES DISPERSED IN GAS PHASE

1.5.1.1 Decomposition of Volatile Metal-containing Precursor

Methods for SWNT synthesis in this category are characterized by formation of SWNT nucleation center through in situ decomposition of volatile metal-containing precursors like carbonyl iron or ferrocene. One example is HiPCO$^{®}$ process which is developed to produce SWNT in a continuous-flow gas phase using CO as the carbon feedstock and $Fe(CO)_5$ as the iron-containing catalyst precursor.[127] Size and diameter distribution of the nanotubes can be roughly selected by controlling the pressure of CO.

Nanotubes as small as 0.7 nm in diameter, which are expected to be the smallest achievable chemically stable SWNTs, have been produced by this method. The average diameter of HiPco SWNTs is approximately 1.1 nm. The yield that could be achieved is approximately 70%. The highest yields and narrowest tubes can be produced at the highest accessible temperature and pressure.[127] SWNT material with 97% purity can be produced at rates of up to 450 mg/h with this process.[49]

1.5.1.2 *Vaporization of Metal from Metal-doped Carbon Electrode*

Arc Discharge

This method creates nanotubes through arc-vaporisation of two carbon rods placed end to end, separated by approximately 1mm, in an enclosure that is usually filled with inert gas (helium, argon) at low pressure (between 50 and 700 mbar). A direct current of 50 to 100 A driven by approximately 20 V creates a high temperature discharge between the two electrodes. The discharge vaporises one of the carbon rods and forms a small rod shaped deposit on the other rod. Producing nanotubes in high yield depends on the uniformity of the plasma arc and the temperature of the deposit form on the carbon electrode. [128]

Insight in the growth mechanism is increasing and measurements have shown that different diameter distributions have been found depending on the mixture of helium and argon. These mixtures have different diffusions coefficients and thermal

conductivities. These properties affect the speed with which the carbon and catalyst molecules diffuse and cool., affecting nanotube diameter in the arc process. This implies that single-layer tubules nucleate and grow on metal particles in different sizes depending on the quenching rate in the plasma and it suggests that temperature and carbon and metal catalyst densities affect the diameter distribution of nanotubes.[128] Figure 1.11 shows an arc discharge apparatus for carbon nanotube synthesis.

Figure 1.12: arc discharge apparatus for carbon nanotube synthesis. (from open source http://www.meijo-u.ac.jp/ST/coe/ENGLISH/seizou.html)

A lot of elements and mixtures of elements have been tested by various authors [129] and it is noted that the results vary a lot, even though they use the same elements. This is not surprising as experimental conditions differ. The quantity and quality of the nanotubes obtained depend on various parameters such as the metal concentration, inert gas pressure, kind of gas, the current and system geometry.

Laser Ablation

In 1995, Smalley's group[130] at Rice University reported the synthesis of carbon nanotubes by laser vaporisation. A pulsed[131], or continuous[132] laser is used to vaporise a graphite target in an oven at 1200 °C. The main difference between continuous and pulsed laser, is that the pulsed laser demands a much higher light intensity (100 kW/cm^2 compared with 12 kW/cm^2). The oven is filled with helium or argon gas in order to keep the pressure at 500 Torr. A very hot vapour plume forms, then expands and cools rapidly. As the vaporised species cool, small carbon molecules and atoms quickly condense to form larger clusters, possibly including fullerenes. The catalysts also begin to condense, but more slowly at first, and attach to carbon clusters and prevent their closing into cage structures. Catalysts may even open cage structures when they attach to them. From these initial clusters, tubular molecules grow into single-wall carbon nanotubes until the catalyst particles become too large, or until conditions have cooled sufficiently that carbon no longer can diffuse through or over the surface of the catalyst particles. It is also possible that the particles become that much coated with a carbon layer that they cannot absorb more and the nanotube stops growing. The SWNTs formed in this case are bundled together by van der Waals forces[133].

Figure 1.13: *Laser ablation apparatus for carbon nanotube synthesis.*

(from open source http://www.nanoscience.com/products */carbon_nanotube_probes.html* *)*

There are some striking, but not exact similarities, in the comparison of the spectral emission of excited species in laser ablation of a composite graphite target with that of laser-irradiated C60 vapour. This suggests that fullerenes are also produced by laser ablation of catalyst-filled graphite, as is the case when no catalysts are included in the target. However, subsequent laser pulses excite fullerenes to emit C2 that adsorbs on catalyst particles and feeds SWNT growth. However, there is insufficient evidence to conclude this with certainty.

Laser ablation is almost similar to arc discharge, since the optimum background gas and catalyst mix is the same as in the arc discharge process. This might be due to very similar reaction conditions needed, and the reactions probably

occur with the same mechanism.

1.5.1.3 *Vaporization of Metal*

This method is based on the synthesis of SWNTs in a controlled flame environment, that produces the temperature, forms the carbon atoms from the inexpensive hydrocarbon fuels and forms small aerosol metal catalyst islands [134, 135]. SWNTs are grown on these metal islands in the same manner as in laser ablation and arc discharge.

These metal catalyst islands can be made in three ways. The metal catalyst (cobalt) can either be coated on a mesh, on which metal islands resembling droplets were formed by physical vapour deposition. These small islands become aerosol after exposure to a flame. The second way [134, 135], is to create aerosol small metal particles by burning a filter paper that is rinsed with a metal-ion (e.g. iron nitrate) solution. The third way, is the thermal evaporating technique in which metal powder (e.g. Fe or Ni) is inserted in a trough and heated.
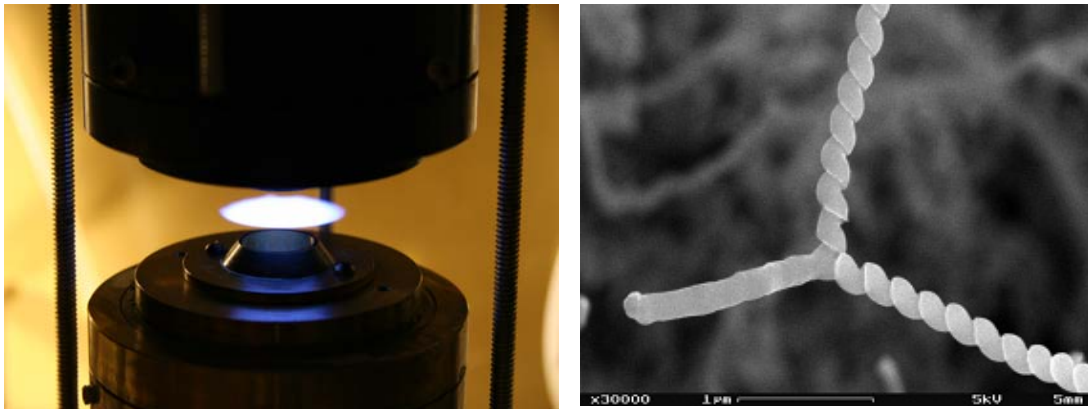
Figure 1.14: *Catalytic Flame Synthesis of Carbon Nanotubes. (from open source http://coewww.rutgers.edu/~sdytse/research.html)*

In a controlled way a fuel gas is partially burned to gain the right temperature of ~800 °C and the carbon atoms for SWNT production. On the small metal particles the SWNTs are than formed. As optimisation parameters the fuel gas composition, catalyst, catalyst carrier surface and temperature can be controlled[50]. In the literature found, the yield, typical length and diameters are not stated.

1.5.2   SWMT GROWN FROM CATALYST NANOPARTICLES SUPPORTED BY POROUS MEDIA

1.5.2.1 Catalyst Supported by Non-uniform Porous Materials

In this category, Fe, Ni, Co or an alloy of the three catalytic metals is initially deposited on high surface area media such as mesoporous or microporous silica,

alumina or magnesium oxide. SWNT synthesis is achieved by putting a carbon source in the gas phase and using an energy source, such as a plasma or a resistively heated coil, to transfer energy to a gaseous carbon molecule. Commonly used gaseous carbon sources include methane, carbon monoxide and acetylene. The energy source is used to "crack" the molecule into reactive atomic carbon. Then, the carbon diffuses towards the catalyst to form SWNT if proper parameters are maintained.

One exemplary method is CoMoCat[®] process developed by Dr. Daniel E. Resasco's group.[136-138] In this method, SWNTs are grown by CO disproportionation at $700 – 950\ ^{\mathrm{o}}$C. The technique is based on a unique Co-Mo catalyst formulation that inhibits the sintering of Co particles and therefore inhibits the formation of undesired forms of carbon that lower the selectivity. During the SWNT reaction, cobalt is progressively reduced from the oxidic state to the metallic form. Simultaneously Molybdenum is converted to the carbidic form (Mo_2C). Co acts as the active species in the activation of CO, while the role of the Mo is possibly dual. It would stabilize Co as a well-dispersed Co^{2+} avoiding its reduction and would act as a carbon sink to moderate the growth of carbon inhibiting the formation of undesirable forms of carbon.[139] It is found that one of the critical conditions for an effective reactor operation is that the space velocity has to be high enough to keep the CO conversion as low as possible. Figure 1.14 shows a fluidized bed reactor for a CoMoCat[®]

process. The most important advantage of fluidised bed reactors is that they permit continuous addition and removal of solid particles from the reactor, without stopping the operation.
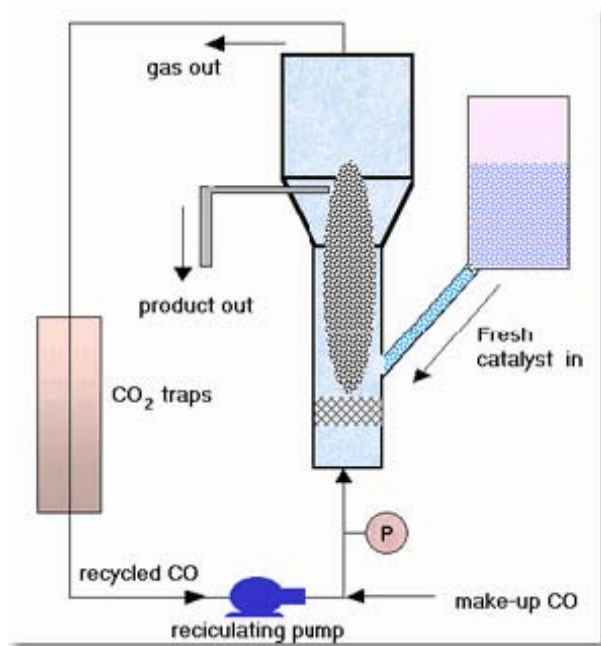
Figure 1.15: Schematic diagram of CoMoCAT® process (from open source www.ou.edu/engineering/nanotube/comocat.html)

This method can be scaled-up without losses in SWNT quality. By varying the operation conditions,SWNTs can be produced with different diameter ranges. The CoMoCat catalyst has a high selectivity towards SWNTs, namely 80 – 90 % .[138]

42

1.5.2.2 Catalyst Supported by Highly Ordered Porous Materials

Contrary to non-uniform porous materials, that has a wide distribution of pore sizes and presents an irregular spacing between particles, zeolites and other molecular sieves offer a very well defined structure that contains specific and uniform pore sizes, thus providing the possibility of controlling diameter of SWNT.
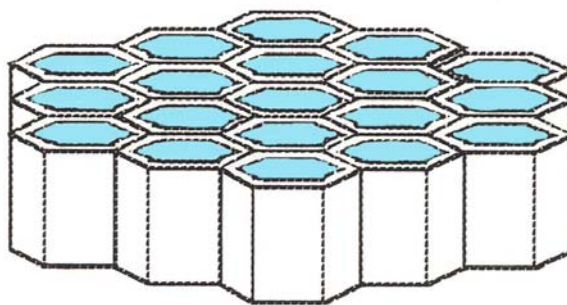
Figure 1.16: *Schematic diagram of MCM-41 (from open source*

www.quanta.kyutech.ac.jp *)*

Among them the mesoporous silica MCM-41 was found to be effective. The MCM-41 (figure 1.15) is a pure-silica material with a regular array of hexagonal, uniform, unidimensional mesopores, which can be systematically varied from 1.5 to 10 nm.

For example, highly ordered cobalt substituted MCM-41 samples were synthesized and characterized for application as catalytic templates for producing aligned SWNT in Dr. Gary Haller's group.[140, 141] Highly reproducible Co-MCM-41

samples were successfully synthesized using alkyl templates with 10, 12, 14, 16, and 18 carbon chain lengths by direct incorporation of cobalt into the siliceous MCM-41 framework using a hydrothermal method; the pore size and the pore volume can be controlled precisely. The catalytic templates showed over 90% selectivity to SWNT with up to 4 wt % carbon yield.

1.5.3   SWMT GROWN FROM CATALYST NANOPARTICLES DEPOSITED ON FLAT SUBSTRATE

1.5.3.1 Catalyst Deposition by Wet (Chemical) Process

Deposition of catalyst nanoparticles on flat surface by wet process normally involves two sequential steps: 1) preparation of metal nanoparticles or metal-containing precursors dispersed and stabilized in liquid phase; 2) formation of catalyst nanoparticles on surface by transferring and immobilizing metal nanoparticles or decomposing precursors. In the first step, metal nanoparticles in solution can be synthesized by using colloidal methods and metal containing precursors in solution have been reported to use metal salt, dendrimer, artificial ferritin, organometallic compound, metal-surfactant complex, metal-copolymer complex, etc. Several examples are given below to illustrate orderly arrayed SWNT grown on flat surface by wet process.

Parallel SWNT by Fast Heating Method

Dr. Jie Liu's group developed this method to grow orderly oriented SWNT.[142-144] A pretreated substrate with catalyst was transferred into the center of the heated furnace to initiate the growth. According to their experimental results, a "kite-mechanism" has been proposed with the catalyst nanoparticle having a long nanotube tail floating in the gas flow, which determines the orientation of SWNT arrays.
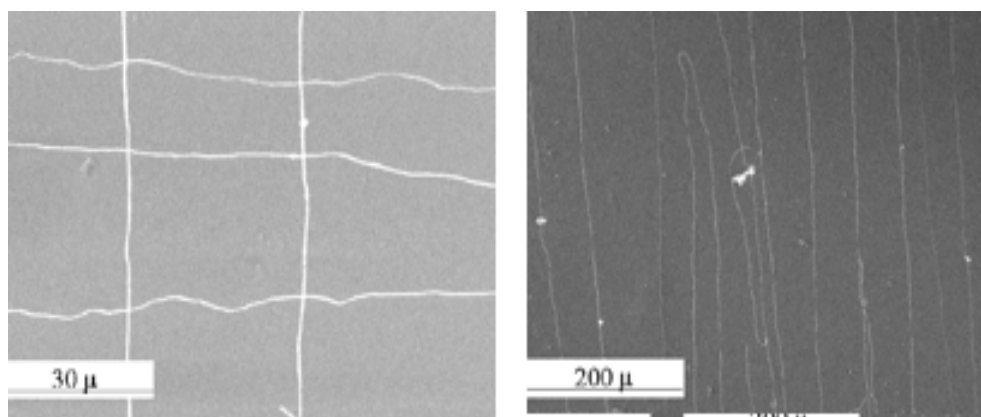
Figure 1.17: aligned SWNT parallel to the substrate (from open source http://www.chem.duke.edu/~jliu/labgroup/research.html)

Vertically Aligned SWNT by Dip-Coating Method

In 2004, Dr. Shegio Maruyama's group reported growth of vertically aligned SWNT on flat surface by alcohol assisted CVD method.[145, 146] In their method, Co/Mo catalyst was deposited by dipping quartz wafer in and pulling it out of

solution of Co and Mo acetate salt. After calcinations, a uniform distribution of CoMo alloy particles is formed on surface.
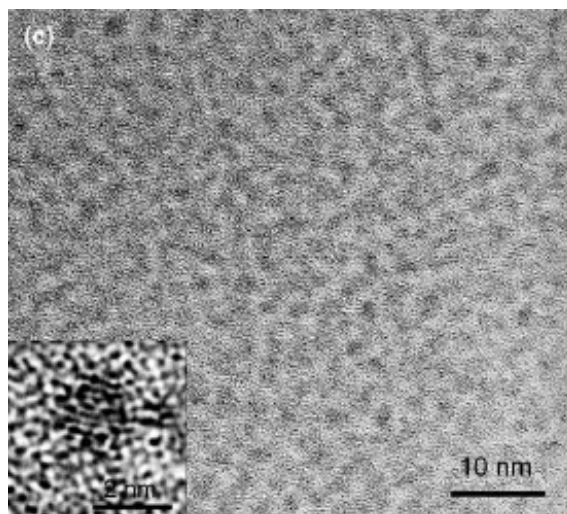
Figure 1.18: Co-Mo catalyst deposited on quartz substrate by dip-coating method. (adapted from "Growth of vertically aligned single-walled carbon nanotube films on quartz substrates and their optical anisotropy", S. Maruyama et al, Chemical Physics Letters, 385(2004) 298-303)

Vertically Aligned SWNT by Drop-Spread-Dry Method

In 2005, our group developed a method to deposit Co/Mo nanoparticles on flat surface by dropping a specially formulated Co/Mo-ligand complex solution on the surface and letting it spread and dry, which we call Drop-Spread-Dry process.[147] The resulted catalyst wafer is put into quartz reactor and a typical CoMoCat process is

conducted to grow vertically aligned SWNT. Our results shows vertically aligned SWNT can be grown not only on flat surface but also on rough surface.
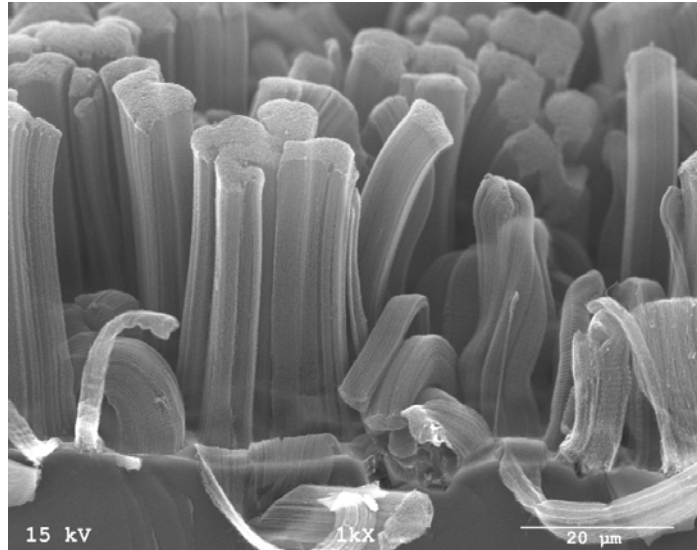
Figure 1.19: Vertically aligned SWTN on rough surface produce in our group.

1.5.3.2 Catalyst Deposition by Dry (Physical) Process

This process uses common physical film deposition methods to coat flat substrate with desired catalyst thin film, such as vacuum evaporation, electron bean evaporation, or sputtering coating. Recently, Dr. Timothy Fisher's group have created a "thin film" containing two layers of aluminum sandwiching one ultra-thin layer of iron using electron-beam evaporation as shown in figure 1.19.[148] Following that, the film was anodized to form a porous anodic alumina template.
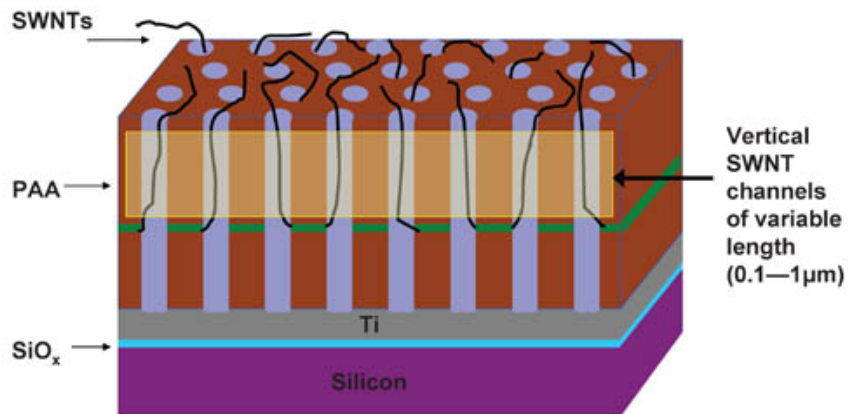
Figure 1.20: Individual carbon nanotubes vertically on top of a

silicon wafer. (from open source http://news.uns.purdue.edu

/html4ever/2006 /060801.Fisher.vertical.html)

A mixture of hydrogen and methane gas was then flowed into the template's holes, and microwave energy was applied to break down the methane, which contains carbon. The iron layer acted as a catalyst that prompted the carbon nanotubes to assemble from carbon originating in the methane, and the tubes then grew vertically out of the cavities.

1.6   REFERENCES

1. Ruoff, R. S.; Lorents, D. C., Mechanical and Thermal-Properties of Carbon Nanotubes. *Carbon* **1995,** 33, (7), 925-930.

2. Hone, J.; Whitney, M.; Piskoti, C.; Zettl, A., Thermal conductivity of single-walled carbon nanotubes. *Physical Review B* **1999,** 59, (4), R2514-R2516.

3. Berber, S.; Kwon, Y. K.; Tomanek, D., Unusually high thermal conductivity of carbon nanotubes. *Physical Review Letters* **2000,** 84, (20), 4613-4616.

4. Dai, H. J., Probing electrical transport in nanomaterials: Conductivity of individual carbon nanotubes (vol 272, pg 523, 1996). *Science* **1996,** 272, (5270), 1861-1861.

5. Ebbesen, T. W.; Lezec, H. J.; Hiura, H.; Bennett, J. W.; Ghaemi, H. F.; Thio, T., Electrical conductivity of individual carbon nanotubes. *Nature* **1996,** 382, (6586), 54-56.

6. Benedict, L. X.; Crespi, V. H.; Louie, S. G.; Cohen, M. L., Static Conductivity and Superconductivity of Carbon Nanotubes - Relations between Tubes and Sheets. *Physical Review B* **1995,** 52, (20), 14935-14940.

7. Dai, H. J.; Wong, E. W.; Lieber, C. M., Probing electrical transport in nanomaterials: Conductivity of individual carbon nanotubes. *Science* **1996,** 272, (5261), 523-526.

8. Lee, R. S.; Kim, H. J.; Fischer, J. E.; Thess, A.; Smalley, R. E., Conductivity enhancement in single-walled carbon nanotube bundles doped with K and Br. *Nature* **1997,** 388, (6639), 255-257.

9. Iijima, S., Helical Microtubules of Graphitic Carbon. *Nature* **1991,** 354, (6348), 56-58.

10. Iijima, S.; Ichihashi, T., Single-Shell Carbon Nanotubes of 1-Nm Diameter (Vol 363, Pg 603, 1993). *Nature* **1993,** 364, (6439), 737-737.

11. Anantram, M.; Delzeit, L.; Cassell, A.; Han, J.; Meyyappan, M., Nanotubes in nanoelectronics: transport, growth and modeling. *Physica E* **2001,** 11, (2-3), 118-125.

12. Bernholc, J.; Brabec, C.; Nardelli, M. B.; Maiti, A.; Roland, C.; Yakobson, B. I., Theory of growth and mechanical properties of nanotubes. *Applied Physics a-Materials Science & Processing* **1998,** 67, (1), 39-46.

13. Gotoh, Y.; Matsumoto, K.; Maeda, T.; Cooper, E. B.; Manalis, S. R.; Fang, H.; Minne, S. C.; Hunt, T.; Dai, H.; Harris, J.; Quate, C. F., Experimental and theoretical results of room-temperature single-electron transistor formed by the atomic force microscope nano-oxidation process. *Journal of Vacuum Science & Technology a-Vacuum Surfaces and Films* **2000,** 18, (4), 1321-1325.

14. Liang, W. J.; Bockrath, M.; Bozovic, D.; Hafner, J. H.; Tinkham, M.; Park, H., Fabry-Perot interference in a nanotube electron waveguide. *Nature* **2001,** 411, (6838), 665-669.

15. Odom, T. W.; Huang, J. L.; Kim, P.; Lieber, C. M., Structure and electronic properties of carbon nanotubes. *Journal of Physical Chemistry B* **2000,** 104, (13), 2794-2809.

16. Salvetat, J. P.; Bonard, J. M.; Thomson, N. H.; Kulik, A. J.; Forro, L.; Benoit, W.; Zuppiroli, L., Mechanical properties of carbon nanotubes. *Applied Physics a-Materials Science & Processing* **1999,** 69, (3), 255-260.

17. Sorescu, D. C.; Jordan, K. D.; Avouris, P., Theoretical study of oxygen adsorption on graphite and the (8,0) single-walled carbon nanotube. *Journal of Physical Chemistry B* **2001,** 105, (45), 11227-11232.

18. Van Lier, G.; Van Alsenoy, C.; Van Doren, V.; Geerlings, P., Ab initio study of the elastic properties of single-walled carbon nanotubes and graphene. *Chemical Physics Letters* **2000,** 326, (1-2), 181-185.

19. White, C. T.; Todorov, T. N., Carbon nanotubes as long ballistic conductors. *Nature* **1998,** 393, (6682), 240-242.

20. Thess, A.; Lee, R.; Nikolaev, P.; Dai, H. J.; Petit, P.; Robert, J.; Xu, C. H.; Lee, Y. H.; Kim, S. G.; Rinzler, A. G.; Colbert, D. T.; Scuseria, G. E.; Tomanek, D.; Fischer, J. E.; Smalley, R. E., Crystalline ropes of metallic carbon nanotubes. *Science* **1996,** 273, (5274), 483-487.

21. Journet, C.; Maser, W. K.; Bernier, P.; Loiseau, A.; delaChapelle, M. L.; Lefrant, S.; Deniard, P.; Lee, R.; Fischer, J. E., Large-scale production of single-walled carbon nanotubes by the electric-arc technique. *Nature* **1997,** 388, (6644), 756-758.

22. Dal, H. J.; Rinzler, A. G.; Nikolaev, P.; Thess, A.; Colbert, D. T.; Smalley, R. E., Single-wall nanotubes produced by metal-catalyzed disproportionation of carbon monoxide. *Chemical Physics Letters* **1996,** 260, (3-4), 471-475.

23. Tans, S. J.; Devoret, M. H.; Dai, H. J.; Thess, A.; Smalley, R. E.; Geerligs, L. J.; Dekker, C., Individual single-wall carbon nanotubes as quantum wires. *Nature* **1997,** 386, (6624), 474-477.

24. Nygard, J.; Cobden, D. H.; Lindelof, P. E., Kondo physics in carbon nanotubes. *Nature* **2000,** 408, (6810), 342-346.

25. Tans, S. J.; Verschueren, A. R. M.; Dekker, C., Room-temperature transistor based on a single carbon nanotube. *Nature* **1998,** 393, (6680), 49-52.

26. Fuhrer, M. S.; Kim, B. M.; Durkop, T.; Brintlinger, T., High-mobility nanotube transistor memory. *Nano Letters* **2002,** 2, (7), 755-759.

27. Liu, K.; Burghard, M.; Roth, S.; Bernier, P., Conductance spikes in single-walled carbon nanotube field-effect transistor. *Applied Physics Letters* **1999,** 75, (16), 2494-2496.

28. Liu, X. L.; Lee, C.; Zhou, C. W.; Han, J., Carbon nanotube field-effect inverters. *Applied Physics Letters* **2001,** 79, (20), 3329-3331.

29. Nygard, J.; Cobden, D. H.; Bockrath, M.; McEuen, P. L.; Lindelof, P. E., Electrical transport measurements on single-walled carbon nanotubes. *Applied Physics a-Materials Science & Processing* **1999,** 69, (3), 297-304.

30. Choi, W. B.; Chung, D. S.; Kang, J. H.; Kim, H. Y.; Jin, Y. W.; Han, I. T.; Lee, Y. H.; Jung, J. E.; Lee, N. S.; Park, G. S.; Kim, J. M., Fully sealed, high-brightness carbon-nanotube field-emission display. *Applied Physics Letters* **1999,** 75, (20), 3129-3131.

31. Bonard, J. M.; Salvetat, J. P.; Stockli, T.; Forro, L.; Chatelain, A., Field emission from carbon nanotubes: perspectives for applications and clues to the emission mechanism. *Applied Physics a-Materials Science & Processing* **1999,** 69, (3), 245-254.

32. Dean, K. A.; Chalamala, B. R., Field emission microscopy of carbon nanotube caps. *Journal of Applied Physics* **1999,** 85, (7), 3832-3836.

33. Dean, K. A.; von Allmen, P.; Chalamala, B. R., Three behavioral states observed in field emission from single-walled carbon nanotubes. *Journal of Vacuum Science & Technology B* **1999,** 17, (5), 1959-1969.

34. Ding, Y.; Hang, Q. L.; Zhang, H. Z.; Feng, S. Q.; Bai, Z. G.; Yu, D. P.; Zhang, Z. X.; Xue, Z. Q.; Shi, Z. J.; Lian, Y. F.; Gu, Z. N., A simple method to make field emitter

using ropes of single-walled carbon nanotubes. *Chinese Physics Letters* **1999,** 16, (2), 117-119.

35.	Saito, Y.; Hamaguchi, K.; Nishino, T.; Hata, K.; Tohji, K.; Kasuya, A.; Nishina, Y., Field emission patterns from single-walled carbon nanotubes. *Japanese Journal of Applied Physics Part 2-Letters* **1997,** 36, (10A), L1340-L1342.

36.	Someya, T.; Small, J.; Kim, P.; Nuckolls, C.; Yardley, J. T., Alcohol vapor sensors based on single-walled carbon nanotube field effect transistors. *Nano Letters* **2003,** 3, (7), 877-881.

37.	An, K. H.; Jeong, S. Y.; Hwang, H. R.; Lee, Y. H., Enhanced sensitivity of a gas sensor incorporating single-walled carbon nanotube-polypyrrole nanocomposites. *Advanced Materials* **2004,** 16, (12), 1005-+.

38.	Kong, J.; Franklin, N. R.; Zhou, C. W.; Chapline, M. G.; Peng, S.; Cho, K. J.; Dai, H. J., Nanotube molecular wires as chemical sensors. *Science* **2000,** 287, (5453), 622-625.

39.	Peng, S.; Cho, K. J.; Qi, P. F.; Dai, H. J., Ab initio study of CNT NO2 gas sensor. *Chemical Physics Letters* **2004,** 387, (4-6), 271-276.

40.	Pengfei, Q. F.; Vermesh, O.; Grecu, M.; Javey, A.; Wang, O.; Dai, H. J.; Peng, S.; Cho, K. J., Toward large arrays of multiplex functionalized carbon nanotube sensors for highly sensitive and selective molecular detection. *Nano Letters* **2003,** 3, (3), 347-351.

41.	Wong, S. S.; Joselevich, E.; Woolley, A. T.; Cheung, C. L.; Lieber, C. M., Covalently functionalized nanotubes as nanometre-sized probes in chemistry and biology. *Nature* **1998,** 394, (6688), 52-55.

42.	Cheung, C. L.; Hafner, J. H.; Lieber, C. M., Carbon nanotube atomic force microscopy tips: Direct growth by chemical vapor deposition and application to high-resolution imaging. *Proceedings of the National Academy of Sciences of the United States of America* **2000,** 97, (8), 3809-3813.

43.	Nguyen, C. V.; Chao, K. J.; Stevens, R. M. D.; Delzeit, L.; Cassell, A.; Han, J.; Meyyappan, M., Carbon nanotube tip probes: stability and lateral resolution in scanning probe microscopy and application to surface science in semiconductors. *Nanotechnology* **2001,** 12, (3), 363-367.

44. Hafner, J. H.; Cheung, C. L.; Lieber, C. M., Direct growth of single-walled carbon nanotube scanning probe microscopy tips. *Journal of the American Chemical Society* **1999,** 121, (41), 9750-9751.

45. Zhang, T.; Nix, M. B.; Yoo, B. Y.; Deshusses, M. A.; Myung, N. V., Electrochemically functionalized single-walled carbon nanotube gas sensor. *Electroanalysis* **2006,** 18, (12), 1153-1158.

46. Hafner, J. H.; Cheung, C. L.; Oosterkamp, T. H.; Lieber, C. M., High-yield assembly of individual single-walled carbon nanotube tips for scanning probe microscopies. *Journal of Physical Chemistry B* **2001,** 105, (4), 743-746.

47. Dresselhaus, M. S.; Dresselhaus, G.; Saito, R., Carbon-Fibers Based on C-60 and Their Symmetry. *Physical Review B* **1992,** 45, (11), 6234-6242.

48. Dresselhaus, M. S.; Eklund, P. C., Phonons in carbon nanotubes. *Advances in Physics* **2000,** 49, (6), 705-814.

49. Dresselhaus, M. S.; Dresselhaus, G.; Saito, R., Physics of Carbon Nanotubes. *Carbon* **1995,** 33, (7), 883-891.

50. Dresselhaus, M. S.; Dresselhaus, G.; Saito, R.; Jorio, A., Raman spectroscopy of carbon nanotubes. *Physics Reports-Review Section of Physics Letters* **2005,** 409, (2), 47-99.

51. Saito, R.; Dresselhaus, G.; Dresselhaus, M. S., Electronic-Structure of Double-Layer Graphene Tubules. *Journal of Applied Physics* **1993,** 73, (2), 494-500.

52. Ajayan, P. M.; Lambert, J. M.; Bernier, P.; Barbedette, L.; Colliex, C.; Planeix, J. M., Growth Morphologies during Cobalt-Catalyzed Single-Shell Carbon Nanotube Synthesis. *Chemical Physics Letters* **1993,** 215, (5), 509-517.

53. Fan, X. D.; Bursill, L. A., Principles for Structure-Analysis of Carbon Nanotubes by High-Resolution Transmission Electron-Microscopy. *Philosophical Magazine a-Physics of Condensed Matter Structure Defects and Mechanical Properties* **1995,** 72, (1), 139-159.

54. Kiang, C. H.; Goddard, W. A.; Beyers, R.; Bethune, D. S., Carbon Nanotubes with Single-Layer Walls. *Carbon* **1995,** 33, (7), 903-914.

55. Su, W.; Dan, Z., Microscopy of Single-Layer Carbon Nanotubes. *Chemical Physics Letters* **1994,** 225, (1-3), 165-169.

56. Meyer, R. R.; Friedrichs, S.; Kirkland, A. I.; Sloan, J.; Hutchison, J. L.; Green, M. L. H., A composite method for the determination of the chirality of single walled carbon nanotubes. *Journal of Microscopy-Oxford* **2003,** 212, 152-157.

57. Colomer, J. F.; Henrard, L.; Lambin, P.; Van Tendeloo, G., Electron diffraction and microscopy of single-wall carbon nanotube bundles produced by different methods. *European Physical Journal B* **2002,** 27, (1), 111-118.

58. Hamon, A. L.; Marraud, A.; Jouffrey, B., A geometrical study of single-walled nanotube ropes by transmission electron microscopy. *Philosophical Magazine B-Physics of Condensed Matter Statistical Mechanics Electronic Optical and Magnetic Properties* **2001,** 81, (11), 1779-1799.

59. Lambin, P.; Meunier, V.; Henrard, L.; Lucas, A. A., Measuring the helicity of carbon nanotubes. *Carbon* **2000,** 38, (11-12), 1713-1721.

60. Henrard, L.; Loiseau, A.; Journet, C.; Bernier, P., Study of the symmetry of single-wall nanotubes by electron diffraction. *European Physical Journal B* **2000,** 13, (4), 661-669.

61. Gao, M.; Zuo, J. M.; Twesten, R. D.; Petrov, I.; Nagahara, L. A.; Zhang, R., Structure determination of individual single-wall carbon nanotubes by nanoarea electron diffraction. *Applied Physics Letters* **2003,** 82, (16), 2703-2705.

62. Wang, S. R.; Liang, Z. Y.; Wang, B.; Zhang, C., Statistical characterization of single-wall carbon nanotube length distribution. *Nanotechnology* **2006,** 17, (3), 634-639.

63. Islam, M. F.; Rojas, E.; Bergey, D. M.; Johnson, A. T.; Yodh, A. G., High weight fraction surfactant solubilization of single-wall carbon nanotubes in water. *Nano Letters* **2003,** 3, (2), 269-273.

64. Lee, J. Y.; Kim, J. S.; An, K. H.; Lee, K.; Kim, D. Y.; Bae, D. J.; Lee, Y. H., Electrophoretic and dynamic light scattering in evaluating dispersion and size distribution of single-walled carbon nanotubes. *Journal of Nanoscience and Nanotechnology* **2005,** 5, (7), 1045-1049.

65. Clauss, W.; Bergeron, D. J.; Johnson, A. T., Atomic resolution STM imaging of a twisted single-wall carbon nanotube. *Physical Review B* **1998,** 58, (8), R4266-R4269.

66. Venema, L. C.; Meunier, V.; Lambin, P.; Dekker, C., Atomic structure of carbon nanotubes from scanning tunneling microscopy. *Physical Review B* **2000,** 61, (4), 2991-2996.

67. Kim, P.; Odom, T. W.; Huang, J. L.; Lieber, C. M., Electronic density of states of atomically resolved single-walled carbon nanotubes: Van Hove singularities and end states. *Physical Review Letters* **1999,** 82, (6), 1225-1228.

68. Klusek, Z.; Kowalczyk, P.; Byszewski, P., Investigations of electronic structure of capped carbon nanotubes by scanning tunneling spectroscopy. *Vacuum* **2001,** 63, (1-2), 145-150.

69. Zhang, Z.; Lieber, C. M., Nanotube Structure and Electronic-Properties Probed by Scanning-Tunneling-Microscopy. *Applied Physics Letters* **1993,** 62, (22), 2792-2794.

70. Olk, C. H.; Heremans, J. P., Scanning Tunneling Spectroscopy of Carbon Nanotubes. *Journal of Materials Research* **1994,** 9, (2), 259-262.

71. Biro, L. P.; Gyulai, J.; Lambin, P.; Nagy, J. B.; Lazarescu, S.; Mark, G. I.; Fonseca, A.; Surjan, P. R.; Szekeres, Z.; Thiry, P. A.; Lucas, A. A., Scanning tunnelling microscopy (STM) imaging of carbon nanotubes. *Carbon* **1998,** 36, (5-6), 689-696.

72. Speck, J. S.; Steinbeck, J.; Dresselhaus, M. S., Microstructural Studies of Laser Irradiated Graphite Surfaces. *Journal of Materials Research* **1990,** 5, (5), 980-988.

73. Ohana, I.; Dresselhaus, M. S.; Endo, M., Raman and X-Ray Study of Asf5/Vapor-Grown Graphite Fibers. *Carbon* **1989,** 27, (3), 417-421.

74. Rao, A. M.; Fung, A. W. P.; Divittorio, S. L.; Dresselhaus, M. S.; Dresselhaus, G.; Endo, M.; Oshida, K.; Nakajima, T., Raman-Scattering and Transmission-Electron-Microscopy Studies of Fluorine-Intercalated Graphite Fibers Cxf (7.8-Greater-Than-or-Equal-to-X-Greater-Than-or-Equal-to-2.9). *Physical Review B* **1992,** 45, (12), 6883-6892.

75. Ohana, I.; Dresselhaus, M. S.; Tanuma, S., Resonant Raman Effect and Fano Distortion in the Stage-2 Graphite Donor Intercalation Compound C/Rb. *Physical Review B* **1991,** 43, (2), 1773-1776.

76. Speck, J. S.; Nicholls, J. T.; Wuensch, B. J.; Delgado, J. M.; Dresselhaus, M. S.; Miyazaki, H., Single-Crystal Structural Studies of Metal Dichloride Graphite-Intercalation Compounds. *Philosophical Magazine B-Physics of Condensed Matter*

Statistical Mechanics Electronic Optical and Magnetic Properties **1991,** 64, (2), 181-206.

77.   Dresselhaus, M. S.; Dresselhaus, G., Fullerenes and Fullerene-Derived Solids as Electronic Materials. *Annual Review of Materials Science* **1995,** 25, 487-523.

78.   Dresselhaus, M. S.; Dresselhaus, G.; Jorio, A.; Souza, A. G.; Saito, R., Raman spectroscopy on isolated single wall carbon nanotubes. *Carbon* **2002,** 40, (12), 2043-2061.

79.   Rao, A. M.; Jorio, A.; Pimenta, M. A.; Dantas, M. S. S.; Saito, R.; Dresselhaus, G.; Dresselhaus, M. S., Polarized Raman study of aligned multiwalled carbon nanotubes. *Physical Review Letters* **2000,** 84, (8), 1820-1823.

80.   Kusunoki, M.; Shibata, J.; Rokkaku, M.; Hirayama, T., Aligned carbon nanotube film self-organized on a SiC wafer. *Japanese Journal of Applied Physics Part 2-Letters & Express Letters* **1998,** 37, (5B), L605-L606.

81.   Saito, R.; Jorio, A.; Hafner, J. H.; Lieber, C. M.; Hunter, M.; McClure, T.; Dresselhaus, G.; Dresselhaus, M. S., Chirality-dependent G-band Raman intensity of carbon nanotubes. *Physical Review B* **2001,** 6408, (8), art. no.-085312.

82.   Rao, A. M.; Richter, E.; Bandow, S.; Chase, B.; Eklund, P. C.; Williams, K. A.; Fang, S.; Subbaswamy, K. R.; Menon, M.; Thess, A.; Smalley, R. E.; Dresselhaus, G.; Dresselhaus, M. S., Diameter-selective Raman scattering from vibrational modes in carbon nanotubes. *Science* **1997,** 275, (5297), 187-191.

83.   Pimenta, M. A.; Jorio, A.; Brown, S. D. M.; Souza, A. G.; Dresselhaus, G.; Hafner, J. H.; Lieber, C. M.; Saito, R.; Dresselhaus, M. S., Diameter dependence of the Raman D-band in isolated single-wall carbon nanotubes. *Physical Review B* **2001,** 6404, (4), -.

84.   Cronin, S. B.; Swan, A. K.; Unlu, M. S.; Goldberg, B. B.; Dresselhaus, M. S.; Tinkham, M., Resonant Raman spectroscopy of individual metallic and semiconducting single-wall carbon nanotubes under uniaxial strain. *Physical Review B* **2005,** 72, (3), -.

85.   Brown, S. D. M.; Jorio, A.; Corio, P.; Dresselhaus, M. S.; Dresselhaus, G.; Saito, R.; Kneipp, K., Origin of the Breit-Wigner-Fano lineshape of the tangential G-band feature of metallic carbon nanotubes. *Physical Review B* **2001,** 6315, (15), -.

86. Souza, A. G.; Kobayashi, N.; Jiang, J.; Gruneis, A.; Saito, R.; Cronin, S. B.; Mendes, J.; Samsonidze, G. G.; Dresselhaus, G. G.; Dresselhaus, M. S., Strain-induced interference effects on the resonance Raman cross section of carbon nanotubes. *Physical Review Letters* **2005,** 95, (21), -.

87. Kim, Y. A.; Muramatsu, H.; Kojima, M.; Hayashi, T.; Endo, M.; Terrones, M.; Dresselhaus, M. S., The possible way to evaluate the purity of double-walled carbon nanotubes over single wall carbon nanotubes by chemical doping. *Chemical Physics Letters* **2006,** 420, (4-6), 377-381.

88. Raravikar, N. R.; Keblinski, P.; Rao, A. M.; Dresselhaus, M. S.; Schadler, L. S.; Ajayan, P. M., Temperature dependence of radial breathing mode Raman frequency of single-walled carbon nanotubes. *Physical Review B* **2002,** 66, (23), -.

89. Bachilo, S. M.; Strano, M. S.; Kittrell, C.; Hauge, R. H.; Smalley, R. E.; Weisman, R. B., Structure-assigned optical spectra of single-walled carbon nanotubes. *Science* **2002,** 298, (5602), 2361-2366.

90. Doorn, S. K.; Heller, D. A.; Barone, P. W.; Usrey, M. L.; Strano, M. S., Resonant Raman excitation profiles of individually dispersed single walled carbon nanotubes in solution. *Applied Physics a-Materials Science & Processing* **2004,** 78, (8), 1147-1155.

91. Doorn, S. K.; O'Connell, M. J.; Sivaram, S.; Strano, M. S., Near infrared Raman characterization of individualized, aggregated, and separated carbon nanotubes. *Abstracts of Papers of the American Chemical Society* **2004,** 227, U1265-U1265.

92. Fantini, C.; Jorio, A.; Souza, M.; Strano, M. S.; Dresselhaus, M. S.; Pimenta, M. A., Optical transition energies for carbon nanotubes from resonant Raman spectroscopy: Environment and temperature effects. *Physical Review Letters* **2004,** 93, (14), -.

93. Heller, D. A.; Barone, P. W.; Swanson, J. P.; Mayrhofer, R. M.; Strano, M. S., Using Raman spectroscopy to elucidate the aggregation state of single-walled carbon nanotubes. *Journal of Physical Chemistry B* **2004,** 108, (22), 6905-6909.

94. Jorio, A.; Fantini, C.; Pimenta, M. A.; Heller, D. A.; Strano, M. S.; Dresselhaus, M. S.; Oyama, Y.; Jiang, J.; Saito, R., Carbon nanotube population analysis from Raman and photoluminescence intensities. *Applied Physics Letters* **2006,** 88, (2), -.

95. O'Connell, M. J.; Bachilo, S. M.; Huffman, C. B.; Moore, V. C.; Strano, M. S.; Haroz, E. H.; Rialon, K. L.; Boul, P. J.; Noon, W. H.; Kittrell, C.; Ma, J. P.; Hauge, R. H.;

Weisman, R. B.; Smalley, R. E., Band gap fluorescence from individual single-walled carbon nanotubes. *Science* **2002,** 297, (5581), 593-596.

96. Strano, M. S.; Doorn, S. K.; Haroz, E. H.; Kittrell, C.; Hauge, R. H.; Smalley, R. E., Assignment of (n, m) Raman and optical features of metallic single-walled carbon nanotubes. *Nano Letters* **2003,** 3, (8), 1091-1096.

97. Strano, M. S., Selective functionalization of single walled carbon nanotubes: Progress towards separation by electronic type. *Abstracts of Papers of the American Chemical Society* **2004,** 227, U1277-U1277.

98. Strano, M. S.; Moore, V. C.; Miller, M. K.; Allen, M. J.; Haroz, E. H.; Kittrell, C.; Hauge, R. H.; Smalley, R. E., The role of surfactant adsorption during ultrasonication in the dispersion of single-walled carbon nanotubes. *Journal of Nanoscience and Nanotechnology* **2003,** 3, (1-2), 81-86.

99. Krishnan, A.; Dujardin, E.; Ebbesen, T. W.; Yianilos, P. N.; Treacy, M. M. J., Young's modulus of single-walled nanotubes. *Physical Review B* **1998,** 58, (20), 14013-14019.

100. Lu, J. P., Elastic properties of single and multilayered nanotubes. *Journal of Physics and Chemistry of Solids* **1997,** 58, (11), 1649-1652.

101. Andrews, R.; Jacques, D.; Rao, A. M.; Rantell, T.; Derbyshire, F.; Chen, Y.; Chen, J.; Haddon, R. C., Nanotube composite carbon fibers. *Applied Physics Letters* **1999,** 75, (9), 1329-1331.

102. Bower, C.; Rosen, R.; Jin, L.; Han, J.; Zhou, O., Deformation of carbon nanotubes in nanotube-polymer composites. *Applied Physics Letters* **1999,** 74, (22), 3317-3319.

103. Curran, S.; Davey, A. P.; Coleman, J.; Dalton, A.; McCarthy, B.; Maier, S.; Drury, A.; Gray, D.; Brennan, M.; Ryder, K.; de la Chapelle, M. L.; Journet, C.; Bernier, P.; Byrne, H. J.; Carroll, D.; Ajayan, P. M.; Lefrant, S.; Blau, W., Evolution and evaluation of the polymer nanotube composite. *Synthetic Metals* **1999,** 103, (1-3), 2559-2562.

104. Gong, X. Y.; Liu, J.; Baskaran, S.; Voise, R. D.; Young, J. S., Surfactant-assisted processing of carbon nanotube/polymer composites. *Chemistry of Materials* **2000,** 12, (4), 1049-1052.

105. Goze, C.; Vaccarini, L.; Henrard, L.; Bernier, P.; Hernandez, E.; Rubio, A., Elastic and mechanical properties of carbon nanotubes. *Synthetic Metals* **1999,** 103, (1-3), 2500-2501.

106. Jia, Z. J.; Wang, Z. Y.; Xu, C. L.; Liang, J.; Wei, B. Q.; Wu, D. H.; Zhu, S. W., Study on poly(methyl methacrylate)/carbon nanotube composites. *Materials Science and Engineering a-Structural Materials Properties Microstructure and Processing* **1999,** 271, (1-2), 395-400.

107. Lourie, O.; Wagner, H. D., Evidence of stress transfer and formation of fracture clusters in carbon nanotube-based composites. *Composites Science and Technology* **1999,** 59, (6), 975-977.

108. Stephan, C.; Nguyen, T. P.; de la Chapelle, M. L.; Lefrant, S.; Journet, C.; Bernier, P., Characterization of singlewalled carbon nanotubes-PMMA composites. *Synthetic Metals* **2000,** 108, (2), 139-149.

109. Tang, B. Z.; Xu, H. Y., Preparation, alignment, and optical properties of soluble poly(phenylacetylene)-wrapped carbon nanotubes. *Macromolecules* **1999,** 32, (8), 2569-2576.

110. Itoh, E.; Suzuki, I.; Miyairi, K., Field emission from carbon-nanotube-dispersed conducting polymer thin film and its application to photovoltaic devices. *Japanese Journal of Applied Physics Part 1-Regular Papers Brief Communications & Review Papers* **2005,** 44, (1B), 636-640.

111. Purcell, S. T.; Binh, V. T.; Baptist, R., Nanoprotrusion model for field emission from integrated microtips. *Journal of Vacuum Science & Technology B* **1997,** 15, (5), 1666-1677.

112. Bonard, J. M.; Salvetat, J. P.; Stockli, T.; de Heer, W. A.; Forro, L.; Chatelain, A., Field emission from single-wall carbon nanotube films. *Applied Physics Letters* **1998,** 73, (7), 918-920.

113. Bonard, J. M.; Kind, H.; Stockli, T.; Nilsson, L. A., Field emission from carbon nanotubes: the first five years. *Solid-State Electronics* **2001,** 45, (6), 893-914.

114. Rosen, R.; Simendinger, W.; Debbault, C.; Shimoda, H.; Fleming, L.; Stoner, B.; Zhou, O., Application of carbon nanotubes as electrodes in gas discharge tubes. *Applied Physics Letters* **2000,** 76, (13), 1668-1670.

115. Nakayama, Y.; Akita, S., Field-emission device with carbon nanotubes for a flat panel display. *Synthetic Metals* **2001,** 117, (1-3), 207-210.

116. Wang, Q. H.; Setlur, A. A.; Lauerhaas, J. M.; Dai, J. Y.; Seelig, E. W.; Chang, R. P. H., A nanotube-based field-emission flat panel display. *Applied Physics Letters* **1998,** 72, (22), 2912-2913.

117. Deheer, W. A.; Chatelain, A.; Ugarte, D., A Carbon Nanotube Field-Emission Electron Source. *Science* **1995,** 270, (5239), 1179-1180.

118. Zeng, B. Q.; Liu, N.; Yang, Z. H., Simulation of vacuum microelectronic triode made of single carbon nanotube. *International Journal of Infrared and Millimeter Waves* **2004,** 25, (11), 1621-1631.

119. Han, J. H.; Lee, T. Y.; Kim, D. Y.; Yoo, J. B.; Park, C. Y.; Choi, J. J.; Jung, T.; Han, I. T.; Kim, J. M., Field emission properties of carbon nanotubes grown on Co/TiN coated Ta substrate for cathode in microwave power amplifier. *Diamond and Related Materials* **2004,** 13, (4-8), 987-993.

120. Milne, W. I.; Teo, K. B. K.; Amaratunga, G. A. J.; Legagneux, P.; Gangloff, L.; Schnell, J. P.; Semet, V.; Binh, V. T.; Groening, O., Carbon nanotubes as field emission sources. *Journal of Materials Chemistry* **2004,** 14, (6), 933-943.

121. Chen, L. H.; Jin, S., Packaging of nanostructured microelectromechanical systems microtriode devices. *Journal of Electronic Materials* **2003,** 32, (12), 1360-1365.

122. Avouris, P.; Hertel, T.; Martel, R.; Schmidt, T.; Shea, H. R.; Walkup, R. E., Carbon nanotubes: nanomechanics, manipulation, and electronic devices. *Applied Surface Science* **1999,** 141, (3-4), 201-209.

123. Simonyan, V. V.; Diep, P.; Johnson, J. K., Molecular simulation of hydrogen adsorption in charged single-walled carbon nanotubes. *Journal of Chemical Physics* **1999,** 111, (21), 9778-9783.

124. Nutzenadel, C.; Zuttel, A.; Chartouni, D.; Schlapbach, L., Electrochemical storage of hydrogen in nanotube materials. *Electrochemical and Solid State Letters* **1999,** 2, (1), 30-32.

125. Zhao, J.; Buldum, A.; Han, J.; Lu, J. P., First-principles study of Li-intercalated carbon nanotube ropes. *Physical Review Letters* **2000,** 85, (8), 1706-1709.

126. Ma, R. Z.; Wei, B. Q.; Xu, C. L.; Liang, J.; Wu, D. H., Development of supercapacitors based on carbon nanotubes. *Science in China Series E-Technological Sciences* **2000,** 43, (2), 178-182.

127. Nikolaev, P.; Bronikowski, M. J.; Bradley, R. K.; Rohmund, F.; Colbert, D. T.; Smith, K. A.; Smalley, R. E., Gas-phase catalytic growth of single-walled carbon nanotubes from carbon monoxide. *Chemical Physics Letters* **1999,** 313, (1-2), 91-97.

128. Ebbesen, T. W.; Ajayan, P. M., Large-Scale Synthesis of Carbon Nanotubes. *Nature* **1992,** 358, (6383), 220-222.

129. Journet, C.; Bernier, P., Production of carbon nanotubes. *Applied Physics a-Materials Science & Processing* **1998,** 67, (1), 1-9.

130. Guo, T.; Nikolaev, P.; Thess, A.; Colbert, D. T.; Smalley, R. E., Catalytic Growth of Single-Walled Nanotubes by Laser Vaporization. *Chemical Physics Letters* **1995,** 243, (1-2), 49-54.

131. Yudasaka, M.; Ichihashi, T.; Komatsu, T.; Iijima, S., Single-wall carbon nanotubes formed by a single laser-beam pulse. *Chemical Physics Letters* **1999,** 299, (1), 91-96.

132. Maser, W. K.; Munoz, E.; Benito, A. M.; Martinez, M. T.; de la Fuente, G. F.; Maniette, Y.; Anglaret, E.; Sauvajol, J. L., Production of high-density single-walled nanotube material by a simple laser-ablation method. *Chemical Physics Letters* **1998,** 292, (4-6), 587-593.

133. Scott, C. D.; Arepalli, S.; Nikolaev, P.; Smalley, R. E., Growth mechanisms for single-wall carbon nanotubes a laser ablation process (vol 72, pg 573, 2001). *Applied Physics a-Materials Science & Processing* **2002,** 74, (1), 11-11.

134. Wal, R. L. V.; Berger, G. M.; Hall, L. J., Single-walled carbon nanotube synthesis via a multi-stage flame configuration. *Journal of Physical Chemistry B* **2002,** 106, (14), 3564-3567.

135. Wal, R. L. V.; Ticich, T. M., Flame and furnace synthesis of single-walled and multi-walled carbon nanotubes and nanofibers. *Journal of Physical Chemistry B* **2001,** 105, (42), 10249-10256.

136. Kitiyanan, B.; Alvarez, W. E.; Harwell, J. H.; Resasco, D. E., Controlled production of single-wall carbon nanotubes by catalytic decomposition of CO on bimetallic Co-Mo catalysts. *Chemical Physics Letters* **2000,** 317, (3-5), 497-503.

137. Resasco, D. E.; Kitiyanan, L.; Alvarez, W. E.; Borgna, A., Effective Co-Mo bimetallic catalysts for the production of single-wall carbon nanotubes by decomposition of Co. *Abstracts of Papers of the American Chemical Society* **2000,** 219, U536-U536.

138. Resasco, D. E.; Alvarez, W. E.; Pompeo, F.; Balzano, L.; Herrera, J. E.; Kitiyanan, B.; Borgna, A., A scalable process for production of single-walled carbon nanotubes (SWNTs) by catalytic disproportionation of CO on a solid catalyst. *Journal of Nanoparticle Research* **2002,** 4, (1-2), 131-136.

139. Herrera, J. E.; Balzano, L.; Borgna, A.; Alvarez, W. E.; Resasco, D. E., Relationship between the structure/composition of Co-Mo catalysts and their ability to produce single-walled carbon nanotubes by CO disproportionation. *Journal of Catalysis* **2001,** 204, (1), 129-145.

140. Pfefferle, L.; Haller, G.; Chen, Y.; Ciuparu, D.; Lim, S.; Yang, Y. H., Mechanism study on cobalt cluster size control in Co-MCM-41 during single wall carbon nanotubes synthesis by Co disproportionation. *Abstracts of Papers of the American Chemical Society* **2005,** 229, U910-U910.

141. Lim, S.; Ciuparu, D.; Pak, C.; Dobek, F.; Chen, Y.; Harding, D.; Pfefferle, L.; Haller, G., Synthesis and characterization of highly ordered Co-MCM-41 for production of aligned single walled carbon nanotubes (SWNT). *Journal of Physical Chemistry B* **2003,** 107, (40), 11048-11056.

142. Huang, S. M.; Fu, Q.; An, L.; Liu, J., Growth of aligned SWNT arrays from water-soluble molecular clusters for nanotube device fabrication. *Physical Chemistry Chemical Physics* **2004,** 6, (6), 1077-1079.

143. Huang, S. M.; Maynor, B.; Cai, X. Y.; Liu, J., Ultralong, well-aligned single-walled carbon nanotube architectures on surfaces. *Advanced Materials* **2003,** 15, (19), 1651-+.

144. Huang, S. M.; Woodson, M.; Smalley, R.; Liu, J., Growth mechanism of oriented long single walled carbon nanotubes using "fast-heating" chemical vapor deposition process. *Nano Letters* **2004,** 4, (6), 1025-1028.

145. Hu, M. H.; Murakami, Y.; Ogura, M.; Maruyama, S.; Okubo, T., Morphology and chemical state of Co-Mo catalysts for growth of single-walled carbon nanotubes vertically aligned on quartz substrates. *Journal of Catalysis* **2004,** 225, (1), 230-239.

146. Maruyama, S.; Einarsson, E.; Murakami, Y.; Edamura, T., Growth process of vertically aligned single-walled carbon nanotubes. *Chemical Physics Letters* **2005,** 403, (4-6), 320-323.

147. Zhang, L.; Tan, Y. Q.; Resasco, D. E., Controlling the growth of vertically oriented single-walled carbon nanotubes by varying the density of Co-Mo catalyst particles. *Chemical Physics Letters* **2006,** 422, (1-3), 198-203.

148. Maschmann, M. R.; Amama, P. B.; Goyal, A.; Iqbal, Z.; Fisher, T. S., Freestanding vertically oriented single-walled carbon nanotubes synthesized using microwave plasma-enhanced CVD. *Carbon* **2006,** 44, (13), 2758-2763.

CHAPTER 2

CONTROLLED SYNTHESIS OF SWNT-POROUS DIELECTRIC COMPOSITES AND THEIR FIELD EMISSION PROPERTIES

2.1 INTRODUCTION

During the last few years, single-walled carbon nanotubes have generated much interest due to their unique structure and properties. It is widely accepted that one of their potential applications might be in field emission devices [1-11]. Among the numerous studies dedicated to nanotube field emitters, great attention has been paid to optimizing the techniques for practical and reliable device fabrication [8, 10-18]. In more fundamental studies, the mechanisms of field-induced electron emission, as well as the relationship between the nanotube structural parameters and emission properties have been the focus of many publications [1, 16, 19-22]. What makes SWNTs good candidates for field emitters is the combination of their natural geometry, chemical stability, and electrical characteristics. They could be used as electron source in a whole range of devices, including flat panel displays,[2, 17, 23-30] light elements,[31-37] e-beam sources for lithography,[38-41] etc. Among these applications, field-emission displays (FEDs) have attracted significant attention as they could become one of the first commercial products using nanotubes. In 1999, Choi et al.[42] built the first SWNT-based FED at Samsung. Carbon nanotube-based FEDs are

characterized by superior display performances such as fast response time, wide viewing angles, wide operation temperatures, cathode ray tube (CRT) like colors, ultra-slim features, low-cost and low-power consumption. FED technology is one of the most promising approaches for direct view displays larger than 60" diagonal [43]. Research efforts are currently devoted to the in-situ growth of vertically aligned nanotubes over a large area of glass substrates at low temperatures. However, while MWNTs can be produced at relatively low temperatures, high synthesis temperatures are required to produce Single-Walled Carbon nanotubes. In this second case, the use of nanotubes produced separately and later deposited on the cathode by techniques such as the screen-printing method might be required.

We have conducted a comparative study of the field emission characteristics of CoMoCAT^{TM} SWNTs still embedded in the silica-supported catalyst used in their synthesis. Researchers at Applied Nanotech Inc have recently shown that deposition of a mixture of nanotubes and dielectric nanoparticles leads to much improved emission characteristics [44]. This development makes a perfect combination with the high quality single-walled carbon nanotubes (SWNTs) produced by the CoMoCAT^{TM} catalytic method that we have developed [45-52]. The CoMoCAT^{TM} product is particularly suitable for this application because it may be used in its as-prepared form, without elimination of the catalyst, given that its main component is silica (SiO_2), in the form of dielectric submicron particles.

In the as-produced CoMoCAT$^®$ product, SWNTs with controlled diameter distribution remain well dispersed and imbedded in the silica support in the form of bundles of different sizes, which can in turn be controlled by adjusting the synthesis parameters .   Such a direct comparison of the FE characteristics of nanotubes with controlled structure and morphology has not been previously done. It is important to compare these values with available theoretical predictions [22, 53-56].

2.2 TAILORING (n,m) STRUCTURE OF SWNT BY

REACTION TEMPERATURE

2.2.1 RESEARCH OBJECTIVES

As mentioned in chapter 1, one of the most attractive features of SWNT is that their electronic properties strongly depend on their diameter and orientation of the carbon hexagons that form their walls. These characteristics are uniquely specified by the chiral vector identified with the integers (n,m), but most synthesis methods result in a wide distribution of (n,m) species. Selective growth of SWNT has several meanings. In the first place, SWNT selectivity can imply the fraction of carbon in the sample forming SWNT as opposed to other forms of carbon. The second type of selectivity is regarding nanotube length, which, as recently shown, can only be controlled in some specific cases. The third and more challenging type of selectivity is what can be called (n,m) selectivity, that is, the controlled production of specific (n,m) structures in much higher proportion than other structures. The first type of selectivity is certainly highly desirable and determines the quality of SWNT. After years of effort, many groups are able now to produce samples of high SWNT selectivity, admittedly in small quantities. More recently, researchers have started to focus on the other two types of selectivity, which may have a great impact in the development of applications. Therefore, one of the objectives of this project is to

develop method leading to precise control of (n,m) structures of SWTNs and their corresponding electronic properties.

2.2.2 EXPERIMENTAL SETUP

2.2.2.1 Synthesis of SWNT

The SWNT used in this study were synthesized by the CoMoCAT [TM] method, described in previous publications [45, 46, 51, 52, 57]. Briefly, the silica-supported Co-Mo catalyst used in this method was prepared using cobalt nitrate and ammonium heptamolybdate as precursors in an aqueous impregnation method. The total metal loading was 2 wt % with a Co/Mo molar ratio of 1/3. Prior to the production of SWNT by the CO disproportionation reaction, the catalyst was heated in H_2 flow to 500°C, and then in He flow to the selected reaction temperature. CO disproportionation was carried out in a fluidized bed reactor in flow of pure CO at a total pressure of 80 Psi and three different temperatures, 750°C, 850°C, and 950°C. The as-produced (raw) nanotube/silica composites are denoted NTR750, NTR850, and NTR950, respectively. Due to the different synthesis temperatures, the surface area of the supported catalyst varies significantly. In order to determine the final surface area, without counting the surface area of the nanotubes, samples of the fresh catalysts were heated in He at the three different reaction temperatures. The

resulting surface areas determined by BET were 98.2 m^2/g at 750°C, 75.8 m^2/g at 850°C, and 29.3 m^2/g at 950°C.

Purified nanotube samples (NTP) from the different as-produced materials were also prepared. To produce these samples, the SWNT/silica composites were attacked with HF solution (49 % HF) as described elsewhere [58]. This purification method results in the complete elimination of the silica support and most of the metal (i.e. residual metal about 2 wt %).

2.2.2.2 *Identification of SWNT Molecular Structure*

The as-produced NTR powder samples were characterized by Raman spectroscopy, optical absorption, and electron microscopy. The Raman spectra were obtained in a Jovin Yvon-Horiba Lab Ram equipped with a charge coupled detector and with He-Ne laser (632 nm) as excitation source.

The nanotubes employed in this study were further characterized by optical absorption measurements in the wavelength range 400-1400 nm. Since this particular characterization must be conducted in liquid suspension, the NTP samples suspended in NaDDBS were used for this purpose. As we have previously shown [58], NaDDBS is an effective surfactant to suspend CoMoCAT® nanotubes. The resulting solution was ultrasonicated for 2 hr and centrifuged at 15,000 rpm for 1.5 hr. Then,

the supernatant fraction was diluted in DI water and characterized by Vis-NIR spectroscopy. The approximate concentrations of SWNT and surfactant in these suspensions were 0.15mg/mL and 3mg/mL, respectively.

2.2.3 RESULTS AND DISCUSSION

Raman spectroscopy is a widely-used technique for characterizing SWNT samples and gaining information about their structure. Figure 1 presents the typical Raman spectra of the as-produced NTR material produced by the CoMoCAT[TM] method at 750°C, 850°C, and 950°C.

The band appearing at about 1580 cm^{-1} (G band) results from the in-plane stretching mode of ordered crystalline graphite-like structures, while the band appearing at around 1340 cm^{-1} (D band) represents disordered carbon structure.[38-41, 59, 60] Consequently, the quality parameter that we have previously defined (1-D/G) can be used as an approximate measure of the nanotube quality. In all the samples used in this study, the observed quality parameter was close to 1, which indicates that concentration of carbonaceous impurities and/or imperfections in carbon
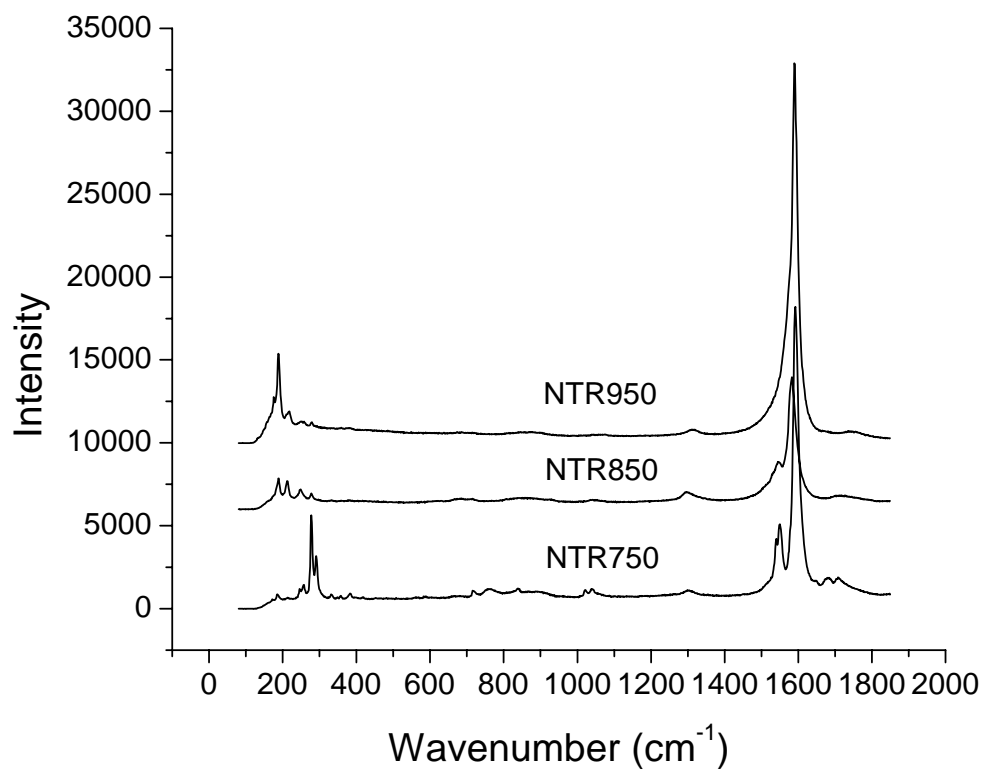
Figure 2.1: *Raman spectra of as-produced SWNT/silica composites synthesized at 750°C, 850°C, and 950°C. The wavelength of excitation laser is 633nm.*

nanotubes was low in all samples. The series of bands in the range 150-400 cm^{-1} are associated with the radial breathing mode (RBM) and are characteristic of single-walled carbon nanotubes. As shown in Fig. 2.1, the position of the intense RBM bands observed for NTR750, NTR850 and NTR950 samples vary with reaction temperature. As the temperature increases, the RBM bands shift to lower wavenumbers. As previously described [57], this systematic shift is consistent with an increase in nanotube diameter as the synthesis temperature increases, since the frequency of the RBM is inversely proportional to the nanotube diameter.[61-63]

Assignment of RBM bands to specific nanotube structures is not straightforward and diameter populations obtained from RBM are not reliable unless a very detailed study is attempted. The dramatic effect of resonance phenomena, complicated by thermal effects[60, 64] and the effect of nanotube aggregation can greatly alter the relative intensities of RBM bands [65]. Therefore, Raman results need to be complemented with an independent technique. Optical absorption is a very powerful technique that can be more quantitative than Raman in the assessment of nanotube populations. It is well known that the quasi-one-dimensionality of SWNT gives origin to sharp van Hove singularities in the density of electronic states. As a result, the optical properties of SWNT are dominated by transitions between van Hove singularities on opposite sides of the Fermi level. Kataura [66] used the tight binding model to calculate energy transitions E_{ii} and generated the well-known

Kataura plot of E_{ii} versus nanotube diameter, which is a function of the structural parameter (n,m). More recently, Weisman and Bachilo [67-70] have modified the Kataura plot on the basis of the photoluminescence method that they developed. This remarkable tool is particularly appropriate to characterize semiconducting nanotubes in the diameter range of those synthesized by our CoMoCAT® method as recently shown [45].

In this case, we have used optical absorption in the 400~1400 nm range. The absorption spectra for the different nanotubes extracted from the NTR750, NTR850 and NTR950 by suspending them in NaDDBS surfactant are shown in Figure 2.2. Only a few sharp absorption peaks with a low background were obtained in the entire Vis-NIR spectrum, in good agreement with previous PL results that evidenced the presence of few nanotube types, with similar diameter and chirality. With such a small number of nanotube types present in the sample, a detailed analysis and (n,m) assignment of the SWNT present in the sample is possible. By matching the corresponding E_{11} and E_{22} of the Weisman plot with the peak lines in the spectrum, it can be seen that a few semiconducting SWNT dominate each of the NTR samples. Using a UV-Vis spectrophotometer, it was observed that the bands corresponding to metallic SWNT are much weaker than those of the semiconducting nanotubes. However, since relative extinction coefficients of metallic and semiconducting nanotubes are not available it is not possible to obtain from the spectra the
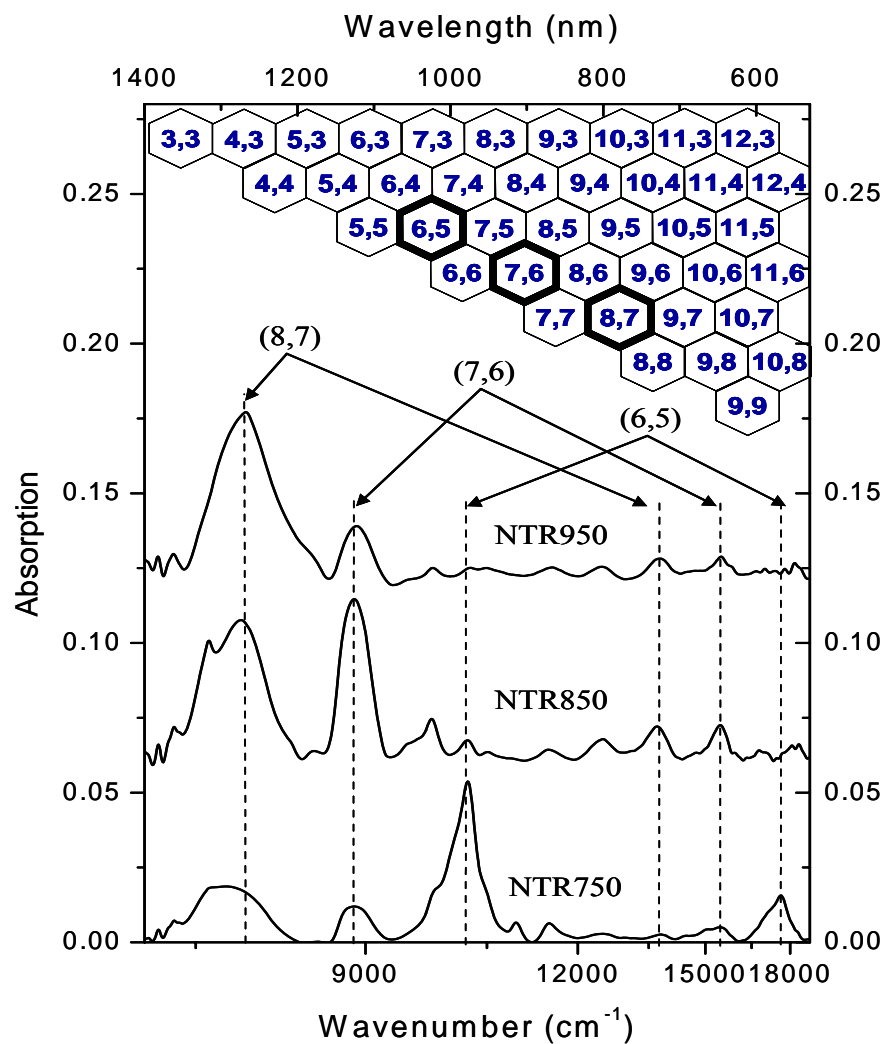
Figure 2.2: *Optical absorption in visible-near IR range for SWNT synthesized at different temperatures. Pure nanotubes suspended in NaDDBS solution (SWNT concentration 0.15mg/mL, surfactant concentration 3mg/mL). The most abundant species in samples produced at three temperatures are also located in the SWNT map at the top.*

metallic/semiconducting population ratio. Within the semiconducting nanotubes in the sample, the (6,5) type is the major constituent of NTR750 sample, while (7,6) dominates in NTR850 and (8,7) in NTR950. This trend is in agreement with the Raman results and previously reported TEM results that indicate that higher synthesis temperatures lead to SWNT of larger diameter [57]. What is now more remarkable is that we can precisely identify the (n,m) types that dominate the nanotube population on the different samples.

The detailed analysis of the optical absorption spectra has allowed us to identify the (n,m) identity of the most abundant nanotube components in each of the as-produced SWNT samples, e.g., the most abundant semiconducting species in NTR750 is the (6,5) nanotube. As we have previously discussed in other contributions [71], the increase in nanotube diameter with synthesis temperature can be explained by a faster growth of the cobalt clusters during the carbon nucleation period. That is, at higher temperatures, by the time carbon has nucleated to form the nanotube cap that determines the nanotube size, the Co cluster responsible for the growth of the nanotube has grown larger. At lower temperatures, the nucleation and cap formation occurs over Co clusters of smaller size.

2.2.4 CONCLUSION TO TAILORING (n,m) STRUCTURE

By using the highly selective CoMoCAT® catalytic method, SWNTs have been synthesized with controlled (n,m) structure on high surface area silica, as characterized by Raman spectroscopy, optical absorption, SEM and TEM. The Vis-NIR optical absorption spectra were used to assign the (n,m) identification parameters to the most abundant nanotubes present on samples synthesized at various temperatures ranging from 750°C to 950°C. (6,5), (7,6), and (8,7) have been found to be the dominant component of semiconducting nanotubes produced respectively at 750°C, $850 \ ^{o}$C, and 950°C. The increase in nanotube diameter with synthesis temperature can be explained by a faster growth of the cobalt clusters during the carbon nucleation period.

2.3 TAILORING AGGREGATION OF SWNT BY REACTION TERPERATURE

2.3.1 RESEARCH OBJECTIVES

In addition to (n,m) selectivity, bundling of SWNT has long been a puzzling question for carbon nanotube researchers. Bundling of SWNT greatly affect the dispersion, modification and applications of SWNT. However, it is under debate how the bundle is formed and how to control the aggregation of SWNT to form bundles, as well as effect of morphology of SWNT bundles on their properties. To answer these questions, we need to first find a way to control the aggregation of SWNTs.

2.3.2 EXPERIMENTAL SETUP

The SWNT used in this study were synthesized by the CoMoCAT ^{TM} method as described in section 2.2.2.1. The morphology of the composites was examined by electron microscopy (SEM and TEM). SEM images were obtained in a JEOL JSM-880 high resolution scanning electron microscope while the TEM pictures were obtained in a JEOL JEM-2000FX transmission electron microscope. For this analysis, each NTR sample was dispersed in isopropanol by ultrasonicating for 10 minutes. A few drops of the suspension were deposited on the TEM grid, then dried, and evacuated before analysis.

2.3.3 RESULTS AND DISCUSSION

SEM and TEM were utilized to directly observe the morphology of the different SWNT samples. Figure 2.3 shows SEM pictures for the three as-produced samples, NTR750, NTR850, and NTR950. Bundles of SWNT are clearly seen meshing with the silica support particles in the three different samples. An interesting conclusion can be derived from the analysis of these images. It is consistently seen that the diameter of the nanotube bundles decreases as the reaction temperature increases. That is, the trend is the opposite to that observed regarding the diameter of each individual SWNT, which as shown above, increases with temperature. The estimated bundle size varies from 20 nm at 750 ^{o}C to 10 nm at 850 ^{o}C, and 5 nm at 950 ^{o}C. Evidently, when the reaction temperature increases to 950 ^{o}C not only the nanotubes, but also the silica support, exhibit a significant morphological change due to a severe thermal sintering. In order to determine whether the support sintering rather than the reaction temperature itself causes the decrease in bundle size we conducted the following experiment. Before the nanotube growth step, the catalyst was preheated in He for 10 min at 950 ^{o}C, then it was cooled down to 750 ^{o}C, at which temperature the nanotube growth was conducted. As shown in Fig. 2.3c, despite the pre-treatment at 950 ^{o}C that caused the silica sintering, the bundle size resulting from the growth at 750 ^{o}C was essentially the same as that obtained at 750 ^{o}C, without previous heating.
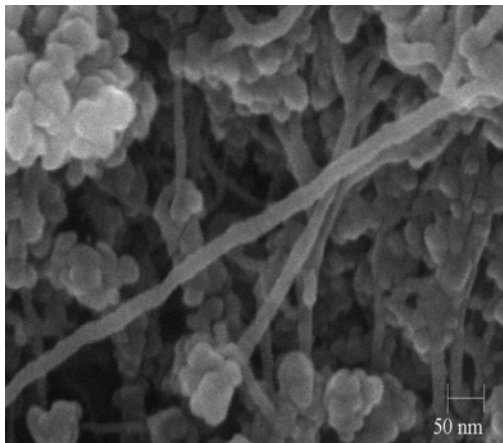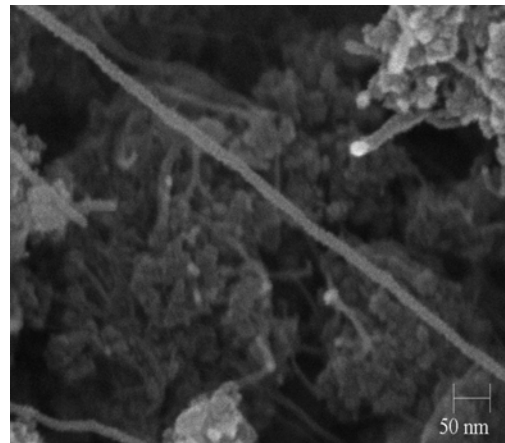
a) NTR750 b) NTR850
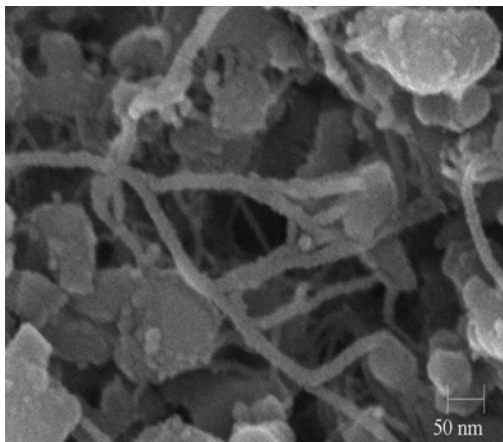
c) NTR750 preheat @950 d) NTR950
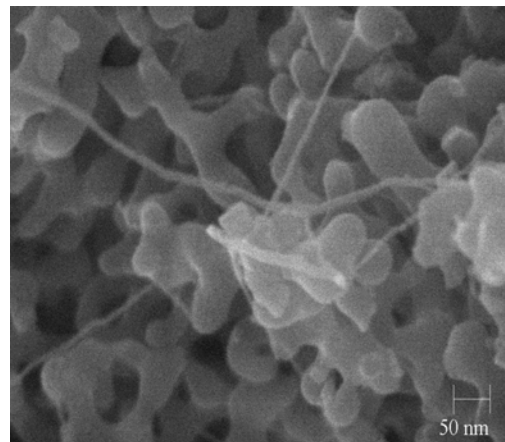
Figure 2.3: SEM images of SWNT/silica composites synthesized at different temperatures. a) Composites produced at $750^{o}C$, b) composites produced at $850^{o}C$, c) composites produced at $750^{o}C$ after preheating at $950^{o}C$, d) composites produced at $950^{o}C$.
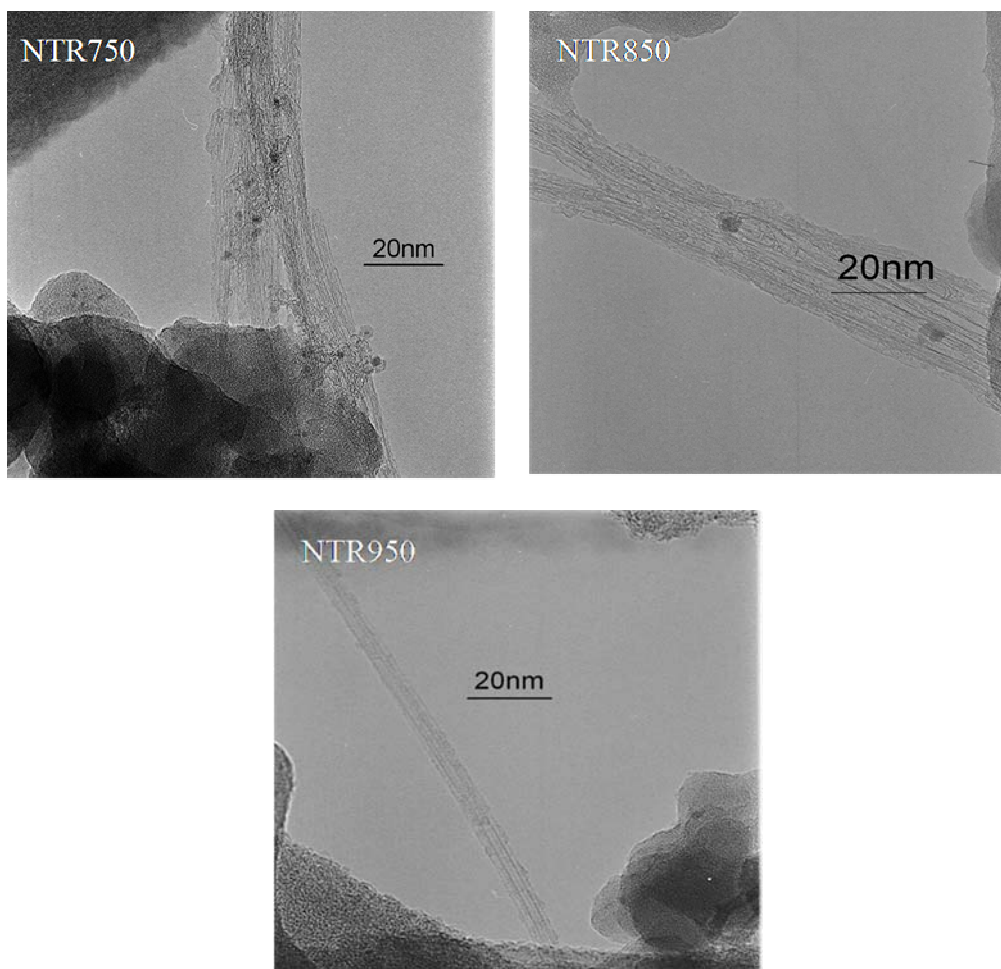
Figure 2.4: *TEM images of SWNT/silica composites at different temperatures. a) Composites produced at 750°C, b) composites produced at 850°C, c) composites produced at 950°C.*

Therefore, it seems that the reaction temperature determines both SWNT diameter and bundle size. The TEM images shown in Fig. 2.4 illustrate the morphology of the typical bundles present in each of the three samples.

By contrast, the tendency to form smaller bundles at higher temperature is harder to explain. Three factors may contribute to this phenomena: 1) thermal effect on the nature of nanotube-nanotube interaction during the bundle formation; 2) morphological change and phase separation of CoMoC at higher temperature: 3) variations in pore structure of the catalyst during the heating. A simple experiment that we conducted to investigate the effect of the support structure on the formation of bundle seems to indicate that this effect is not the most critical. Heating at 950°C causes a significant drop in surface area and pore volume since the high temperature pretreatment causes an irreversible sintering on the silica pore structure. However, when the catalyst was heated to 950°C for 10 minutes and then cooled down to 750 $^{\circ}$C for the SWNT growth, the resulting bundle size was the same as that obtained without the pre-heating step. One can expect that the changes in morphology and aggregation state that can be reproducibly obtained by our catalytic method should have an impact on the work function and other electrical characteristics that determine the field emission properties of composites.

2.3.4 *CONCLUSION TO CONTROLLING AGGREGATION OF SWNT*

As apposed to the increasing trend of diameter of SWNTs with temperature, the aggregation of SWNTs appeared to decrease with temperature due to thermal effect or stronger aggregation tendency of smaller tubes. The average size of SWNT bundle produced at 750$^{\text{o}}$C, 850$^{\text{o}}$C, and 950$^{\text{o}}$C has been found to be 20nm, 16nm, and 5nm respectively. The aggregation of SWNTs is probably affected by thermal effect or larger aggregation tendency of smaller tubes.

2.4 FIELD EMISSION FROM SWNT-POROUS DIELECTRIC COMPOSITES

2.4.1 *RESEARCH OBJECTIVES*

SWNTs are perfect for field emitters due to the combination of their natural geometry, chemical stability, and electrical characteristics. Researchers at Applied Nanotech Inc have recently shown that deposition of a mixture of nanotubes and dielectric nanoparticles leads to much improved emission characteristics. In the as-produced CoMoCAT® product, SWNTs with controlled diameter distribution remain well dispersed and imbedded in the silica support in the form of bundles of different sizes, which can in turn be controlled by adjusting the synthesis parameters. However a direct comparison of the FE characteristics of nanotubes with controlled structure and morphology has not been previously done. Therefore, in this project, we attempt to develop method to prepare SWNT/silica based electrode for field emission and to investigate the relations of structure of SWNT/silica composites to their field emission properties. Fitting experimental data with field emission simulation is also desired to understand better the field emission mechanism of SWNT.

2.4.2 EXPERIMENTAL SETUP

The field emission measurements were conducted in a simple diode setup, placed in a vacuum chamber with $10^{-6} \sim 10^{-7}$ Torr base pressure. The cathode and anode in the diode were separated by a ceramic spacer of well-controlled thickness (250 μm). For each measurement with the as-produced (NTR) material, the sample was ground to a very fine powder and mixed with a conducting Ag-based fluro-elastomer binder in order to form the emitting film. The film was attached to the stainless steel cathode by a double-faced copper tape.

For the measurement of the purified sample (NTP), the SWNTs were suspended in the NaDDBS solution by ultrasonicating for 10 minutes. The SWNT to surfactant weight ratio was kept at 1:2. The NaDDBS-based NTP suspension was then pressure-filtrated through a 0.5 μm stainless steel frit. The SWNT-coated frit was attached to the cathode with a double faced copper tape.

The I-V curves were recorded using a Keithley 2410 sourcemeter. To investigate the field emission process, a sequential sweeping method was employed. In this method, the voltage is increased in a sequence of 6 different ranges: 1-100 V, 1-300 V, 1-500 V, 1-700 V, 1-900 V, 1-1100 V. Each sweep was run twice to determine the irreversibility of the process. As a result, the sample in the last 1-1100 V cycle has been ramped twelve times.

2.4.3 RESULTS AND DISCUSSION

Most previous field emission studies involving SWNT have employed purified nanotubes. By contrast, the as-produced SWNT material used in this study contains the porous silica support and the catalytic metals. The practical importance of this study arises from the possibility of using the as-produced material, thus avoiding the purification step. In this way, not only the cost of the material would be reduced, but the potential damage of the nanotubes by the acid treatment is prevented. Figure 2.5 compares the field emission characteristics of the as-produced SWNT/silica composite (NTR750) with that of purified SWNT (denoted NTP). The SWNT content in the films is around 0.0003 mg/mm^3 and 0.011mg/mm^3, respectively. The two curves demonstrate the NTR has comparable electron emission characteristics as the NTP with a much lower SWNT density. One reason for the higher effective utilization of the nanotubes in the NTR samples could be the reduced shielding [21]due to the presence of the dielectric silica particles intermixed with the nanotubes, as opposed to the densely entangled SWNT that are present in the purified film.
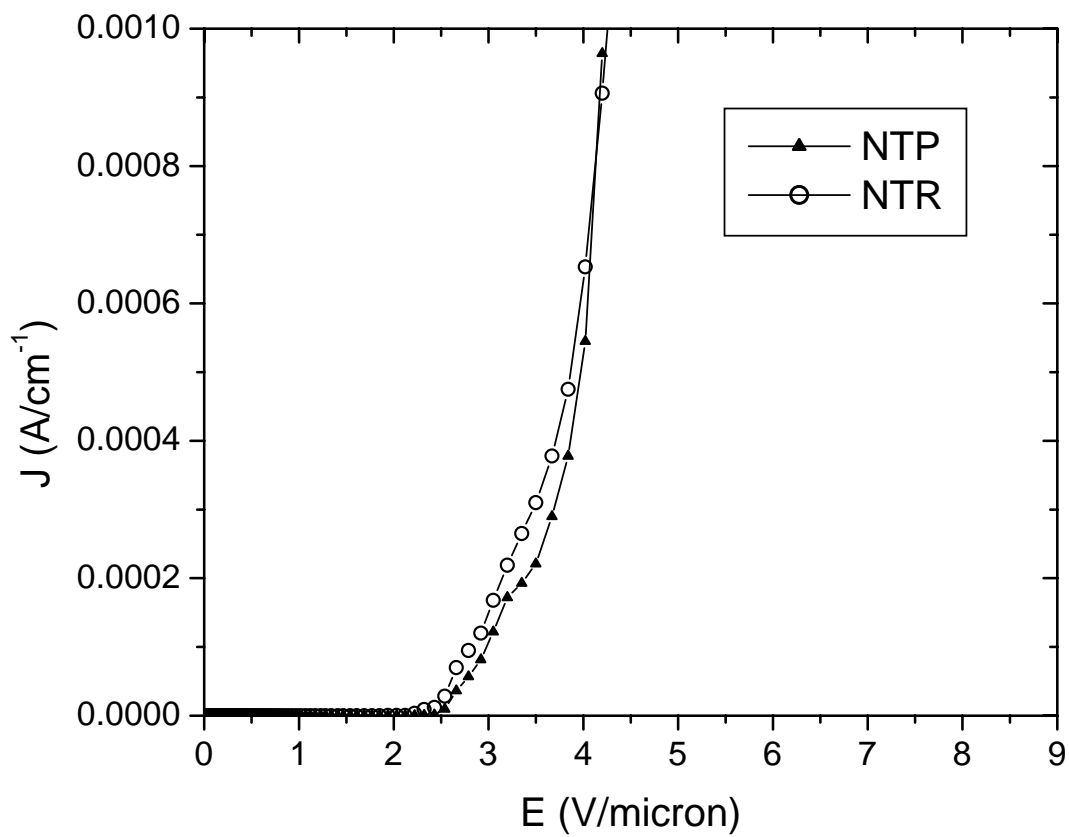
Figure 2.5: *Emission current as a function of field from purified SWNT (NTP) and as-produced SWNT/silica composites (NTR)*

To investigate the field emission properties of the as-produced composites, we performed current-voltage measurements on the NTR750, NTR850, and NTR950 samples as well as on the composite synthesized at 750°C after preheating in inert gas at 950 $^{\circ}$C. Figure 2.6 compares the electron emission characteristics of the composites synthesized at different temperatures. A trend in extraction field with nanotube synthesis temperature is observed. NTR950, with the smallest bundle size but largest nanotube diameter has the lowest extraction field, 0.6 V/μm. This sample reaches the target of 1 mA/cm^2 at a field of 1.8 V/μm, showing the best emission performance among the three samples. While the other two samples, NTR850 and NTR750 also show very good field emission properties, the extraction fields for them was 1.6 and 2.2 V/μm, respectively, in a clear trend with the synthesis temperature; the field needed for generating the current density of 1 mA/cm^2 was 3.4 and 4.3 V/μm, respectively. In separate measurements the maximum current density achieved with each sample was determined. In this case, it was observed that the maximum current density decreased with synthesis temperature; that is, the maximum values for NTR750, NTR850 and NTR950 were 13.7, 12.1 and 3.44 mA/cm^2, respectively. Thus, it appears that while increasing the synthesis temperature, there is an improvement in extraction field, the maximum current density deteriorates. An intermediate temperature might be the optimal solution.
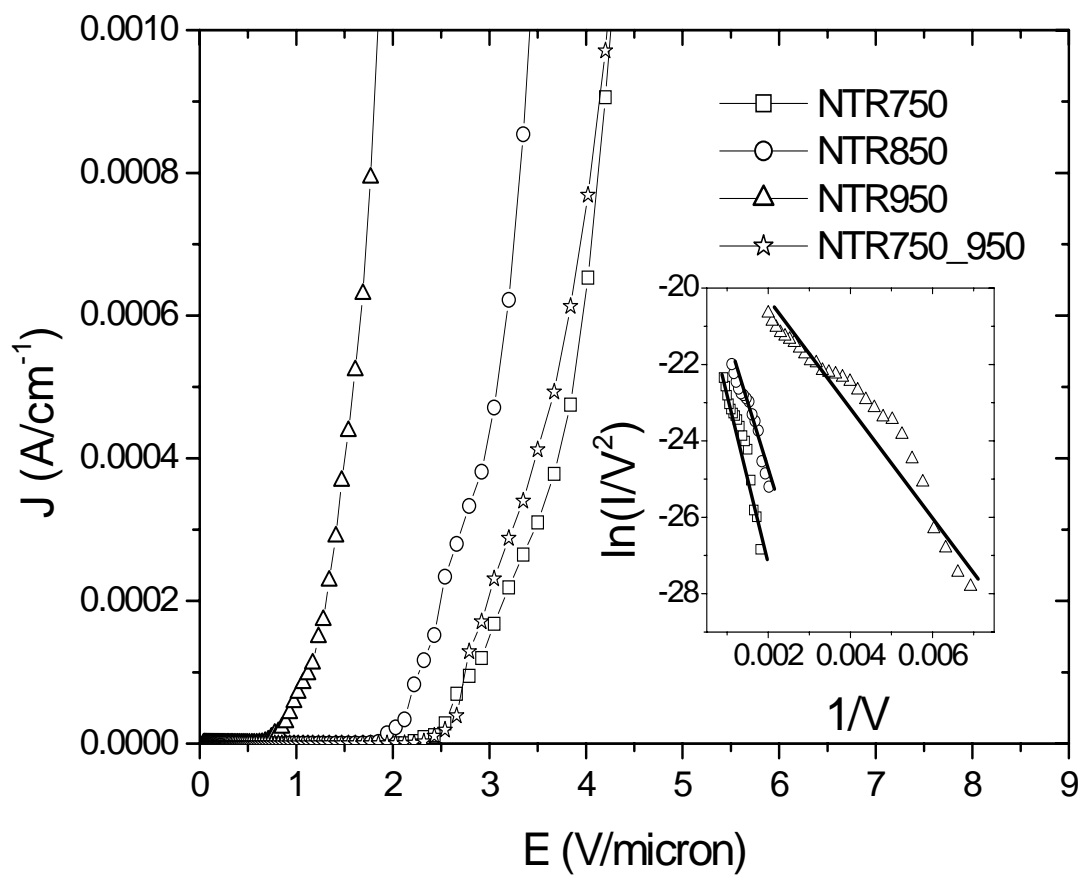
Figure 2.6: Emission current as a function of field from SWNT/silica composites (NTR) synthesized at different temperatures. Inset is the Fowler-Nordheim plot derived from field emission data of NTR750, NTR850 and NTR950.

From the well known Fowler-Nordheim theory, the emission current density J can be written and simplified as [72]:

$$J = 1.54 \times 10^{-6} \frac{E^2}{\phi} \exp\left[-6.83 \times 10^7 \frac{\phi^{1.5}}{E}\right] \tag{1}$$

where J is in A/cm^2, the electric field E is in V/μm and the work function Φ is in eV. For plotting convenience, we use I and V to replace J and E, respectively, from the relations:

$$J = \frac{I}{S} \qquad E = \beta V$$

where S is the emitting area, equal to 0.1926 cm^2 in our case, and β is the field enhancement factor that accounts for the geometry of the emitter. Different empirical formulas have been provided to calculate this factor. Here, we choose the paraboloid approximation

$$\beta = \frac{2}{r \ln(2R/r)} \tag{2}$$

where R is the distance between the emitter tip and the anode while r is the radius of curvature of the tip. By rearranging (1), we obtain

$$\ln(I/V^2) = -6.83 \times 10^7 \frac{\phi^{1.5}}{\beta} \times (1/V) + \ln(1.54 \times 10^{-6} \times S \frac{\beta^2}{\phi}) \tag{3}$$

$$= A(1/V) + B$$

Thus, the F-N plots in the inset of Figure 6 can be fitted to equation (3) to calculate the parameter β and subsequently r.

	NTR 750	NTR 850	NTR 950
Ln(I/V2)= A*(1/V) + B	A = -4449.3 B = -18.136	A = -3277.2 B = -18.28	A = -1307.2 B = -17.779
Theoretical Work Function Φ (eV)	5.24	5.16	5.10
Field Enhancement Factor β (cm^{-1})	184658	244282	601775
Size of emitter (nm)	22.3	15.8	5.6

Table 2.1: *Calculated results from the experimental field emission data for NTR750, NTR850 and NTR 950*

It is widely accepted that the work function can be obtained from I Vs. V curves only on those cases in which single emitters are being used. A more common practice has been to assume a given work function for the emitter and then calculating the parameter β. Some authors [73, 74] have used work function values typical of graphite (i.e. about 5 eV). In this case, the fitting of the data in Fig. 2.6 was conducted using the theoretical work functions of the most abundant species in

each sample; that is (6,5), (7,6), and (8,7). As shown below, the small variations in the work functions for the different nanotubes do not have a significant impact on the resulting extraction field values. Therefore, the only adjustable parameter resulting from the fitting is the field enhancement factor, from which the emitter size can be directly calculated. The resulting parameters are summarized in Table 2.1. The calculated emitter sizes for the different samples are in excellent agreement with the trend in bundle size observed experimentally by SEM. These results indicate that the geometrical factors that determine the field enhancement play a more important role in determining the extraction field in nanotube samples than differences in the work functions of the specific nanotubes present in the sample.

To further illustrate the influence of these two parameters, we have simulated I-V emission curves for several hypothetical conditions. These simulated curves are depicted in Fig. 2.7. The following cases are considered: a) emission from individual SWNT, in which the emitter size is the radius of the individual nanotube and the work function is the theoretical value [75] for each nanotube, i.e. 5.24, 5.16, and 5.10 eV for the (6,5), (7,6), and (8,7) nanotubes, respectively; b) the work functions are
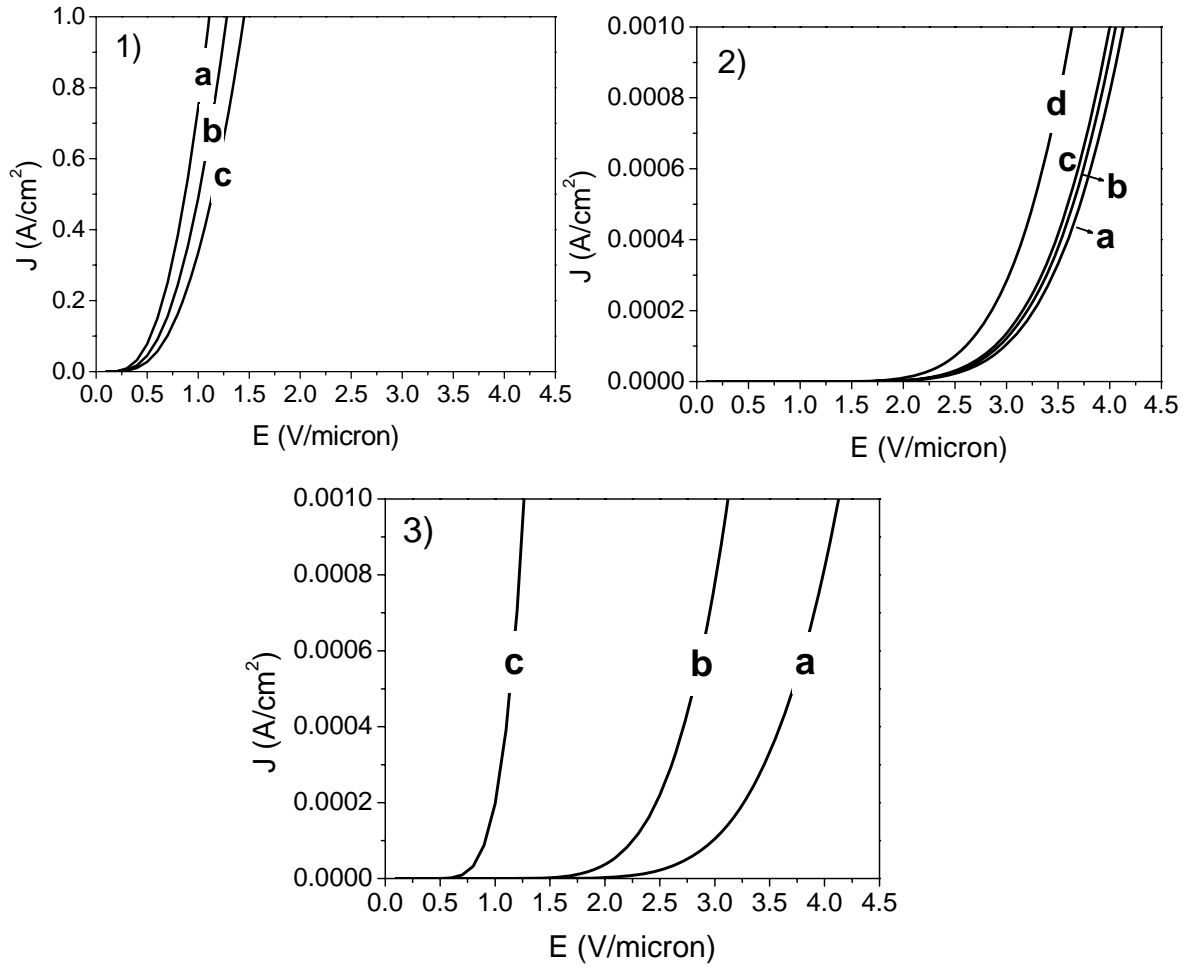
Figure 2.7: *Simulated field emission with different assumptions. 1) the emitter size is the radius of the individual nanotube and the work function is the theoretical value for each nanotube, i.e. a) 5.24 eV for (6,5), b) 5.16 eV for (7,6), and c) 5.10 eV for (8,7); 2) the work functions are those characteristic of the a) (6,5), b) (7,6), c) (8,7), and d) (6,6) nanotubes, emitter size is constantly 20 nm for bundles composed of each type of tubes; 3) the emitters are a) 20nm bundle of (6,5), b) 15 nm bundle of (7,6) and c) 5 nm bundle of (8,7).*

92

those characteristic of the (6,5), (7,6), (8,7), and (6,6) nanotubes, respectively; the emitter size is considered fixed at 20 nm, representing bundles of the same size; c) the work functions are those characteristic of the (6,5), (7,6), and (8,7) nanotubes, respectively; the emitter sizes are those observed in SEM and TEM pictures, i.e. 20nm, 15nm and 5nm. It should be mentioned that even for metallic tube (6,6), which has similar diameter as semiconducting tubes (6,5), (7,6), and (8,7), but has lower work function of 4.7 eV, the field emission enhancement is really small compared to the one caused by difference in bundle size. Hence, it can be inferred that the greatest variation of field emission properties arise from differences in emitter size, rather than differences in work function

2.4.4 CONCLUSION TO FIELD EMISSION FROM SWNT/SILICA

The synthesis reaction temperature was found to affect the nanotube diameter and bundle size in opposite directions, that is, as the synthesis temperature increased the nanotube average diameter was larger, but the bundle size smaller. A gradual and consistent reduction in the emission onset field was observed as the synthesis temperature was increased. Experiments and simulation demonstrate the bundle size, rather than the nanotube diameter or differences in work function are more important in determining the field emission properties of SWNT/silica composites.

2.5 REFERENCES

1. Wang, Q. H.; Corrigan, T. D.; Dai, J. Y.; Chang, R. P. H.; Krauss, A. R., Field emission from nanotube bundle emitters at low fields. *Applied Physics Letters* **1997,** 70, (24), 3308-3310.

2. Deheer, W. A.; Chatelain, A.; Ugarte, D., A Carbon Nanotube Field-Emission Electron Source. *Science* **1995,** 270, (5239), 1179-1180.

3. Rinzler, A. G.; Hafner, J. H.; Nikolaev, P.; Lou, L.; Kim, S. G.; Tomanek, D.; Nordlander, P.; Colbert, D. T.; Smalley, R. E., Unraveling Nanotubes - Field-Emission from an Atomic Wire. *Science* **1995,** 269, (5230), 1550-1553.

4. Collins, P. G.; Zettl, A., A simple and robust electron beam source from carbon nanotubes. *Applied Physics Letters* **1996,** 69, (13), 1969-1971.

5. Rupesinghe, N. L.; Chhowalla, M.; Teo, K. B. K.; Amaratunga, G. A. J., Field emission vacuum power switch using vertically aligned carbon nanotubes. *Journal of Vacuum Science & Technology B* **2003,** 21, (1), 338-343.

6. deHeer, W. A.; Bonard, J. M.; Fauth, K.; Chatelain, A.; Forro, L.; Ugarte, D., Electron field emitters based on carbon nanotube films. *Advanced Materials* **1997,** 9, (1), 87-&.

7. Saito, Y.; Hamaguchi, K.; Nishino, T.; Hata, K.; Tohji, K.; Kasuya, A.; Nishina, Y., Field emission patterns from single-walled carbon nanotubes. *Japanese Journal of Applied Physics Part 2-Letters* **1997,** 36, (10A), L1340-L1342.

8. Bonard, J. M.; Maier, F.; Stockli, T.; Chatelain, A.; de Heer, W. A.; Salvetat, J. P.; Forro, L., Field emission properties of multiwalled carbon nanotubes. *Ultramicroscopy* **1998,** 73, (1-4), 7-15.

9. Dean, K. A.; Chalamala, B. R., Field emission microscopy of carbon nanotube caps. *Journal of Applied Physics* **1999,** 85, (7), 3832-3836.

10. Bonard, J. M.; Kind, H.; Stockli, T.; Nilsson, L. A., Field emission from carbon nanotubes: the first five years. *Solid-State Electronics* **2001,** 45, (6), 893-914.

11. Yuan, Z. H.; Huang, H.; Dang, H. Y.; Cao, J. E.; Hu, B. H.; Fan, S. S., Field emission property of highly ordered monodispersed carbon nanotube arrays. *Applied Physics Letters* **2001,** 78, (20), 3127-3129.

12.   Bonard, J. M.; Salvetat, J. P.; Stockli, T.; de Heer, W. A.; Forro, L.; Chatelain, A., Field emission from single-wall carbon nanotube films. *Applied Physics Letters* **1998,** 73, (7), 918-920.

13.   Bonard, J. M.; Salvetat, J. P.; Stockli, T.; Forro, L.; Chatelain, A., Field emission from carbon nanotubes: perspectives for applications and clues to the emission mechanism. *Applied Physics a-Materials Science & Processing* **1999,** 69, (3), 245-254.

14.   Bonard, J. M.; Gaal, R.; Garaj, S.; Thien-Nga, L.; Forro, L.; Takahashi, K.; Kokai, F.; Yudasaka, M.; Iijima, S., Field emission properties of carbon nanohorn films. *Journal of Applied Physics* **2002,** 91, (12), 10107-10109.

15.   Zhou, G.; Duan, W. H.; Gu, B. L., Electronic structure and field-emission characteristics of open-ended single-walled carbon nanotubes. *Physical Review Letters* **2001,** 8709, (9), art. no.-095504.

16.   Jo, S. H.; Tu, Y.; Huang, Z. P.; Carnahan, D. L.; Wang, D. Z.; Ren, Z. F., Effect of length and spacing of vertically aligned carbon nanotubes on field emission properties. *Applied Physics Letters* **2003,** 82, (20), 3520-3522.

17.   Umnov, A. G.; Matshushita, T.; Endo, M.; Takeuchi, Y., Field emission from flexible arrays of carbon nanotubes. *Chemical Physics Letters* **2002,** 356, (3-4), 391-397.

18.   Jo, S. H.; Banerjee, D.; Ren, Z. F., Field emission of zinc oxide nanowires grown on carbon cloth. *Applied Physics Letters* **2004,** 85, (8), 1407-1409.

19.   Zhou, G.; Duan, W. H.; Gu, B. L., Dimensional effects on field emission properties of the body for single-walled carbon nanotube. *Applied Physics Letters* **2001,** 79, (6), 836-838.

20.   Bonard, J. M.; Croci, M.; Klinke, C.; Kurt, R.; Noury, O.; Weiss, N., Carbon nanotube films as electron field emitters. *Carbon* **2002,** 40, (10), 1715-1728.

21.   Feng, Y. T.; Deng, S. Z.; Chen, J.; Xu, N. S., Effect of carbon nanotube structural parameters on field emission properties. *Ultramicroscopy* **2003,** 95, (1-4), 93-97.

22.   Liang, S. D.; Xu, N. S., Chirality effect of single-wall carbon nanotubes on field emission. *Applied Physics Letters* **2003,** 83, (6), 1213-1215.

23.   Sarangi, D.; Arfaoui, I.; Bonard, J. M., Carbon nanotube growth on borosilicate glass for flat panel displays. *Physica B-Condensed Matter* **2002,** 323, (1-4), 165-167.

24. Maschmann, M. R.; Amama, P. B.; Goyal, A.; Iqbal, Z.; Fisher, T. S., Freestanding vertically oriented single-walled carbon nanotubes synthesized using microwave plasma-enhanced CVD. *Carbon* **2006,** 44, (13), 2758-2763.

25. Jung, H. Y.; Jung, S. M.; Gu, G. H.; Suh, J. S., Anodic aluminum oxide membrane bonded on a silicon wafer for carbon nanotube field emitter arrays. *Applied Physics Letters* **2006,** 89, (1), -.

26. Cao, A.; Zhang, X.; Xu, C.; Liang, J.; Wu, D.; Wei, B., Thinning and diluting aligned carbon nanotube films for uniform field emission. *Applied Physics a-Materials Science & Processing* **2002,** 74, (3), 415-418.

27. Deng, S. Z.; Wu, Z. S.; Xu, N. S.; Chen, J., Characterization of a high voltage flat panel display unit using nanotube-based emitters. *Ultramicroscopy* **2001,** 89, (1-3), 105-109.

28. Zhu, C. C.; Liu, W. H.; Huangfu, L. J., Flat-panel structure for field-emission displays with carbon nanotube cathode. *Journal of Vacuum Science & Technology B* **2001,** 19, (5), 1691-1693.

29. Xu, N. S.; Wu, Z. S.; Deng, S. Z.; Chen, J., High-voltage triode flat-panel display using field-emission nanotube-based thin films. *Journal of Vacuum Science & Technology B* **2001,** 19, (4), 1370-1372.

30. Wang, Q. H.; Yan, M.; Chang, R. P. H., Flat panel display prototype using gated carbon nanotube field emitters. *Applied Physics Letters* **2001,** 78, (9), 1294-1296.

31. Aguirre, C. M.; Auvray, S.; Pigeon, S.; Izquierdo, R.; Desjardins, P.; Martel, R., Carbon nanotube sheets as electrodes in organic light-emitting diodes. *Applied Physics Letters* **2006,** 88, (18), -.

32. Qian, L.; Teng, F.; Jin, Z. S.; Zhang, Z. J.; Zhang, T.; Hou, Y. B.; Yang, S. Y.; Xu, X. R., Improved optoelectronic characteristics of light-emitting diodes by using a dehydrated nanotube titanic acid (DNTA)-polymer nanocomposite. *Journal of Physical Chemistry B* **2004,** 108, (37), 13928-13931.

33. Croci, M.; Arfaoui, I.; Stockli, T.; Chatelain, A.; Bonard, J. M., A fully sealed luminescent tube based on carbon nanotube field emission. *Microelectronics Journal* **2004,** 35, (4), 329-336.

34. Jang, Y. T.; Lee, Y. H.; Ju, B. K.; Ahn, J. H.; Go, C. K.; Park, G. S., Application of carbon nanotubes to the cathode ray tube-electron gun. *Vacuum* **2002,** 68, (1), 79-85.

35. Dai, L. M., Light-emitting polymers and carbon nanotube electron emitters for optoelectronic displays. *Smart Materials & Structures* **2002,** 11, (5), 645-651.

36. Fournet, P.; Coleman, J. N.; Lahr, B.; Drury, A.; Blau, W. J.; O'Brien, D. F.; Horhold, H. H., Enhanced brightness in organic light-emitting diodes using a carbon nanotube composite as an electron-transport layer. *Journal of Applied Physics* **2001,** 90, (2), 969-975.

37. Fournet, P.; O'Brien, D. F.; Coleman, J. N.; Horhold, H. H.; Blau, W. J., A carbon nanotube composite as an electron transport layer for M3EH-PPV based light-emitting diodes. *Synthetic Metals* **2001,** 121, (1-3), 1683-1684.

38. Hata, K.; Takakura, A.; Ohshita, A.; Saito, Y., Brightness of electron beam emitted from a single pentagon on a multiwall carbon nanotube tip. *Surface and Interface Analysis* **2004,** 36, (5-6), 506-509.

39. de Jonge, N.; Lamy, Y.; Schoots, K.; Oosterkamp, T. H., High brightness electron beam from a multi-walled carbon nanotube. *Nature* **2002,** 420, (6914), 393-395.

40. Milne, W. I.; Teo, K. B. K.; Chhowalla, M.; Amaratunga, G. A. J.; Yuan, J.; Robertson, J.; Legagneux, P.; Pirio, G.; Pribat, D.; Bouzehouane, K.; Bruenger, W.; Trautmann, C., Carbon films for use as the electron source in a parallel e-beam lithography system. *New Diamond and Frontier Carbon Technology* **2001,** 11, (4), 235-247.

41. Leopold, J. G.; Zik, O.; Cheifetz, E.; Rosenblatt, D., Carbon nanotube-based electron gun for electron microscopy. *Journal of Vacuum Science & Technology A* **2001,** 19, (4), 1790-1795.

42. Choi, W. B.; Chung, D. S.; Kang, J. H.; Kim, H. Y.; Jin, Y. W.; Han, I. T.; Lee, Y. H.; Jung, J. E.; Lee, N. S.; Park, G. S.; Kim, J. M., *Applied Physics Letters* **1999,** 75, 3129.

43. Sato, F.; Seki, M. In Proceedings of Asia Display/IDW'01, Nagoya, Japan, 2001; Nagoya, Japan, 2001; p 1153.

44.   Mao, D. S.; Fink, R. L.; Monty, G.; Thuesen, L.; Yaniv, Z. In Proceedings of 9th International Display Workshops/IDW'02, Hiroshima, Japan, 2002; Hiroshima, Japan, 2002; p 1415.

45.   Bachilo, S. M.; Balzano, L.; Herrera, J. E.; Pompeo, F.; Resasco, D. E.; Weisman, R. B., Narrow (n,m)-distribution of single-walled carbon nanotubes grown using a solid supported catalyst. *Journal of the American Chemical Society* **2003,** 125, (37), 11186-11187.

46.   Resasco, D. E.; Alvarez, W. E.; Pompeo, F.; Balzano, L.; Herrera, J. E.; Kitiyanan, B.; Borgna, A., A scalable process for production of single-walled carbon nanotubes (SWNTs) by catalytic disproportionation of CO on a solid catalyst. *Journal of Nanoparticle Research* **2002,** 4, (1-2), 131-136.

47.   Alvarez, W. E.; Pompeo, F.; Herrera, J. E.; Balzano, L.; Resasco, D. E., Characterization of single-walled carbon nanotubes (SWNT) produced by CO disproportionation on CO-MO catalysts. *Abstracts of Papers of the American Chemical Society* **2002,** 223, U630-U631.

48.   Alvarez, W. E.; Pompeo, F.; Herrera, J. E.; Balzano, L.; Resasco, D. E., Characterization of single-walled carbon nanotubes (SWNTs) produced by CO disproportionation on Co-Mo catalysts. *Chemistry of Materials* **2002,** 14, (4), 1853-1858.

49.   Herrera, J. E.; Balzano, L.; Borgna, A.; Alvarez, W. E.; Resasco, D. E., Relationship between the structure/composition of Co-Mo catalysts and their ability to produce single-walled carbon nanotubes by CO disproportionation. *Journal of Catalysis* **2001,** 204, (1), 129-145.

50.   Alvarez, W. E.; Kitiyanan, B.; Borgna, A.; Resasco, D. E., Synergism of Co and Mo in the catalytic production of single-wall carbon nanotubes by decomposition of CO. *Carbon* **2001,** 39, (4), 547-558.

51.   Resasco, D. E.; Kitiyanan, L.; Alvarez, W. E.; Borgna, A., Effective Co-Mo bimetallic catalysts for the production of single-wall carbon nanotubes by decomposition of Co. *Abstracts of Papers of the American Chemical Society* **2000,** 219, U536-U536.

52. Kitiyanan, B.; Alvarez, W. E.; Harwell, J. H.; Resasco, D. E., Controlled production of single-wall carbon nanotubes by catalytic decomposition of CO on bimetallic Co-Mo catalysts. *Chemical Physics Letters* **2000,** 317, (3-5), 497-503.

53. Liu, X.; Pichler, T.; Knupfer, M.; Fink, J.; Kataura, H., Electronic properties of potassium-intercalated C-60 peapods. *Physical Review B* **2004,** 69, (7), -.

54. Mayer, A.; Miskovsky, N. M.; Cutler, P. H., Three-dimensional simulations of field emission through an oscillating barrier from a (10,0) carbon nanotube. *Journal of Vacuum Science & Technology B* **2003,** 21, (1), 395-399.

55. Mayer, A.; Miskovsky, N. M.; Cutler, P. H., Theoretical comparison between field-emission properties of carbon protrusions ranging from an isolated atom to multi-wall nanotubes. *Journal of Physics-Condensed Matter* **2003,** 15, (4), R177-R191.

56. Mayer, A.; Miskovsky, N. M.; Cutler, P. H., Simulations of transport and field-emission properties of carbon nanotubes. *Journal of Vacuum Science & Technology B* **2003,** 21, (4), 1545-1549.

57. Herrera, J. E.; Balzano, L.; Pompeo, F.; Resasco, D. E., Raman characterization of single-walled nanotubes of various diameters obtained by catalytic disproportionation of CO. *Journal of Nanoscience and Nanotechnology* **2003,** 3, (1-2), 133-138.

58. Matarredona, O.; Rhoads, H.; Li, Z. R.; Harwell, J. H.; Balzano, L.; Resasco, D. E., Dispersion of single-walled carbon nanotubes in aqueous solutions of the anionic surfactant NaDDBS. *Journal of Physical Chemistry B* **2003,** 107, (48), 13357-13367.

59. Dresselhaus, M. S.; Dresselhaus, G.; Jorio, A.; Souza, A. G.; Pimenta, M. A.; Saito, R., Single nanotube Raman spectroscopy. *Accounts of Chemical Research* **2002,** 35, (12), 1070-1078.

60. Dresselhaus, M. S.; Eklund, P. C., Phonons in carbon nanotubes. *Advances in Physics* **2000,** 49, (6), 705-814.

61. Dresselhaus, M. S.; Dresselhaus, G.; Saito, R., Physics of Carbon Nanotubes. *Carbon* **1995,** 33, (7), 883-891.

62. Dresselhaus, M. S.; Jorio, A.; Pimenta, M. A., Resonance Raman spectroscopy in one-dimensional carbon materials. *Anais Da Academia Brasileira De Ciencias* **2006,** 78, (3), 423-439.

63. Dresselhaus, M. S.; Jorio, A.; Souza, A. G.; Dresselhaus, G.; Saito, R., Raman spectroscopy on one isolated carbon nanotube. *Physica B-Condensed Matter* **2002,** 323, (1-4), 15-20.

64. Raravikar, N. R.; Keblinski, P.; Rao, A. M.; Dresselhaus, M. S.; Schadler, L. S.; Ajayan, P. M., Temperature dependence of radial breathing mode Raman frequency of single-walled carbon nanotubes. *Physical Review B* **2002,** 66, (23), -.

65. Heller, D. A.; Barone, P. W.; Swanson, J. P.; Mayrhofer, R. M.; Strano, M. S., Using Raman spectroscopy to elucidate the aggregation state of single-walled carbon nanotubes. *Journal of Physical Chemistry B* **2004,** 108, (22), 6905-6909.

66. Kataura, H.; Kumazawa, Y.; Maniwa, Y.; Umezu, I.; Suzuki, S.; Ohtsuka, Y.; Achiba, Y., Optical properties of single-wall carbon nanotubes. *Synthetic Metals* **1999,** 103, (1-3), 2555-2558.

67. Weisman, R. B.; Bachilo, S. M., Dependence of optical transition energies on structure for single-walled carbon nanotubes in aqueous suspension: An empirical Kataura plot. *Nano Letters* **2003,** 3, (9), 1235-1238.

68. Weisman, R. B., Fluorimetric analysis of single-walled carbon nanotube samples. *Abstracts of Papers of the American Chemical Society* **2004,** 227, U1265-U1265.

69. Weisman, R. B.; Bachilo, S. M.; Tsyboulski, D., Fluorescence spectroscopy of single-walled carbon nanotubes in aqueous suspension. *Applied Physics a-Materials Science & Processing* **2004,** 78, (8), 1111-1116.

70. Bachilo, S. M.; Strano, M. S.; Kittrell, C.; Hauge, R. H.; Smalley, R. E.; Weisman, R. B., Structure-assigned optical spectra of single-walled carbon nanotubes. *Science* **2002,** 298, (5602), 2361-2366.

71. Herrera, J. E.; Resasco, D. E., Role of Co-W interaction in the selective growth of single-walled carbon nanotubes from CO disproportionation. *Journal of Physical Chemistry B* **2003,** 107, (16), 3738-3746.

72. Purcell, S. T.; Binh, V. T.; Baptist, R., Nanoprotrusion model for field emission from integrated microtips. *Journal of Vacuum Science & Technology B* **1997,** 15, (5), 1666-1677.

73. Kang, D. W., Suh J. S. , *Journal of Applied Physics* **2004,** 96, 5324.

74. Sun J. P., Z. Z. X., Hou S. M., Zhang G. M., Gu Z. N., Zhao X. Y., Liu W. M., Xue Z. Q.,, *Applied Physics a-Materials Science & Processing* **2002,** 75, 479.

75. Zhao, J. J.; Han, J.; Lu, J. P., Work functions of pristine and alkali-metal intercalated carbon nanotubes and bundles. *Physical Review B* **2002,** 65, (19), -.

CHAPTER 3

CONTROLLED GROWTH OF VERTICALLY ALIGNED SWNT (VSWNT) ON FLAT SURFACE

3.1 INTRODUCTION

Being one dimensional nanostructures, SWNTs exhibit outstanding structural, mechanical and electronic properties,[1-5] which leads to highly feasible proposals for them to function as essential components for fabrication of non-volatile random access memory,[6-10] interconnects in 3 dimensional architecture,[6-18] field emitter, [19-22] molecular recognition probes,[23, 24] and so on. Their unique structure-property relation and great application potential make them promising building blocks for molecular electronics and give numerous researchers tremendous passion to develop techniques assembling these building blocks into functional arrays to realize their potential applications.

Since most of these applications are based on flat substrate, questions are brought out that how to appropriately incorporate SWNTs into these systems. The first method one may figure out to assemble SWNTs on flat surface is by post-dispersion and deposition of bulk-produced SWNTs. However, the impurities and defects introduced in the purification and dispersion process impose a big threat in fabrication of SWNT-based devices. Moreover, the lengthy process and difficulty in

transferring SWNT to nano-structures compromise the benefit of this method. In regard of these disadvantages, another tempting bottom-up method was intuitively attempted by in-situ fabrication of SWNT-base devices. Unlike bulk production of SWNT on porous materials of high surface area[25-28] or in aerosol environment,[29-31] the first problem emerging before researchers is how to disperse and stabilize nana-sized particles on flat surface because agglomeration may occur on the surface. To surmount the problem, generally two categories of approaches have been tried by researchers. One of them is by employing the latest thin film technology through physical vapor deposition, normally called as dry process, such as sputter coating or vacuum evaporation.[32-42] For example, the synthesis of SWNT on a flat silicon surface was reported by several groups, but the produced SWNTs were accompanied by MWNT due to agglomerated catalyst metals with large diameters.[35, 37] Delzeit et al [38]synthesized SWNTs with relatively high quality and selectivity by pre-depositing 20 nm of Al underlayer on a silicon surface before depositing 1nm of Fe-Mo catalyst, which however resulted in significant surface roughness due to agglomeration of Al. In addition, other quantum dots like Ni catalyst particle was also used to for synthesus of SWNTs on Al layer by Zhang et al.[39]

As opposed to dry process, wet methods involving solution-based catalyst precursors have recently attracted much more attention due to their low cost (no need for expensive photo- or electro-lithography facilities), the advantages in easily tuning

103

the composition and concentration of the catalysts, and the ability to form various complex configurations of catalyst patterns by adjusting the physical properties (such as surface free energy and viscosity) of the solution. These features make it possible to investigate a new class of customer-designed catalysts, which allow better control of the diameters of the nanotubes, the density of the nanotubes in the patterns, and their orientation and morphology on the substrates. For example, Li et al. [43]proposed that ferritin protein was utilized for sparsely located iron nanoparticles on a flat silicon wafer to synthesize SWNTs. Homma et al. [44, 45]dispersed commercially available Fe or Fe_2O_3 nanoparticles in ethanol and loaded them onto an Si substrate. Recently Amama et al. [46, 47]reported a method to deliver nearly monodispersed catalyst nanoparticles stabilized by dendrimer to SiO_2/Si, Ti/Si, sapphire and porous anodic alumina (PAA) substrates.

After solving the problem of immobilizing nano-seeds for SWNT growth on flat substrate, another issue of manipulating growth of SWNTs, especially in alignment, raised to direct the technology to the end application. Alignment of CNT is subcategorized into horizontal alignment (parallel to surface) and vertical alignment (perpendicular to surface). Horizontal alignment has been realized by presence of electric[48-55], magnetic field[56] or by direction of gas flow[57-61]. Vertical alignment of multi-wall carbon nanotubes has been mastered by researchers for several years.[62-71] However, the growth of vertically aligned SWNT (or V-SWNT)

on substrates has remained a challenging task. Only recently, substantial progress has been made on this controlled growth first by some research groups in Japan.[72-77] The special environmental conditions required for the V-SWNT growth have been carefully investigated by Maruyama et al. [72, 73] who pointed out the importance of achieving total cleanliness in the vacuum chamber where the growth is conducted.[10] Hata and co-workers[74-77] have explored the effect of flow rate and the molar ratio of co-feeding gases, ethylene, He, and water. Dai et al. [78] further investigated the effect of O_2 and H_2 in optimizing growth of VSWNT. Much less attention has been paid to the state of the catalyst particles, such as the distribution of the metal particles that act as seeds for the growth of the nanotubes. In addition, the growth mechanism has not been explored completely such as why all the SWNT that forms the "forest" appear to have the same growth rate and length.

In this project, a new catalyst preparation method was developed such that a controllable uniform Co-Mo nanoparticles distribution was able to be achieved based on CoMoCAT® process. VSWNTs have been synthesized in conventional thermal CVD reactor from this catalyst thin film. Detailed analysis of structures of VSWNT and their growth process was conducted to understand the growth mechanism.

3.2 DEVELOPMENT OF CVD METHOD FOR SWNT GROWTH ON FLAT SUBSTRATE

3.2.1 RESEARCH OBJECTIVES

CoMoCAT® has long been proved to be an effective way to selectively produce SWNTs of controlled structures by disproportionation of CO on Co-Mo bimetallic catalyst.[27, 79-82] In chapter 2, it has been demonstrated that reaction temperature can be used as controlling knob to tailor (n,m) structure of SWNTs. Interaction between support materials and catalyst was found to tuning (n,m) structure as well by Giulio et al. in our group. Based on the knowledge learned from CoMoCAT® process about optimized reaction condition and growth mechanism, growth of SWNTs on flat surface are supposed to be possible in controlled conditions as does in reaction occurring on porous materials. Therefore, the objectives of the research is

- ➢ To develop a versatile and controllable method to deposit Co-Mo nanoparticles on flat substrate
- ➢ To control the distribution of Co-Mo nanoparticles for SWNT growth
- ➢ To optimize the reaction conditions for SWNT growth

3.2.2 EXPERIMENTAL SETUP

3.2.2.1 Production of SWNTs on Si substrate

Catalyst solution of various concentration (ranging from 0.09~0.38% in total metal weight) was prepared by dissolving salts of Co and Mo into isopropanol while keeping molar ratio of Co/Mo constant to 1:3. Then a drop of catalyst solution was put on a 2x1cm p-type Si wafer and it spreaded all over the surface and dried in a covered Petri dish (which is called slow drying because of slow solvent transport due to confined convection and rate-limiting diffusion under small concentration gradient) to form a uniform catalyst film. Following that, the wafer with catalyst film was baked in convection oven at 100 ^{o}C for 10 min and 500 ^{o}C for 15 min.

After pretreatment, the wafer was placed in quartz reactor parallel to the flowing direction. Prior to the production of SWNT by the CO disproportionation reaction, the catalyst was heated in H_2 flow to 500°C, and then in He flow to the 750 ^{o}C. The flow rate of gases was 1000 sccm for each stage. The pressure through the whole process was atmosphere.

Patterned catalyst on substrate was prepared by two kinds of methods: natural pattern and manual pattern. Natural pattern process is to dry Si wafer wetted with catalyst solution in air (fast drying). Manual pattern process is to use TEM parallel grid as mask and sputter coat Au/Pd on calcined catalyst/wafer prepared by slow drying.

3.2.2.2   Characterization of catalyst substrates and SWNTs

The as-produced SWNTs and catalyst/wafer were characterized by Raman spectroscopy, and electron microscopy and probe microscopy. The Raman spectra were obtained in a Jovin Yvon-Horiba Lab Ram equipped with a charge coupled detector. SEM images were obtained in a JEOL JSM-880 high resolution scanning electron microscope while the TEM pictures were obtained in a JEOL JEM-2000FX transmission electron microscope. AFM were operated with tapping mode on NanoScope III by Digital Instruments.

3.2.3   RESULTS AND DISCUSSION

3.2.3.1   Formation of Co-Mo Nanoparticles on Flat Substrate

As mentioned in the instruction part, wet method owns several advantages over dry method to deposit catalyst nanoparticles on flat substrate. In theory, the key to successful deposition of nanoparticle is to suppress the polymerization of metal ions or atoms in solvent and to minimize the surface tension of solvent for wetting effect as well as to keep nanoparticles on surface from agglomerating during drying and decomposition of metal-containing precursors. Maruyama et al. [73] developed a so-called "dip coating" method to prepare catalyst by immersing substrate into ethanol solution of Co and Mo acetate salts and pulling it out at constant slow rate. We found that a real solution of Co-Mo can be achieved by stabilizing Co and Mo ions with complex ligands such as isopropoxide or Cl in isopropanol. When dropped on

surface, the solution spreads quickly to cover the whole area and a uniform catalyst thin film forms if the liquid is let dried slowly by limiting the convection and diffusion of vaporized solvent. One of the advantages of this method is it is very easy to control the surface density and size distribution of nanoparticles by adjusting the concentration of catalyst solution. The morphology and chemical status of Co-Mo nanoparticles will be discussed in chapter 3.4.

3.2.3.2   *SWNT Morphology on Flat Surface Controlled by Catalyst Concentration*

Figure 3.1 shows an obvious trend how concentrations of catalyst solution affect growth of SWNTs on Si substrate, which was visualized by SEM. Vertically aligned SWNTs (forest) were grown on substrate deposited with catalyst solution of 0.19% metal concentration. On wafers deposited with catalyst solution of 0.38% and 0.02% metal concentration, random network of SWNTs (grass) were observed after reaction. Apparently, catalyst solution of either higher or lower concentration is not suitable for growth of forest. Besides, it was observed grass grown with catalyst solution of higher concentration was reasonably denser than that with catalyst solution of lower concentration. We have tried to push the reaction to a limit by raising the metal concentration up to 3.8% and lowering down to 0.001%. It turned out that very high concentration of catalyst resulted in carbon fiber and multi-walled carbon nanotubes while extremely low concentration of catalyst produced largely

scattered SWNTs. It is clear forest only grow on substrates with catalyst solution of concentration in a proper range.

Characterizations of VSWNTs were performed by Raman and TEM. Figure 3.2 shows Raman spectrum of as-produced VSWNTs with three excitation lasers (633 nm, 514 nm, and 488 nm). It is well known peaks for radial breathing mode (RBM) of SWNTs are related to diameter of SWNTs by $\omega_{RBM} = 234/d_{SWNT} + 10$ [cm^{-1}][83]. Main RBM features with 3 lasers for VSWNT covered a range from 130 cm-1 to 300 cm-1. The corresponding diameter range was from 0.8 nm to 1.9 nm. Therefore, as-produced VSWNTs had a wide size distribution and large average diameter, which was reflected by convergence of G- and G+ features and broad base of the whole G band. [83] TEM images in figure 3.3 perfectly agree with Raman results. Meanwhile, these images display clean VSWNTs free of impurities like metal particles.
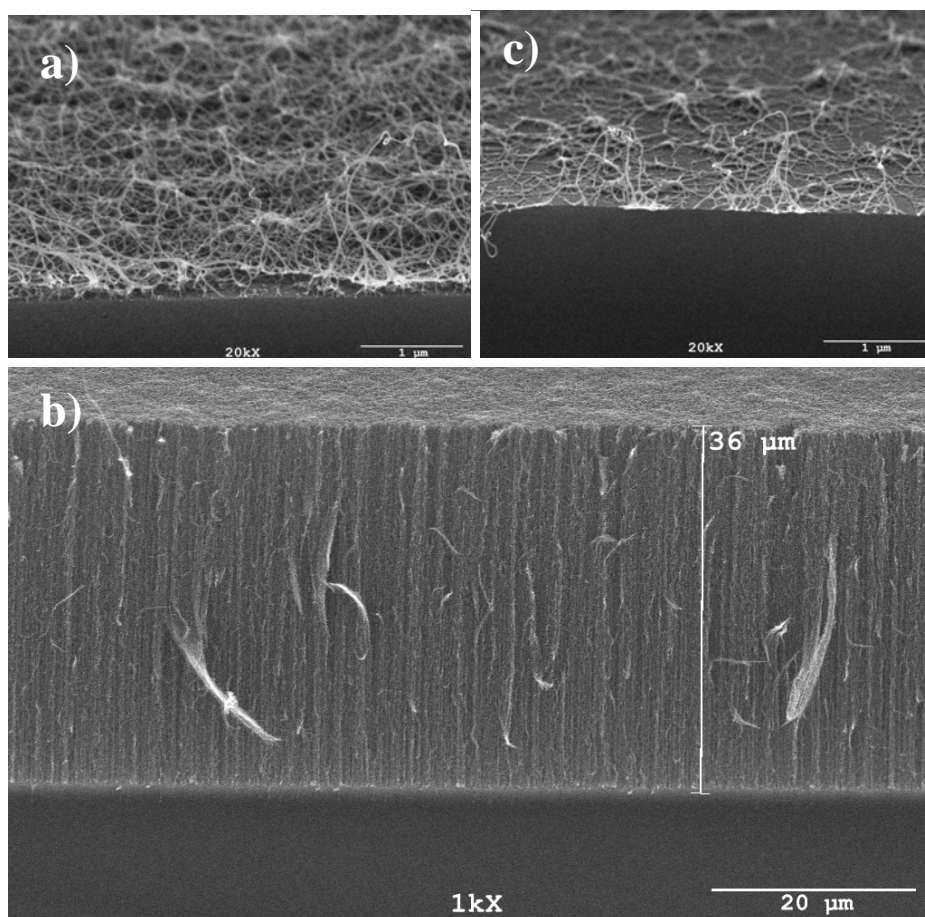
Figure 3.1: SEM images of SWNTs produced on silicon wafers with catalyst solution of different concentrations: a) 0.38%, b) 0.19%, c) 0.02%. Concentration is in total metal weight.
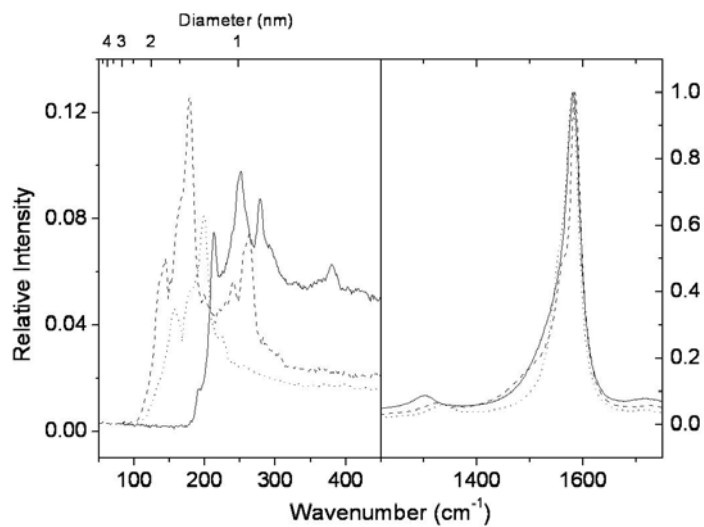
Figure 3.2: *Resonance Raman spectrum of as-produced VSWNTs with lasers of various wavelength: 633 nm (solid line), 514 nm (dotted line), and 488 nm (dashed line).*
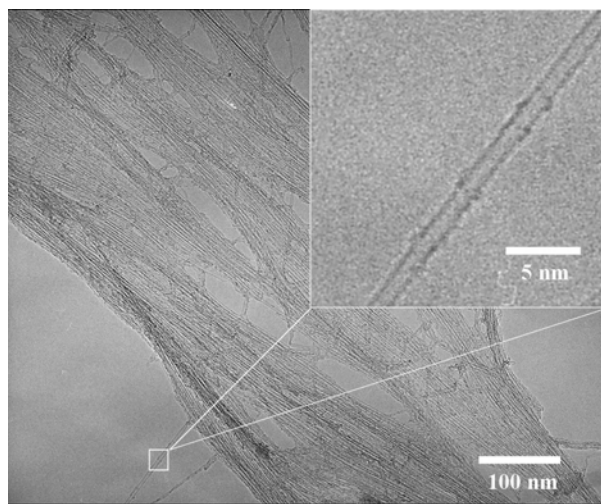
Figure 3.3: *TEM images of VSWNTs removed off silicon wafer.*

3.2.3.3 *Optimization of Reaction Conditions for Growth of VSWNT*

❖ *Effect of Catalyst Solution Concentration*
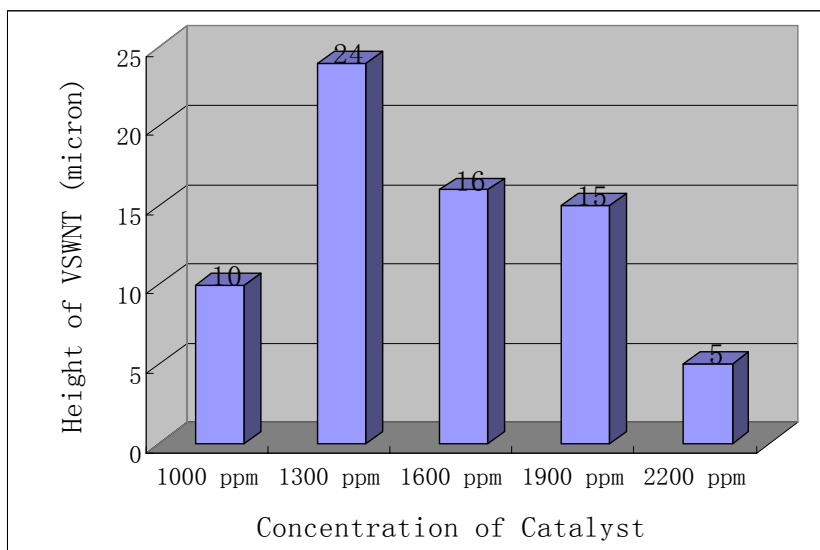
Figure 3.4: Height of VSWNT as a function of catalyst concentration in solution (total metal in solution by weight). Reactions were conducted at 750℃ for 1hr with atmospheric pressure.

As demonstrated earlier, VSWNT only grow on flat substrate with catalyst solution of concentration in a proper range. It needs to further investigate what is the working range and how the fine tune of catalyst concentration in the range affects the growth of VSWNT. Figure 3.4 shows how the height of VSWNT changes with the concentration of catalyst solution in the range where VSWNT is able to be achieved. Clearly, the height of VSWNT reached maximum (24 μm) in the middle of the working range (1300 ppm of total metal concentration).   Since the catalyst

concentration determines the surface density of catalyst nanoparticles, it is reasonable to infer that surface density of catalyst at 1300 ppm either optimized the mass transfer of carbon source during reaction or enhanced the neighboring effect for aligned growth.

❖ *Effect of Reaction Pressure*
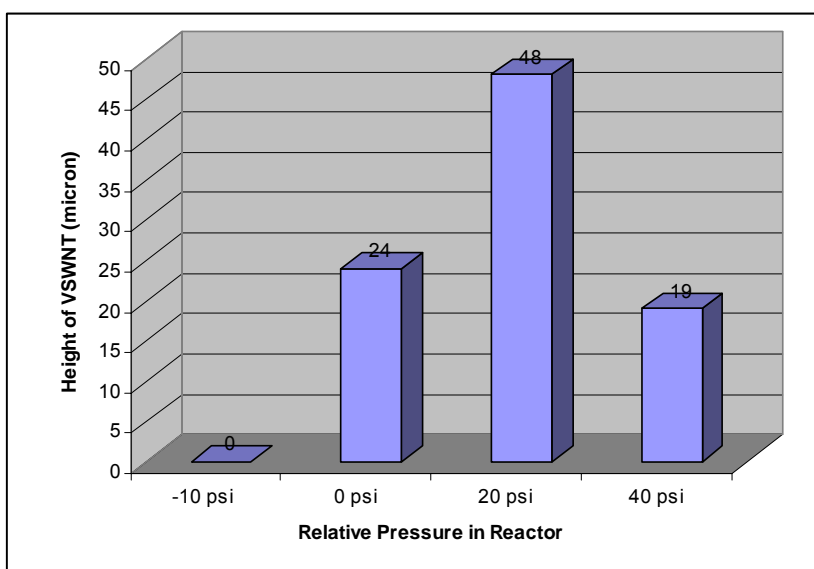
Figure 3.5: Height of VSWNT as a function of relative pressure in reactor. Reactions were conducted at 750°C for 1hr with 1300 ppm of total metal concentration in solution.

Figure 3.5 shows the effect of reaction pressure on the growth of VSWNT. In the case of reaction at -10 psi, 0 height means there is no VSWNT, but random

network of SWNT of 1~3 molecular tube thickness. The height of VSWNT increased with pressure until it reached 48 μm at 20 psi and turned down after that point. The reaction below 20 psi seems to be mass transfer limited while the CO pressure above 20 psi probably over reduces the Co-Mo catalyst.

❖ *Effect of Reaction Temperature*
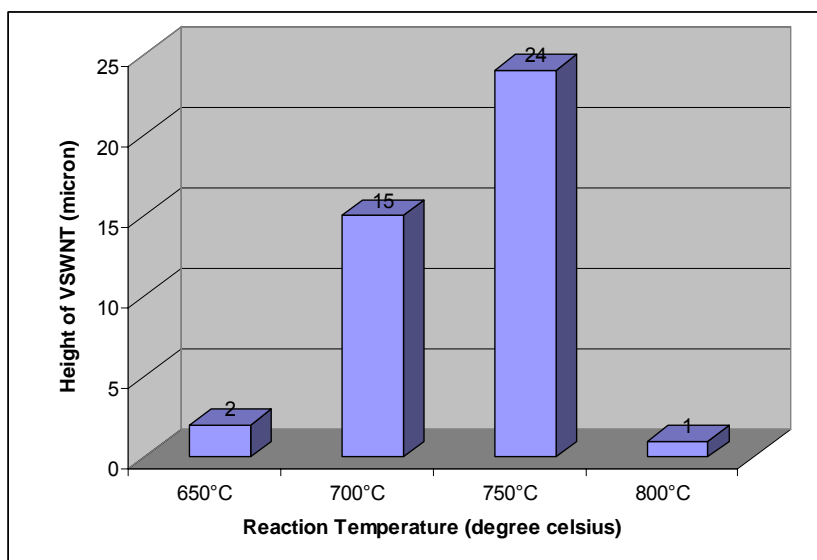
Figure 3.6: Height of VSWNT as a function of reaction temperatures. Reactions were conducted for 1hr with 1300 ppm of total metal concentration in solution.

It is surprising VSWNT can be produced in the broad temperature window ranging from 650 °C to 800 °C. A dramatic drop of VSWNT height from 24 μm to 1

µm when changing temperature from 750 °C to 800 °C can be explained by slow reaction rate due to either sintering of nucleation center for SWNT growth or over-reduction of Co-Mo catalyst.

3.2.4 CONCLUSION TO DEVELOPMENT OF METHOD FOR GROWTH OF SWNT ON FLAT SUBSTRATE

We have developed a simple method to grow various forms of SWNTs on substrates by regular atmospheric CVD method. Before any pretreatment, a uniform thin layer of Co-Mo nanopartiles is deposited on flat substrate by our "drop-spread-dry" process. This process is easy to control the surface density of nanoparticles by adjusting the catalyst concentration in solution. VSWNTs were found to only grow in a proper range of catalyst concentration and the height of VSWNT varies with catalyst concentration finely tuned in the working range. Reaction pressure and temperature were also optimized to increase the height of produced VSWNT.

3.3 MICROANALYSIS OF STRUCTURE AND PROPERTIES OF VSWNT

3.3.1 RESEARCH OBJECTIVES

In the CoMoCAT® process, (n,m) structure of SWNT can be tailored by reaction temperature and interaction between catalyst and substrate. When VSWNT are grown on flat substrate, interesting questions are brought up whether the VSWNT growth is as selective as CoMoCAT® process. Thus, a detailed analysis of VSWNT by electron microscopy and optical spectroscopy is needed to explore the structures of VSWNTs.

Due to its one dimensional structure, SWNTs have quantization of the circumferential wave vectors, creating strong divergences in the electronic density of states known as van Hove singularities, which formulate discrete energy levels or "subbands".[848] The resulting unique properties make SWNTs an important candidate for various electronic and optical applications.[85-87] In particular, since the intersubband gap energies correspond to infrared to visible light, several innovative optical applications have been proposed. [85-87] The 1D shape of a SWNT would be advantageous in polarization-sensitive optical devices, provided one has a sound understanding of its anisotropic optical properties. Despite their significant potential,

there have been few experimental studies on the anisotropic optical absorption of SWNTs to provide confirmation to earlier theoretical works in the inter-subband[88] and higher energy regions.[89] So far, such investigations using aligned SWNTs embedded in a polymer matrix [90] and magnetically aligned SWNTs in gel[91] have been reported. In addition to optical absorption, polarized Raman scattering has also been employed to study the anisotropic optical properties of SWNTs. So far several studies employing polarized RRS on SWNTs, either bundled or isolated, have been reported.[92-102] Hwang et al.[90] and Duesberg et al.[93] performed polarized RRS experiments on nearly isolated SWNTs on a glass plate and presumably bundled SWNTs aligned in a melt-spun PMMA fiber, respectively, and showed that the scattering intensities of both RBM and G peaks are maximized when the polarization of the light is parallel to the SWNT axis and are suppressed when perpendicular.

As a macroscopic one-dimensional aligned structure, VSWNT is a perfect object to study anisotropic optical properties. Maruyama et al.[103] have investigated anisotropic properties of SWNTs determined from polarized optical absorption and Raman scattering measurements of a vertically aligned SWNT film. Therefore, polarized optical measurements can be used to determine the ordered and disordered structures of VSWNT provided the measurements can be applied on VWNT disclosing information from different positions along aligned direction of VSWNT.

So far, no polarized optical measurements for such purpose have been reported. Thus, in our project, several tasks need to be accomplished:

➢ Use electron microscopy to determine molecular structure of VSWNT.

➢ Use optical measurement to determine the (n,m) and diameter distribution of VSWNT.

➢ Use position-resolved micro Raman and angle-resolved X-ray absorption near edge structure to determine the ordered and disordered structure of VSWNT.

3.3.2   *EXPERIMENTAL SETUP*

Production of VSWNT is as described in section 3.2.2.1.   As produced VSWNT on silicon wafer was cleaved by leaning and push a surgery blade against the edge of silicon wafer. A small chip of VSWNT/silicon wafer was mounted on specimen carrier by copper tape. SEM imaging and analysis was conducted in JEOL JSM-880 High Resolution SEM equipped with backscattered electron detector, transmitted electron detector, electron channelling imaging , and Kevex X-ray analyzer with IXRF software

VSWNT was removed from wafer by mechanical method and dispersed in isopropanol. One drop of VSWNT/isopropanol dispersion was dropped on carbon lacy grid for TEM imaging in JEOL 2000-FX Intermediate Voltage STEM equipped

with secondary electron detector, Gatan Digi-PEELS Electron Energy Loss Spectrometer, Kevex Quantum 10 mm2 X-ray detector, and IXRF X-ray analyzer with digital imaging capability.

The optical absorption equipment used in this study was a combination of a Bruker Equinox 55 FTIR and a Shimadzu double-beam spectrometer UV-2101. A 10-mm light path "I" grade quartz cuvette was used for the measurements. Raman spectra were obtained on a Jovin Yvon-Horiba LabRam 800 equipped with a charge-coupled device detector. The laser excitation energy was 1.96 eV (633 nm).

Position-resolved micro Raman along the length of VSWNT was carried out at Oak Ridge National Lab with red laser polarization direction parallel and perpendicular to the grow direction of VSWNT. The angle-dependent C K-edge XANES spectra were taken under UHV with total electron yield (TEY) mode at the bending magnet beamline 9.3.2 of Advanced Light Source (ALS) in Lawrence Berkeley National Laboratory (LBNL). The XANES data were collected at various angles ranging from $\theta=10°$ ("glancing geometry") to $\theta=80°$ ("normal geometry"), where θ denotes the angle between the sample normal and the direction of the electric vector of the X-ray beam.

3.3.3   RESULTS AND DISCUSSION

3.3.3.1   Molecular Structure of VSWNT Determined by Electron Microscopy

❖ *<u>Scanning Electron Microscopic Method</u>*

The most direct method to visualize VSWNT is scanning electron microscopy. Figure 3.7 shows secondary electron SEM images at different angles and positions. Crosssectional view from 60° direction at lower magnification presents VSWNT with well aligned bundles of uniform height. The surface on the top seems smooth indicating the apparent growth rate for each SWNT bundles is the same. The SEM pictures imaging the bottom and middle of VSWNT from the side at higher magnification shows a combination of major well aligned SWNT bundles and minor branches sticking out of stems instead of perfectly parallel SWNT bundles. Thus, the real world of VSWNT is composed of ordered and disordered structures. When moving view to the top of VSWNT, one can see an apparent SWNT layer in the form of random network, which is called "crust". The aligning mechanism and function of crust will be further discussed in chapter 3.4.
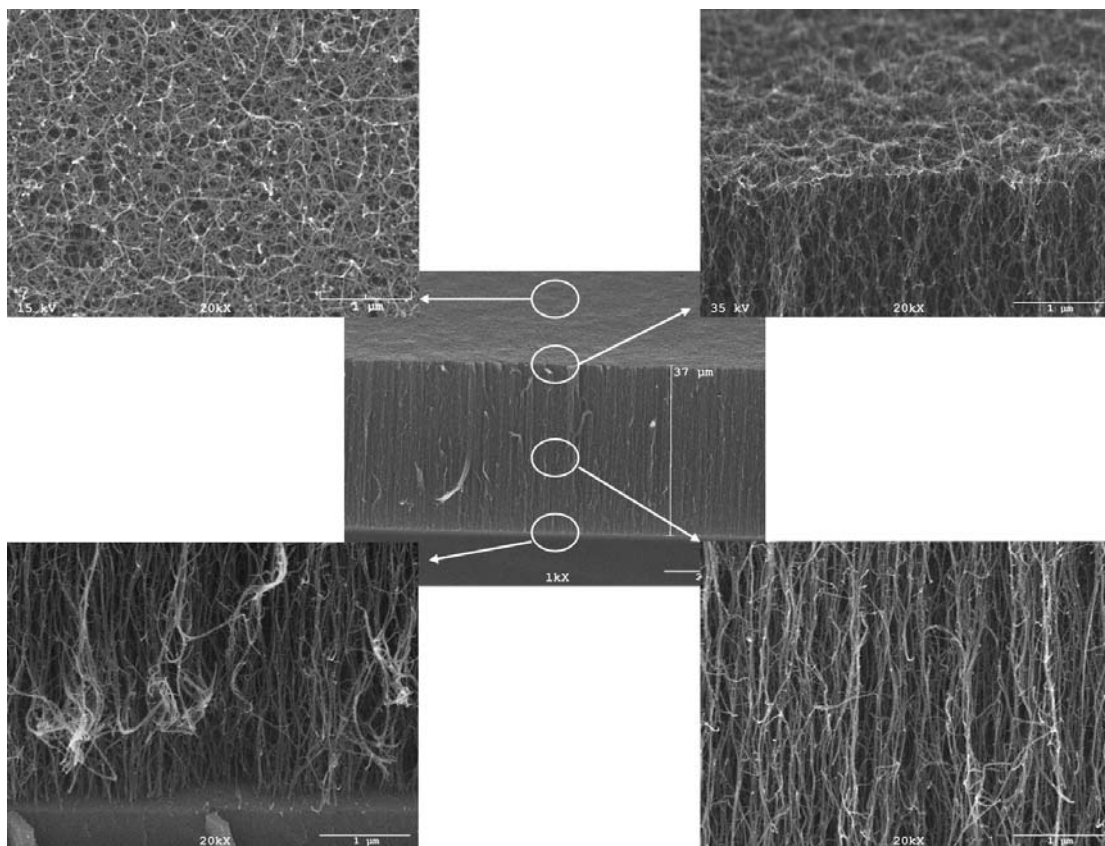
Figure 3.7: *SEM images of VSWNT. Top left is the top view of VSWNT, top right is the side view of VSWNT's top, bottom left is the side view of VSWNT's bottom, bottom right is the side view of VSWNT's middle.*

122

❖ ***Transmission Electron Microscopic Method***
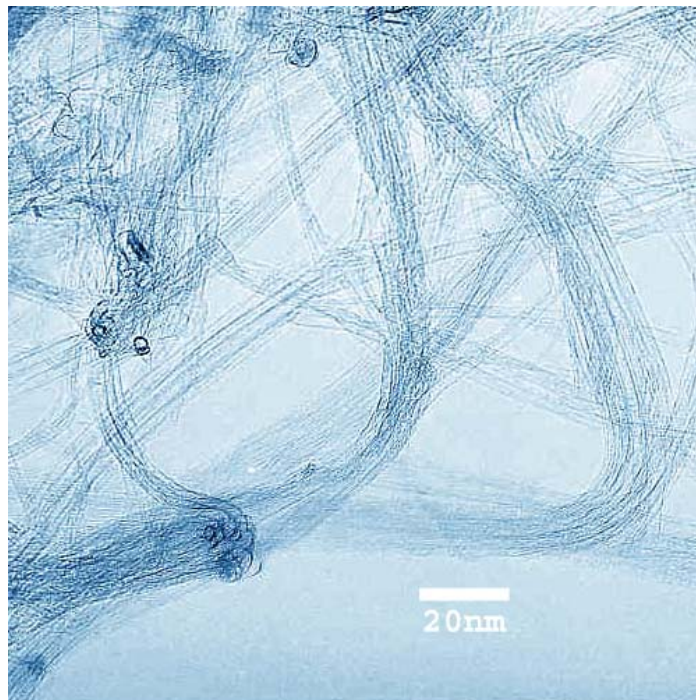
Figure 3.8: *TEM image of VSWNT after being recovered from the silicon wafer and deposited on lacy carbon grid.*

High resolution transmission electron microscopy is able to resolve VSWNT structure at molecular level. As shown in figure 3.8, VSWNTs are clean single walled carbon nanotubes without metal impurities. No multi-walled or double-walled carbon nanotubes are observed in TEM. By measuring diameter of VSWNTs representative in the sample, the diameter of VSWNT is determined to range from 1 nm to 4 nm, which is composed of mainly large tubes and few small tubes.

Apparently, the size distribution of VSWNT is broader than that of conventional CoMoCAT® tubes and the average diameter is larger too.

3.3.3.2 *Electronic Structure of VSWNT Determined by Optical Absorption and Raman Scattering*
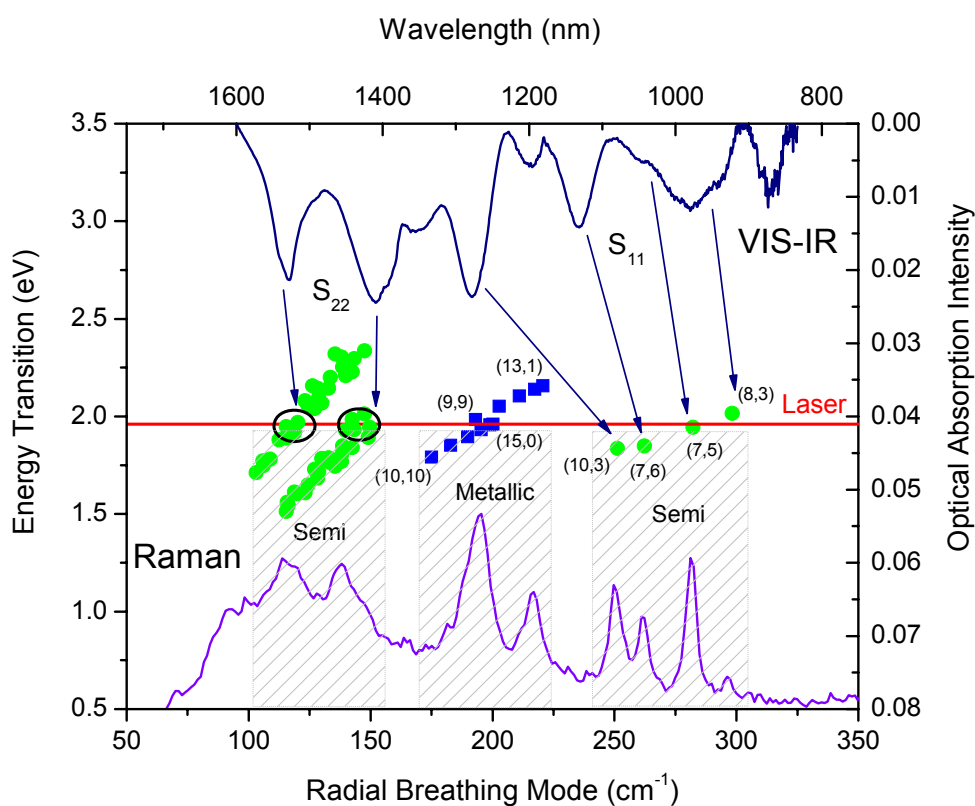
Figure 3.9: *Near IR absorption (spectrum at the top) and Raman shift in the radial breathing mode of VSWNT dispersed in carbomethylcellulose aqueous solution.*

As discussed in chapter 2.2, Raman spectroscopy provides useful information about VSWNT structure. The lower panel in Figure 3.9 presents the radial breathing mode of Raman shift of the VSWNT dispersed in carbomethylcellulose (CMC) solution. The series of bands in the range 150-400 cm^{-1} are characteristic of single-walled carbon nanotubes. As it is well-known, the frequency of the RBM is related to the nanotube diameter by $\omega_{RBM} = 234/d_{SWNT} + 10$ [cm^{-1}].[104] However, assignment of RBM bands to specific nanotube structures is not straightforward and diameter populations obtained from RBM are not reliable unless a very detailed study is attempted. The dramatic effect of resonance phenomena, complicated by thermal effects and the effect of nanotube aggregation can greatly alter the relative intensities of RBM bands [105]. Therefore, Raman results need to be complemented with an independent technique. Optical absorption is a very powerful technique that can be more quantitative than Raman in the assessment of nanotube populations. It is well known that the quasi-one-dimensionality of SWNT gives origin to sharp van Hove singularities in the density of electronic states. As a result, the optical properties of SWNT are dominated by transitions between van Hove singularities on opposite sides of the Fermi level. Kataura [3] used the tight binding model to calculate energy transitions E_{ii} and generated the well-known Kataura plot of E_{ii} versus nanotube diameter, which is a function of the structural parameter (n,m). More recently, Weisman and Bachilo [106] have modified the Kataura plot on the basis of the photoluminescence method that they developed. This remarkable tool is particularly

appropriate to characterize semiconducting nanotubes in the diameter range of those synthesized by our CoMoCAT $^®$ method as recently shown [107].

In this case, we have used optical absorption in the 800~1600 nm range. The absorption spectra for the VSWNT dispersed in CMC solution are shown in Figure 3.9. As compared to only a few sharp absorption peaks with a low background in the entire Vis-NIR spectrum, much more features are found in VSWNT sample. By matching the corresponding S_{11} or S_{22} of the Weisman plot with the peak lines in the spectrum, individual nanotube or group of nanotubes can be determined. The result is combined with resonant Raman spectra to determine stereo and electronic structures of VSWNT. 3 groups of peaks were found in the radial breathing mode of resonant Raman as shown in figure 3.9. Because those peaks are generated by resonance with red laser of 633 nm, not all nanotube species are expected to be probed by the laser. However, diameter distribution of VSWNT probed by red laser is typical of VSWNT observed by TEM as demonstrated in figure 3.8. Peaks in the range of 100~150 cm^{-1} and 240~300 cm^{-1} correspond to semiconducting tubes of larger diameter and small diameter respectively. By correlating RBM peaks with data from the Weisman plot, it can be seen that in the small tube range (n,m) structures are able to be specified as (8,3), (7,5), (7,6), (10,3) as shown by solid green circles while in the large tube range (n,m) structures are hard to differentiate because large number of big tubes resonant in that range. Those RBM peaks are in

perfect agreement with absorption peaks in Near IR range. Absorption peak in the range between 900 nm and 1300 nm are S11 transition for (8,3), (7,5), (7,6), (10,3). Absorption peaks in the range of 1400~1600 nm correspond to S22 transition for semiconducting tubes presented in the group of Raman shifts in the range of 100~150 cm^{-1}. In addition to semiconducting tubes, metallic tubes are also found in the Raman spectrum. The peaks in the range of 170~230 cm^{-1} are referred to as metallic tubes, which are out of range in the Near IR absorption.

The detailed analysis of the optical absorption spectra has allowed us to identify the (n,m) identity of the most abundant nanotube components in VSWNT sample. As compared to major (6,5) in conventional CoMoCAT® sample produced at 750 °C, VSWNT has broader size and (n,m) distribution and consist of small tubes with several (n,m) structures and big tubes with much more nanotube species.

3.3.3.3   *Ordered and Disordered Structure of VSWNT Studied by Polarized Photon Flux*

❖ *Polarized Raman Scattering on Full Length of VSWNT*

The features in the Raman spectra of single-wall carbon nanotubes in the range 1550~1600 cm-1 as shown in figure 3.10 are identified as the tangential stretch *G*-band modes and can be understood by zone-folding of the 2D graphite phonon

dispersion relations and therefore show a number of characteristics that relate to the low dimensionality of the carbon nanotube. Unlike graphite, the tangential G mode in SWNTs gives rise to a multi-peak feature, also named the G band, where up to six Raman peaks can be observed in a first-order Raman process. However, a simple analysis can be carried out considering the two most intense peaks, that basically originate from the symmetry breaking of the tangential vibration when the graphene sheet is rolled to make a cylindrically shaped tube. The two most intense G peaks are labelled G^+, for atomic displacements along the tube axis, and G^-, for modes with atomic displacement along the circumferential direction, and the lowering of the frequency for the G^- mode is caused by the curvature of the nanotube which softens the tangential vibration in the circumferential direction. The D-band is activated in the first-order scattering process by the presence of in-plane substitutional hetero-atoms, vacancies, grain boundaries or other defects and by finite size effects, all of which lower the crystalline symmetry of the quasi-infinite lattice.

Polarization of the incident and scattered light is not an important issue for a sample of misaligned carbon nanotubes, but polarization effects are very important for the Raman response of a sample of aligned carbon nanotubes (either aligned bundles or a single straight carbon nanotube). Although strict polarization studies require selection rules and phonon/electron symmetry analysis, there is a general and simple polarization behavior that one should have in mind when acquiring the

Raman spectra from a sample of aligned carbon nanotubes. Carbon nanotubes behave as antennas, with the absorption/emission of light being highly suppressed for light polarized perpendicular to the nanotube axis[96, 108]. Therefore, if one wants to measure Raman spectra from a sample of aligned carbon nanotubes, the largest Raman intensity will be generally observed for light polarized along the tube axes, and almost no signal will be observed for cross polarized light.

VSWNT is a good model to study the polarization effect of Raman due to its aligned structure. But as shown in the SEM image in figure 3.7, VSWNT is a combination of ordered and disordered structures. This is the reason why the G band of VSWNT (figure 3.10) with laser polarization perpendicular to growth direction is pronounced instead of no signal in the ideal model as discussed above. In our experiment, micro Raman with polarization direction parallel and perpendicular to the alignment direction was conducted along the length of a 70 μm high VSWNT sample. Since the intensity of G band is sensitive to the direction of incident and scattered optical E fields with respect to the direction of alignment while the intensity of D band is not, it is not surprising that the G/D ration along the length of VSWNT measured with laser polarization parallel to the growth direction is higher than that measured with laser polarization perpendicular to the growth direction, as shown in figure 3.11. Interestingly, the G/D ration in the parallel direction goes down to merge with G/D ratio in the perpendicular direction when scattering location

moves to the top of VSWNT. The explanation for this might be the existence of disordered structure of crust, at which polarized laser in either direction will be scattered with the same efficiency.

Laser polarization parallel to growth direction

Laser polarization perpendicular to growth direction
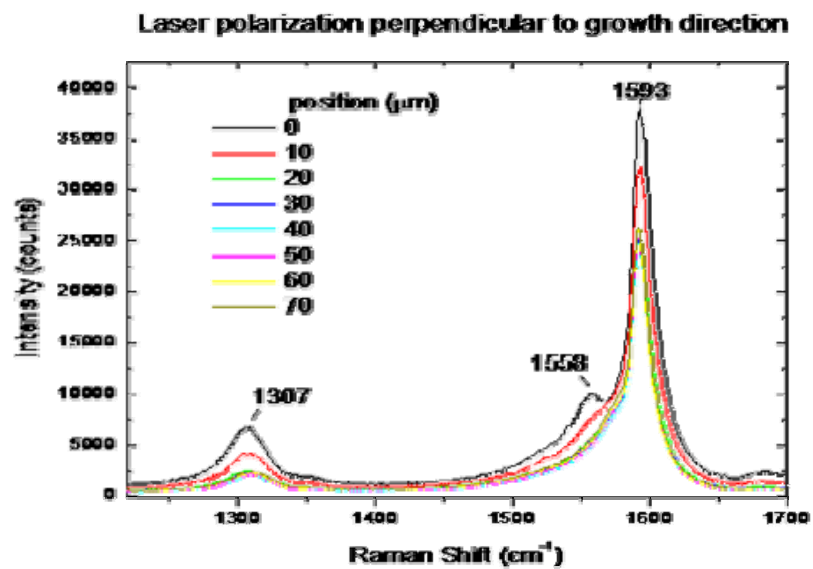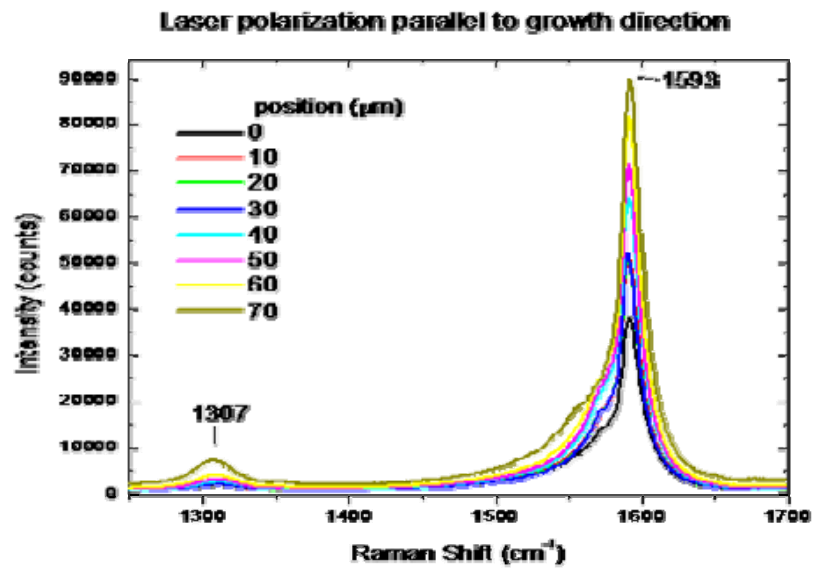
Figure 3.10: *Polarized Raman along the length of VSWNT: top panel was measured with laser polarization parallel to growth direction, bottom panel was measured with laser polarization perpendicular to growth direction.*
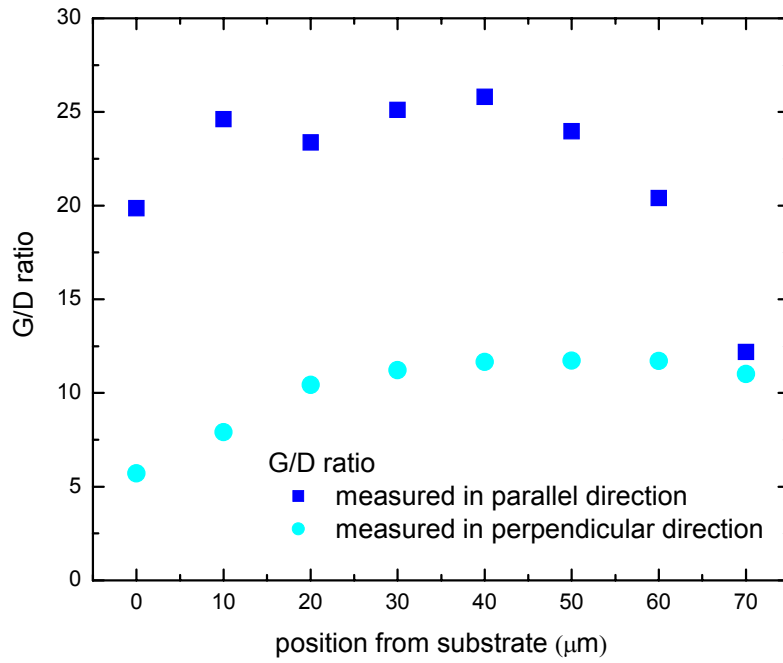
Figure 3.11: *G/D ratio of Raman shift as the function of the length of VSWNT: data in square labels was measured with laser polarization parallel to growth direction, data in round labels was measured with laser polarization perpendicular to growth direction.*

❖ *Angle-resolved X-ray Absorption Near Edge Structure Analysis on VSWNT*

The X-ray absorption near edge structure (XANES) technique involves the excitation of electrons from a core shell (in our case C1s) to unfilled states. The peak positions and spectral line shape in a XANES spectrum are directly associated with the nature of these unoccupied electronic states. Accordingly XANES can be used to obtain qualitative bonding information for a full range of the sp^2/sp^3 bonding ratios. It can be used to identify specific bonds in molecules (*e.g.* C=C, C-C, and C-O bonds) as well as the presence of chemisorbed species. Of greater importance for this study, by using linearly polarized X-ray beam, angle-dependent XANES can be used to investigate the angular dependence of the specific orbitals involved in the transition $1s \rightarrow \pi^*$ and $1s \rightarrow \sigma^*$.

Figure 3.12a shows the changes in the XANES spectra of the SWNT forest for different incident angles θ, which is also the angle between the axis of the vertical nanotubes and the electric field vector of the X-ray beam. In all the spectra, the pre-edge and post-edge regions were normalized to 0 and 1, respectively. Several characteristic peaks can be identified at the C K-edge which is similar to that of graphite,[109] and has been previously discussed.[110] The spectra are characterized by a sharp C(1s)-to-π^* transition near 285.4 eV, a sharp C(1s)-to-σ^* transition near 291.5 eV, two other σ^* transitions from 292 to 298 eV and broader (σ+π) transitions

between 301 and 309 eV. The position and width of these resonances are typical of C-C single bonds. Two smaller peaks in the 287-290 eV region can be assigned to oxygenated surface functionalities, perhaps associated to a small level of defects of the nanotubes. These peaks would correspond to π^* C=O and σ^* C-O resonances.

The XANES spectra were fitted to an arctangent step corresponding to the excitation edge of carbon, a smooth decreasing background, and a series of Gaussians,. The fitting program EDG_FIT by G. N. George, SSRL, available from http://ssrl.slac.stanford.edu/exafspak.html, which utilizes the double-precision version of the public domain MINPAK fitting library[111] was used for the fit. All spectra were fit over the range of 275-325 eV. Pseudo-Voigt line shapes of a fixed 1:1 ratio of the Lorentzian to Gaussian contribution were used to model the π^* and σ^* resonances features and successfully reproduce the spectra. Functions modeling the background contributions to the pre-edge features were chosen empirically to give the best fit and included pseudo-Voigt functions that mimicked shoulders on the rising edge. For all spectra, a fit was considered acceptable only if it successfully reproduced the data as well as the second derivative of the data. The resonance peak area after the background subtraction was obtained by integrating over a range of 10 eV.
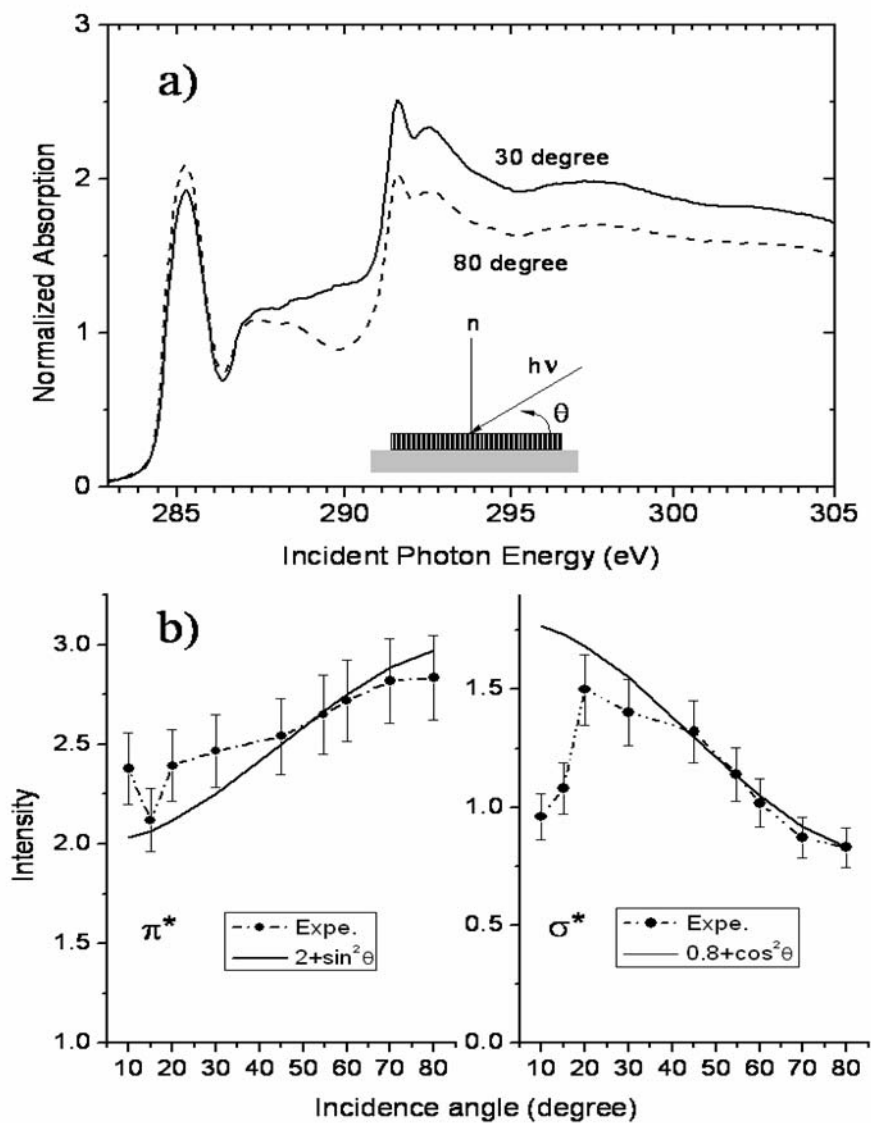
Figure 3.12: *a) XANES spectra of V-SWNT at different angles with respect to top surface of V-SWNT; b) Experimental and fitted data of σ* and π* peak intensity.*

The local order of the SWNTs is clearly evident in the angular dependence of the XANES series. Since the synchrotron light is linearly polarized horizontally, the intensity of the π^* transition is sensitive to the orientation of the π^* orbital with respect to the polarization vector. Thus, since the π^* orbitals in the nanotube specimen are oriented with respect to the incident photon beam, a rotation of the specimen with respect to the incoming photon shows a measurable angular dependence. At normal incidence, the electric field **E** is in the same cross section plane as the π^* orbitals, and thus, the π^* resonance peak is the highest at this angle, as opposed to at glancing angles. Conversely, when **E** is normal to the surface, the field lies along the tube axis (along z) and is perpendicular to the plane of the π^* orbitals, the intensity of the π^* resonance is at its minimum. Specifically, there is an increase in the intensity of the π^* resonance with increasing angle of X-ray beam incidence. The local contribution to the π^* excitation XAS intensity is proportional to the square of the scalar product of the local normal and **E.** As shown before, the π^* resonance intensity is proportional to the sine-squared function of the incidence angle. Indeed, a plot of the π^* excitation *vs.* the incidence angle shows an approximate sine-squared dependence, as shown in left panel of Fig. 3.12b. By contrast, a C–C σ^* orbital orthogonal to the π^* orbital should show an opposite trend. The σ^* orbitals can be viewed as combination of two perpendicular components, one is parallel to tube axis direction ($\sigma^*_{//}$), another along circumferential direction (also perpendicular to the tube axis, $\sigma^*_{\perp}$). The local contribution to the σ^* excitation XAS

135

intensity at 291.5 eV is proportional to the sum of the squared scalar products of the two components and electric polarization vector. With a simple calculation by accounting for all σ* contributions on the entire tube circumference, we found the intensity of the σ* bound resonance at 291.5 eV is indeed roughly proportional to $(0.8 + \cos^2\theta)$. However, deviations from the predicted trend are observed for both σ* and π* transition at low angles. These deviations are consistent with a fraction of the tubes, most noticeable at grazing angles, oriented parallel to the surface, rather than perpendicular as the majority of the tubes in the forest.

3.3.4   CONCLUSION TO MICROANALYSIS OF VSWNT

Detailed characterization was conducted on VSWNT by SEM, TEM, optical absorption, Raman scattering, and XANE. SEM and TEM demonstrate the morphology and molecular structure of VSWNT. Composed of almost pure single walled carbon nanotubes, VSWNT consist of 2 parts: top layer of crust with random network of SWNTs and ordered body with mainly aligned SWNTs. Combined optical absorption in the near IR range and Raman scattering determine the (n,m) and diameter distribution of VSWNT, showing broader distribution and larger average diameter than conventional CoMoCAT® tubes. Polarized Raman scattering and angle-resolved XANE show the effect of disordered structure crust on the polarization dependence of anisotropic optical properties of VSWNT.

3.4 EXPLORATION OF GROWTH MECHANISM OF VSWNT

3.4.1 RESEARCH OBJECTIVES

Despite large uncertainties in the measurements and differences in the synthesis methods employed, it is well recognized that, in an unrestricted state, the growth rate of single-walled carbon nanotubes is at least higher than several microns-per-second.[112-114] By contrast, when the growth occurs via catalytic decomposition of carbon-containing molecules on high surface-area catalysts, such as $CoMo/SiO_2$, the growth takes place in a scale of hours. As previously proposed,[115, 116] while the amount of carbon deposits slowly increases with time, this does not necessarily mean that the growth of a given nanotube is so slow. It is plausible that the slow rate observed for overall rate of carbon deposition is in fact a slow rate of nucleation followed by a fast nanotube growth rate. Accordingly, new nucleation sites will appear on a high-surface area material and each site will give rise to a nanotube that grows relatively fast. Of course, the nanotubes that grow later will do it constricted by the presence of those that grew earlier. As a result, control of nanotube length during growth appeared as an almost impossible task for a long time. However, recent studies of SWNT growth on flat substrates have shown that, in fact, length of SWNT can be controlled.[78, 117, 118] We have found that the density and distribution of the catalyst moieties on the flat surface is crucial to determine whether the nanotubes grow in vertically oriented fashion ("forest" or V-SWNT) or a random network

parallel to the surface ("grass"). We found that different forms of SWNT arrays can be reproducibly obtained on flat silicon substrates when the Co-Mo catalyst particles have the appropriate distribution, which can be readily controlled by simply varying the concentration of catalyst solution.

The difference between this type of flat catalyst and the high surface-area catalyst, is that on a flat surface the nanotube growth is, in principle, less constricted by the catalyst structure due to the absence of porosity. However, the growth of a nanotube is still constricted by the presence of the other nanotubes, which as we will show make them grow vertically oriented (V-SWNT). A question that remains unanswered is why all the SWNT that forms the "forest" appear to have the same length and what is most puzzling is the smoothness of the top of the forest clearly observed in the SEM images.

3.4.2 EXPERIMENTAL SETUP

VSWNT was synthesized as described in section 3.2.2.1. Morphology of catalyst on the silicon wafer after calcinations was characterized by atomic force microscopy (AFM) with tapping mode on NanoScope III by Digital Instruments. The chemical status of catalyst was characterized by X-ray photoemission spectroscopy (XPS) on a PHI 5800 ESCA Monochromatized XPS Spectrometer, which uses Al(kα) radiation (1486 eV) as a probe. To decrease the influence of oxidation and

contamination for XPS samples, these substrates were sealed in a glove bag filled with He gas as soon as they were removed from the furnace or the CVD reactor, and then transferred to an analysis chamber (2.0×10−9 Torr) through a loading chamber (5.3×10−6 Torr) for XPS measurements. All these procedures were finished in 30 min. Binding energies (BEs) were referenced to the C 1s peak at 284.6 eV to compensate for the charging effect. The surface atomic ratios of the calcined and the reduced Co–Mo catalysts on substrate were estimated from peak intensities in the XPS spectra and atomic sensitivity factors.

As produced VSWNT on silicon wafer was cleaved by leaning and push a surgery blade against the edge of silicon wafer. A small chip of VSWNT/silicon wafer was mounted on specimen carrier by copper tape. SEM imaging and analysis was conducted in JEOL JSM-880 High Resolution SEM equipped with backscattered electron detector, transmitted electron detector, electron channelling imaging , and Kevex X-ray analyzer with IXRF software

3.4.3   RESULTS AND DISCUSSION

3.4.3.1   Chemical Analysis of Catalyst Immobilized on Flat Surface

To investigate the chemical status of Co-Mo immobilized on flat surface is key to understanding the mechanism of high selectivity and activity for Co–Mo catalysts

in controlling the growth and structure of SWNTs. Figure 3.13a shows binding energy (BE) of Co 2p levels for the calcined and the reduced Co–Mo catalysts on the Si substrates. The reduced samples showed slight differences from calcined ones in the range of 778 ~784 (2p 3/2 spin orbit). It was found BE for Co Molybdate at 782 eV slightly shifted to lower eV, which may result from the change in the oxidation state of Co during reduction. Interestingly, after reduction there is no BE appearing at 778 eV which is attributed to metallic Co. Figure 3.13b shows BEs of Mo 3d levels for the calcined and the reduced catalysts on the Si substrates. Both spectra exhibit a pair of spin-orbit BEs at 233 and 236 eV. The Mo 3d5/2 BE at 233 eV is attributed to Mo6+ in MoO3 and/or nonstoichiometric Co molybdates, stoichiometric $CoMoO_4$. These results indicate that the decomposition of Mo complex resulted in the formation of Mo^{6+} in MoO3 and/or $CoMoO_x$. Because the metallic Co did not appear after reduction and BEs for Co 2p and Mo3d changed almost nothing, we infer that the calcination of CoMo catalyst decomposed Co complex into Co oxide species existing mostly as CoMoOx, and CoMoOx help to stabilize Co in oxide state during the subsequent reduction.

Table 3.1 shows the surface atomic ratios of the calcined and the reduced Si substrates coated with Co–Mo catalysts. The calcined and the reduced samples had Co/Mo atomic ratios of 0.48~0.51, apparently higher than initial ratio of Co to Mo in solution 0.33, which means excessive Co exits on the surface of catalyst

140

nanopartiles. It is noteworthy that the atomic ratios of Co and Mo to total elements didn't change much after reduction, respectively. This further proves the existence of stable phase of Co Molybdate.

Based on the XPS data, a model is proposed to describe the evolution in morphology and chemical state of Co–Mo catalysts on the Si substrates during calcination and reduction. After "drop-speard-dry" process, a thin layer of bimetallic catalysts (initial Co:Mo 1:3 in atomic ratio) is formed on surface. After calcination in air at 500 °C, metal complex are decomposed into CoMoOx and MoO3, which exist as well-dispersed nano-sized particles. After reduction in H_2 at 500 ∘C, existing CoMoOx remains unchanged. Finally, the growth of SWNTs starts with the reaction of disproportionation of CO on catalyst surface. Upon contact with carbon, Co molybdate is converted into Mo carbides and release active metallic Co particles from which SWNTs selectively grow during the CVD reaction.

	O1s	Si2p	Co2p	Mo3d	Co/Mo
CoMoWafer, after calcination	69.5	28.16	0.76	1.58	0.48
CoMoWafer, reduced at 500°C	68.63	29.11	0.76	1.49	0.51

Table 3.1: *Chemical composition of catalyst particles on silicon wafer after calcination and reduced at 500℃. The original atomic ratio of Cobalt to Molybdenum in the catalyst solution is 0.33.*
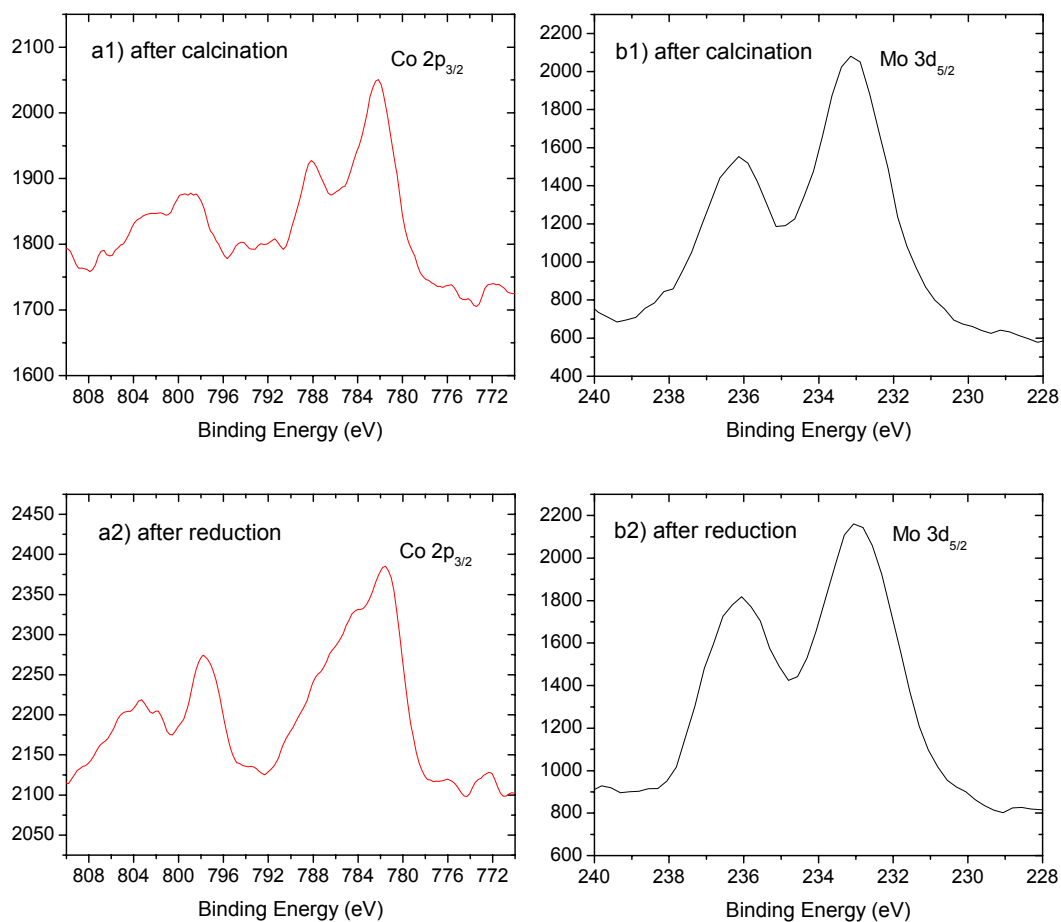
Figure 3.13: *XPS spectra for Co 3d5/2 and Mo 3d5/2 in two cases: top panels are for catalyst after calcinations, bottom panels are for catalyst after reduction at 500°C.*

3.4.3.2 Morphological Analysis of Catalyst Immobilized on Flat Surface

AFM, known to be a powerful tool to explore 3-D surface profile of materials, was employed to probe morphology of catalyst particles on Si wafers. In Figure 3.14 higher-magnification SEM pictures of SWNTs and AFM images of calcined catalyst/substrates are arranged side by side for comparison. Catalyst particles formed with solution of 0.02% metal concentration were small and widely separated. As a result, grass grown from that was sparse and almost lying down on the surface completely. In the case of 0.19% metal concentration, catalyst was densely distributed on substrate in relatively uniform nano-particles. The average distance between those particles were around 60-70 nm, which matched the average distance between bundles of forest in (b1) of figure 4. When the concentration of catalyst solution was high enough (0.38%), catalyst started aggregating to form big particles as shown in (a2) of figure 4 and there was still small particles remained between thosre big ones just like nano-particles formed with solution of 0.19% metal concentration. It is speculated that conglomeration of Co/Mo alloy blocks the nucleation of SWNTs and thus poisons part of surface while small particles maintain the capability to grow SWNT bundles.
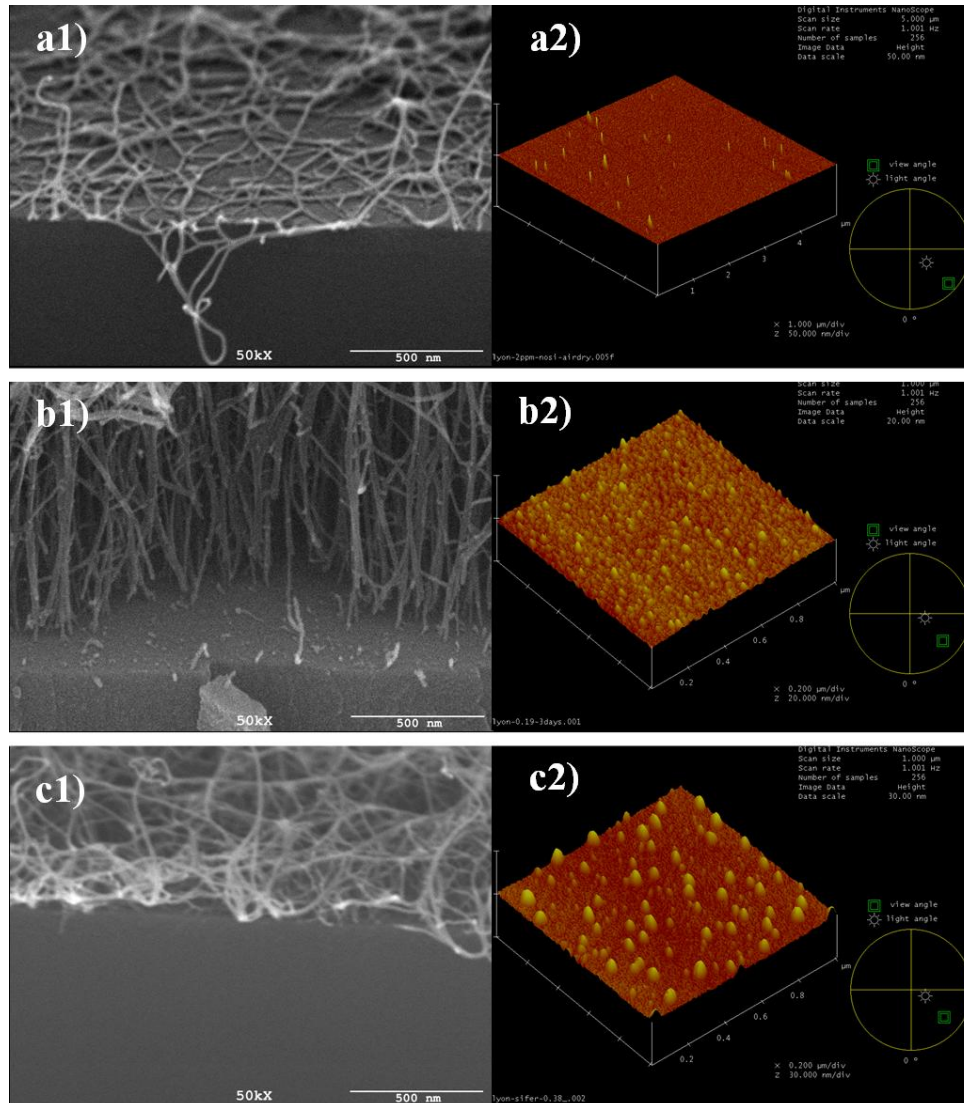
Figure 3.14: *Side-by-side comparison of SEM pictures (left column) of SWNTs with AFM images (right column) of corresponding silicon wafers with catalyst solution of different concentrations: a) 0.38%, b) 0.19%, c) 0.02%. Concentration is in total metal weight. AFM were done after silicon wafers were calcined in oven at 500 °C.*

3.4.3.3   Evolution of VSWNT with Time
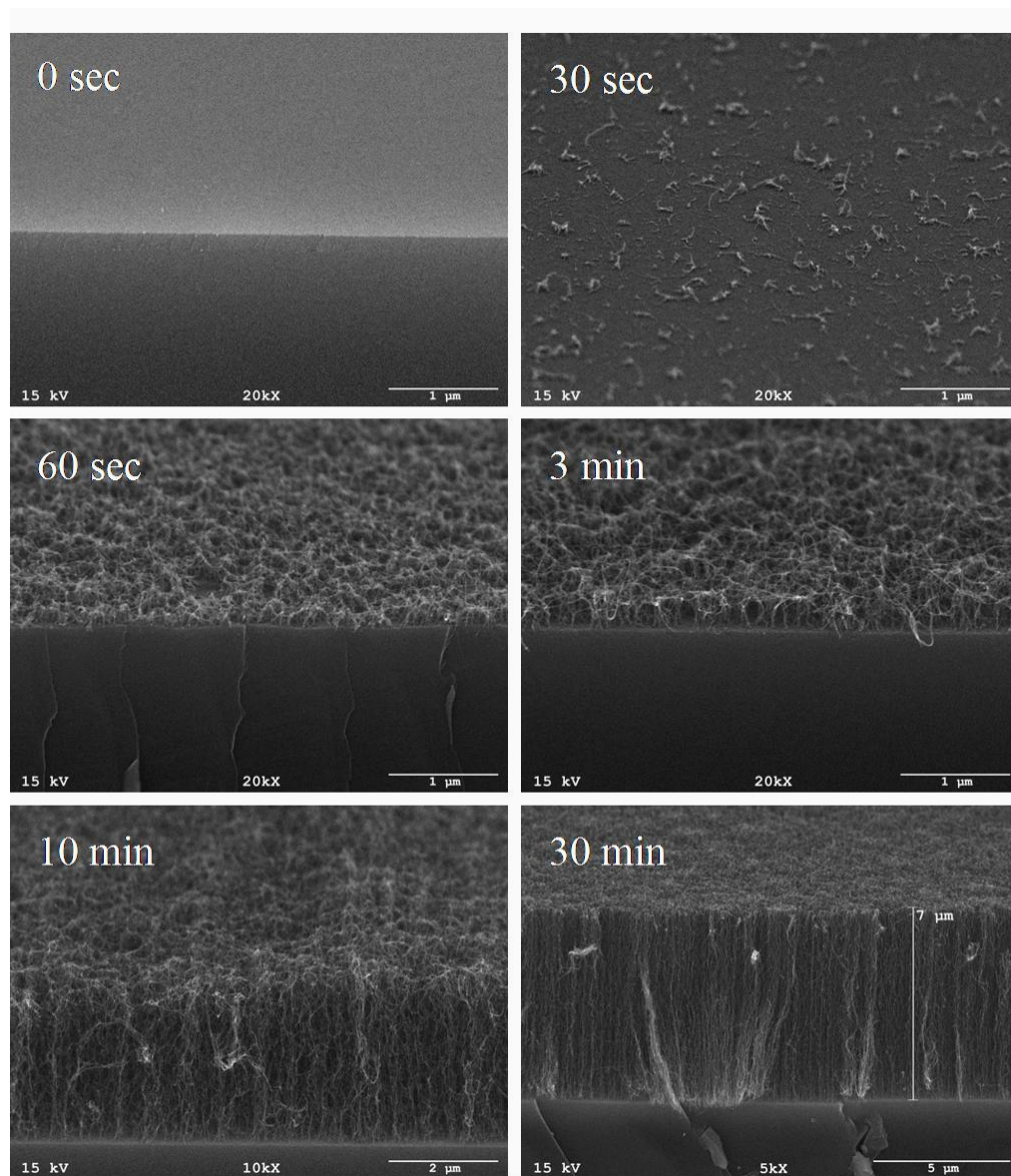
Figure 3.15: *SEM Images of V-SWNT obtained for a series of reaction time period. The scale bars in those images are 1 μm for 0, 30, 60 seconds and 3 minutes, 2 μm for 10 minutes and 5 μm for 30 minutes.*

To investigate how this crust develops during the growth process, we have followed the evolution of the forest structure as a function of time. Fig. 3.15 clearly shows the different morphologies of the nanotube layer observed as a function of time. The first image shows the flat catalyst surface before any carbon was deposited. Next, the appearance of short SWNT is observed after only 30 s. of reaction time. It is evident that the early growth does not occur over the entire surface, but rather on some preferential spots which are those in which the development of the active Co-Mo catalyst and nucleation of nanotube caps occurs first, as proposed earlier.[14] It is important to note that during the early stages of the growth process, there is no indication of a vertically oriented structure. During the following 30 s., it appears that the entire surface as been covered by nanotubes, with evidence of sites being activated at a later time than the first ones. As a result, a thin layer of randomly oriented SWNT gets woven. After 3 min., a uniform crust with very short aligned SWNT bundles underneath can be clearly seen. This is a critical moment. It is obvious that the entangling of SWNT bundles due to different growth rate and random orientation has stopped at this stage; instead, as the nanotube growth continues from the root, the crust is pushed up, but being rather rigid, the overall growth is now concerted. Consequently, a microscopically uniform growth is forced and a somewhat vertical alignment of every nanotube occurs.
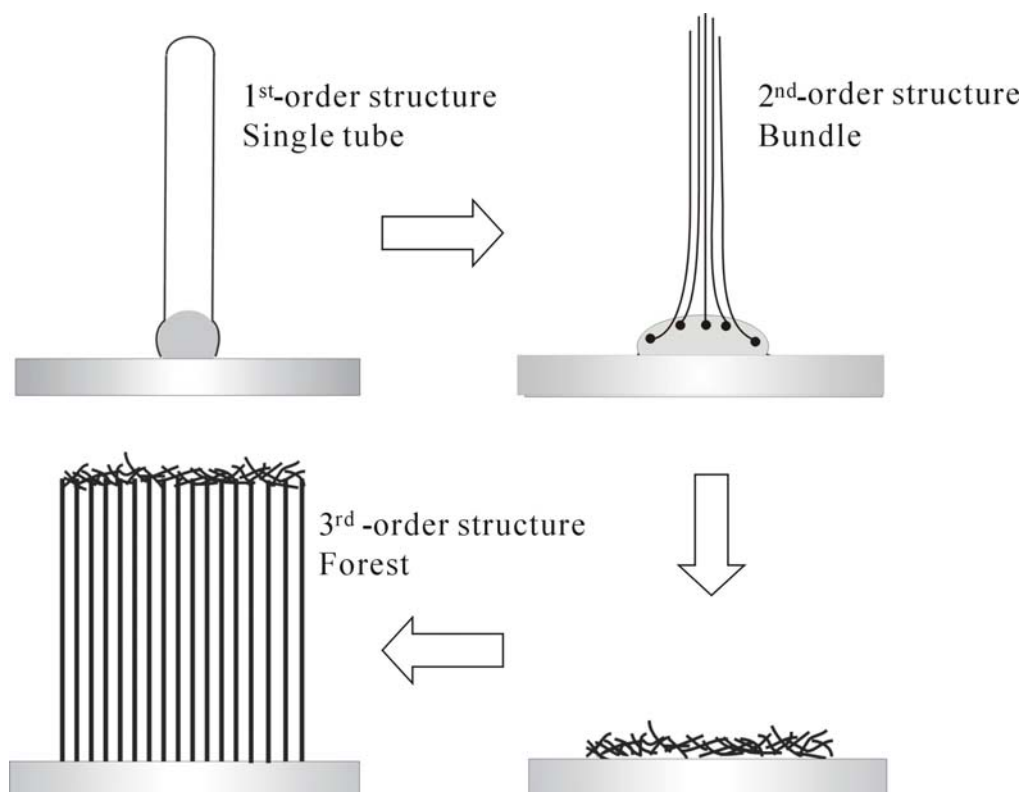
Figure 3.16: Schematic diagram of growth process of VSWNT

The results above lead us to propose a two-step mechanism for growth of VSWNTs on flat surfaces as shown schematically in figure 3.16. The first step is formation of crust of random network of SWNT. Based on the fact that as-produced VSWNTs are completely free of metal particles as shown in figure 3.8 and VSWNTs are able to grow on used substrate after removing previously grown VSWNTs, It could be inferred individual SWNTs follow bottom growth mechanism: the active nano-clusters remain on the substrate through the whole reaction and SWNT nucleation occurs with uplift of graphitic cap from the cluster surface while carbon atoms supply via surface diffusion. Recent molecular dynamics simulation also proved this process[14]. As we discussed previously, Cobalt molybdate transforms into molybdenum carbide after absorbing carbon disproportionated from carbon monoxide and release cobalt nano-clusters in the beginning of reaction. Experimental results and theoretical calculation illustrated the function of molybdenum as a carrier to stabilize active cobalt nano-clusters. Therefore, it is reasonably deluded a SWNT bundle generally originates from a Co/Mo alloy particle which has several active sites on surface for SWNT nucleation. Images for 0.19% metal concentration in Figure 3.14 clearly demonstrates how VSWNTs bundles originate from the alloy particles at the bottom. The average distance between alloy particles plays an import role here. As shown in figure 3.14, the average distance for VSWNTs was determined to be around 60-70 nm. When the average distance is larger than that, as in the case of 0.02% metal concentration, the elongating SWNT bundles are not able

148

to sustain their upward growth tendency and start bending toward any direction and end up lying down on the surface. Touching each other of bundles during growth even make things worse by holding back each other. In the case of 0.38% metal concentration, aggregated alloy particles flatten cobalt nano-clusters due to size effect and lose their activity as template for SWNT nucleation. Therefore, those big particles poison part of surface and make the actual average distance between active particles larger than that necessary for VSWNT, though small particles are still origin of SWNT bundles. When the average distance is in the proper range, the elongating bundles touch each other before losing their upward growth tendency and support each other for synergetic growth. The second step in the growth of VSWNT is aligned growth led by crust. During formation of crust, the initially different growth rate for each nanotube or bundles become averaged by crust. Finally, the crust lead all the nanotube or bundles grow at the same apparent rate toward to some direction. That is the reason why the top of forest is always smooth and uniformly high.

3.4.3.4   *Simulation of VSWNT Growth*

To further understand the growth process of VSWNT, a simulation based our previous data can be used to investigate the mechanism. The mechanism of carbon filament formation assumes that the carbon atoms, formed on the metallic surface from the hydrocarbon decomposition, will react forming surface metallic carbide.

The process of decomposition-segregation of this carbide allows the carbon atoms to penetrate into the metallic particle, and finally regenerate the metallic surface. The evolution of the carbon concentration at the interface of the metallic carbide and the metal particle, C_B, can be expressed according to first-order kinetics,

$$dC_B/dt = k_B(C_S - C_B), \tag{1}$$

where the parameter k_B represents the coefficient of segregation-diffusion of the surface metallic carbide. It depends on the diffusivity of the carbon through the surface carbide, the carbide phase thickness, and the exposed surface area of this carbide. C_S represents the carbon surface concentration generated from the fed hydrocarbon decomposition. This parameter is mainly affected by the gas composition, pressure, and temperature during reaction. It will also vary with the remnant surface activity of the metal particles in the catalyst,

$$C_S = C_{S0} * a, \tag{2}$$

where C_{S0} is the carbon concentration at the gas side of the metallic particles when the catalyst is not deactivated. This model also considers that the catalyst can be deactivated by the formation of encapsulating coke. This coke can be partially removed from the catalyst surface by gasification with the hydrogen present in the reaction atmosphere. Consequently, the rate of catalyst deactivation is expressed as [31,32]

$$-da/dt = k_d a - k_r(1 - a) = k_G(a - a_S), \tag{3}$$

150

where k_d and k_r are the deactivation and regeneration kinetic constants, respectively. For a given catalyst, both kinetic parameters are a function of the operating conditions, namely temperature and gas composition. The catalyst residual activity, a_S, and the parameter k_G, dependent on k_d and k_r, are expressed as follows:

$$a_S = k_r/(k_d + k_r), \qquad k_G = k_d + k_r, \tag{4}$$

The evolution in time of the surface carbon concentration is deduced from Eqs. (2) and (3):

$$C_S = C_{S0}(a_S + (1- a_S) \exp(-k_G t), \tag{5}$$

The carbon formation (CNT) rate can be expressed as a function of the gradient of carbon concentration across the metallic particle, once the surface carbide has been produced,

$$r_C = k_C(C_B - C_F) \approx k_C C_B, \tag{6}$$

where C_B is the carbon concentration at the interface of the surface carbide and the metal particle and CF is the carbon concentration generated after diffusion through the metal particle. It can be supposed that CF is low, and so, its value is negligible with respect to CB. The effective carbon transfer coefficient, kC, depends on several factors such as the carbon diffusion coefficient, the average size of the metallic particles, and the exposed metallic surface area of the catalyst. The evolution of carbon concentration in the interface carbide-metal particle, C_B, is deduced from Eqs. (1) and (5):

$$C_B(t) = C_{S0} (a_S + k_G \alpha \exp(-k_G t)- k_B \beta \exp(-k_B t), \tag{7}$$

The terms α and β are given by

$$\alpha = k_B(1- a_S)/k_G(k_B - k_G), \qquad (8)$$

$$\beta = (k_B - k_G a_S)/k_B(k_B - k_G), \qquad (9)$$

From Eqs. (6) and (7), the evolution of carbon formation rate in time can be expressed as

$$r_C(t) = r_{C0} [a_S + k_G\alpha \exp(-k_G t)- k_B\beta \exp(-k_B t)], \qquad (10)$$

where the term r_{C0} represents the maximum rate of CNT formation that can be attained in the absence of deactivation:

$$r_{C0} = k_C C_{S0}, \qquad (11)$$

Finally the evolution of the carbon content accumulated on the catalyst, equivalent to CNTs production, can be calculated as

$$m_C(t) = \int r_C(t)\, dt, \qquad (12)$$

The integration of Eq. (10) gives the following expression:

$$m_C(t) = r_{C0} [a_S t +\alpha(1- \exp(-k_G t)) - \beta(1 - \exp(-k_B t))], \qquad (13)$$

In the case that the catalyst does not suffer deactivation, the above expression is simplified to

$$m_C(t) = r_{C0} [t - 1/k_B (1 - \exp(-k_B t))], \qquad (14)$$

Eq. (13) allows the prediction of the carbon content evolution over the catalyst as a function of the operating conditions. All the parameters of this kinetic model, r_{C0}, k_B, k_d, and k_r, have a real physical meaning and show the great influence of the catalyst properties and the operating conditions on the CNT formation rate.

By using the above model, the time evolution data in chapter 3.4.3.3 can be fitted to find those parameters in the kinetic model. Here we use 2 functions to express carbon content m_c: height of VSWNT and G/Si ratio in the Raman spectrum of VSWNT. Figure 3.17 shows the experimental data and fitted growth curve of VSWNT growth. The generated kinetic parameters are listed in Table 3.2. From the calculation, the maximum growth rate of SWNT in this system is estimated to be 0.75 µm/min, that is approximately 12.5 nm/min. This value is much smaller compared to the data obtained by L. X. Zheng et al. [58]. In their case, individual SWNTs were grown freely in the air close to the surface of silicon wafer without perturbation from other tubes while in our case the growth of SWNTs was constrained by entangling with neighboring tubes.
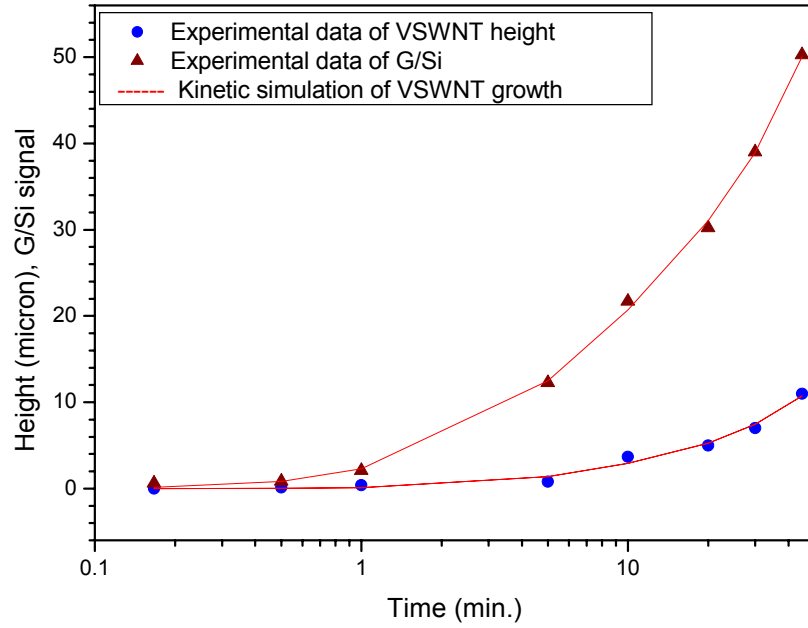
Figure 3.17: *Kinetic study of VSWNT growth with time. Triangles are experimental data of VSWNT height and circles are experimental data of G/Si for VSWNT. Red lines are fitted curve for those data. (Courtesy of Prof. Antonio Monzon, University of Zaragoza, Spain)*

Parameters	G/Si signal	Height
$r_{C0}=$	3.48223	0.75355
$k_B=$	3.04279	0.35372
$k_d=$	0.12455	0.25114
$k_r=$	0.03302	0.10234
$a_s=$	0.209557657	0.289521331

Table 3.2: *Fitted parameters in kinetic model for two expressions.*

3.4.3.5 *Restarted Growth of VSWNT*

Restarted growth of VSWNT originates from the idea catalyst remains active after the reaction is disrupted. The experiment was conducted by starting reaction as normal synthesis of VSWNT in the thermal CVD reactor and terminating reaction after 10 min with inert gas. After 5 min, reaction was restarted by switching back to CO. The produced VSWNT is shown in figure 3.18. A clear line in the middle of VSWNT is seen to separate VSWNT into 2 parts: the top part grown before disruption and the bottom part grown after disruption. Magnified image in the middle of VSWNT shows the line is a thin layer of disordered SWNTs. We may infer that some of nanotubes may still remain connected to the catalyst when the reacting species is depleted by inert gas. When reaction was turned off, discontinued growth of VSWNT made the whole film relaxed and settled back down to the surface. When reaction was turned on, the initial growth rate varies from one tube or bundle to another just as a fresh reaction begins before forming a first crust. Then the different growth rate and flexible nature of SWNT push them to bend or deviate from the original growth direction before termination. Relaxation of VSWTN after termination of reaction and the random growth forms a second layer of crust, which averages the grow rate again and start growing up together.
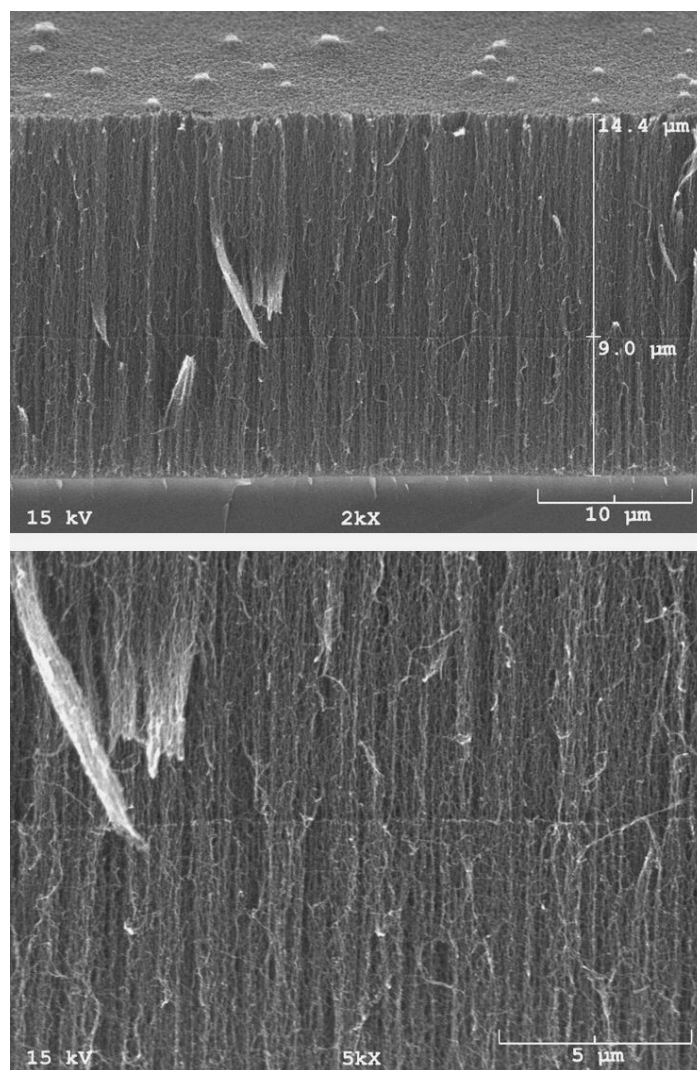
Figure 3.18: SEM Images of V-SWNT obtained with a short period of disruption by flushing system with He during production.

3.4.3.6 Patterned Growth of VSWNT

Further demonstrations of the role of the crust in determining the structure of the resulting forest have been obtained by depositing the Co-Mo catalyst in a non-uniform manner over the flat substrate. For example, when the catalyst was deposited on the rough surface side of the silicon wafer, instead of obtaining a uniform catalyst film, the catalyst preferentially deposited on the shallow depressions of the unsmooth surface (see Fig. 3.19b). As a result, the nanotube growth occurred on separate domains, with each domain generating a separate crust. Therefore, the height and orientation of each domain was somewhat different, as illustrated in Fig. 3.19c. The curvature of the top of the crust in these small domains contrasts with the much flatter surface observed on the broader area forests, for which the effects of the edges is less pronounced. One can imagine that when the crust is pushed away from the surface as the nanotube growth proceeds, the edges will be unevenly pushed up, which causes the curvature. To investigate the effects of the edges on the forest, we prepared samples in which the catalyst was only deposited on certain regions. For example, the effect of the edge is illustrated in Fig. 3.19d, which shows the separation between a region with catalyst and the bare substrate. It can be seen that the entangled crust is resting on the substrate at the border where no catalyst is present, this interaction with the substrate anchors the whole crust, and the nanotubes growing beneath make the crust curve.   Similarly, Fig. 3.19e shows the case in which, using a very fast drying rate, circular spots of dried catalyst were produced.

The small size of these islands (roughly 4 µm in diameter) and non-uniformity of catalyst distribution make the edge effect more pronounced.
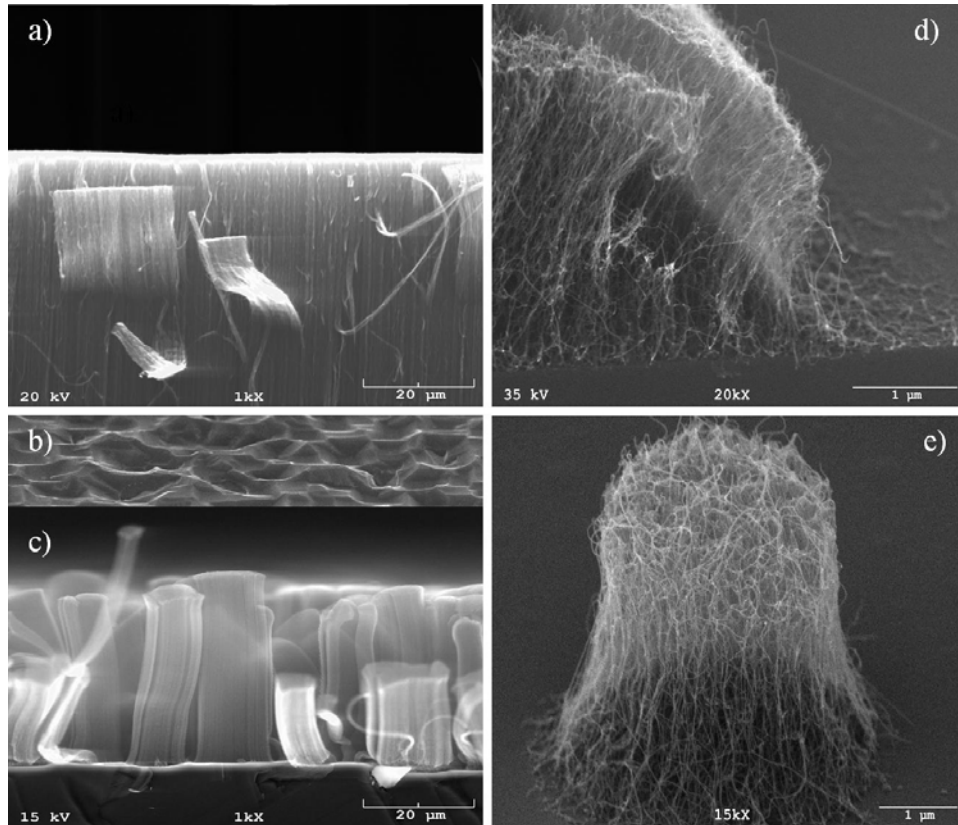
Figure 3.19: *SEM image of V-SWNT grown on a) a flat silicon wafer surface, c) a rough silicon wafer surface, d) end of a region covered with non-uniform distribution of catalyst, e) a small circular spot covered with catalyst on a bare silicon surface. b) is a rough silicon wafer surface after deposition of Co-Mo catalyst.*

3.4.4 CONCLUSION TO GROWTH MECHNISM OF VSWNT

The growth mechanism of VSWNT is explored by investigation of morphology and chemical state of Co-Mo catalyst immobilized on flat surface as well as study of evolution of VSWNT with time. Detailed characterization of catalyst by XPS and AFM demonstrate catalyst after calcinations forms well dispersed nanoparticle with chemical composition as Co Molybdate and Molybdenum oxide. The distribution of catalyst nanoparticles determines whether a VSWNT is formed or not. By studying the time evolution of VSWNT growth, VSWNT is formed through a two-step process. The first step is the weaving of a crust of entangled SWNT which grow with different rates and with random orientation over the surface. The second step is a concerted growth of vertically aligned SWNT constrained by the uniform top crust. Several examples are presented to demonstrate that the crust influences the morphology of the resulting forest. Catalysts which are non-uniformly distributed on the substrate produce curved crusts instead of the consistent forest with a flat top obtained when the catalyst layer is uniform.

3.5   PROCESSING OF VSWNT

3.5.1   *RESEARCH OBJECTIVES*

As we discussed previously, VSWNTs have broad diameter and (n,m) structure distribution. Optical absorption and Raman scattering show that semiconducting tubes in VSWNT are composed of small tube group and large tube group. Temperature programmed oxidation (TPO) performed on VSWNT also shows two peaks indicating those two group of tubes, as shown in figure 3.20.
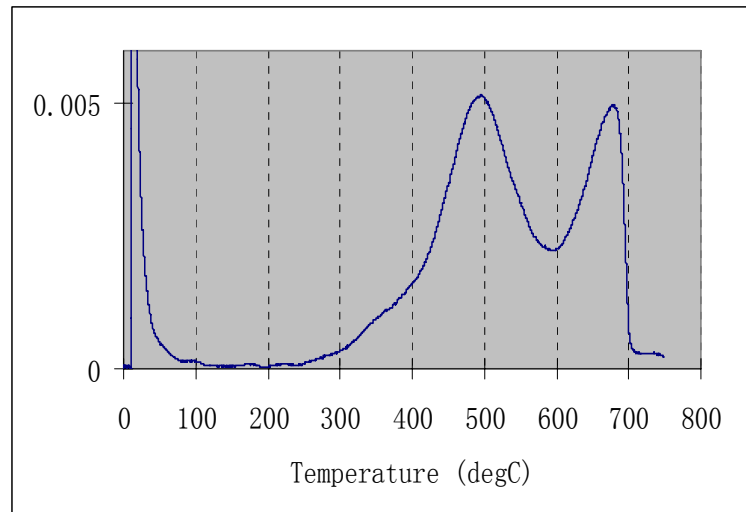
Figure 3.20: TPO of VSWNT with 5% O_2 in He. Temperature ramp is 10 ℃ per min

It is then preferable for some application if one can separate or remove one group from another. Since two group of tubes are burned with O_2/He gas at different

temperatures, selective oxidation might be a good option to accomplish the goal. Theoretically, small tubes is oxidized first at lower temperature because of their high reactivity resulted from higher degree of C-C bond bending. Thus, one of the research objectives is to investigate effect of selective oxidation by O_2.

VSWNTs have been propose to be a good candidate for several applications such as nano heat sink, light emission display, photovoltaic device, and biosensor. For these applications, VSWNT is required to mount on a conductive substrate. Since direct synthesis of VSWNT on conductive substrate has not been realized yet, transfer of VSWNT to another substrate is attempted. Therefore, another objective in this project is to develop method to transfer VSWNT without damaging its ordered structure.

3.5.2   *EXPERIMENTAL SETUP*

Selective oxidation of VSWNT was conducted in a horizontal CVD reactor by flowing 5% O_2 /He at required temperature for 20 min. Partially oxidized VSWTN was characterized by SEM and TEM. SEM imaging was finished in JEOL JSM-880 High Resolution SEM equipped with backscattered electron detector, transmitted electron detector, electron channelling imaging , and Kevex X-ray analyzer with IXRF software. TEM imaging was carried out in JEOL 2000-FX Intermediate Voltage STEM equipped with secondary electron detector, Gatan Digi-PEELS

Electron Energy Loss Spectrometer, Kevex Quantum 10 mm2 X-ray detector, and IXRF X-ray analyzer with digital imaging capability.

3.5.3   RESULTS AND DISCUSSION

3.5.3.1   Oxidation of VSWNT

Figure 3.21 shows VSWNT selectively oxidized at different temperatures. To determine the thermal effect, one VSWNT sample was heated in He environment without burning tubes. It was found in figure a) and d), VSWNT after annealing at 550 °C apparently shows no difference from the original VSWNT as shown in figure 3.7. Compared to the big cracks in the oxidized VSWNT of b) and c), annealed VSWNT remains continuous film of SWNT because the heat stress generated during heating is dissipated by the ordered structure. From image b) and c), it seems oxidation starts from the bottom where catalyst connects with SWNT, which is evidenced by the fact, . The non-uniform oxidation at the bottom and other part of VSWNT generates enough stress to break the whole VSWNT. Once the crack is formed, SWNTs on the edge of crack seem to be burned at first. It is noteworthy that top of VSWNT appears smoother after burning. A close look at the VSWNT from the top shows more open structure in f) with small braches being burned already.
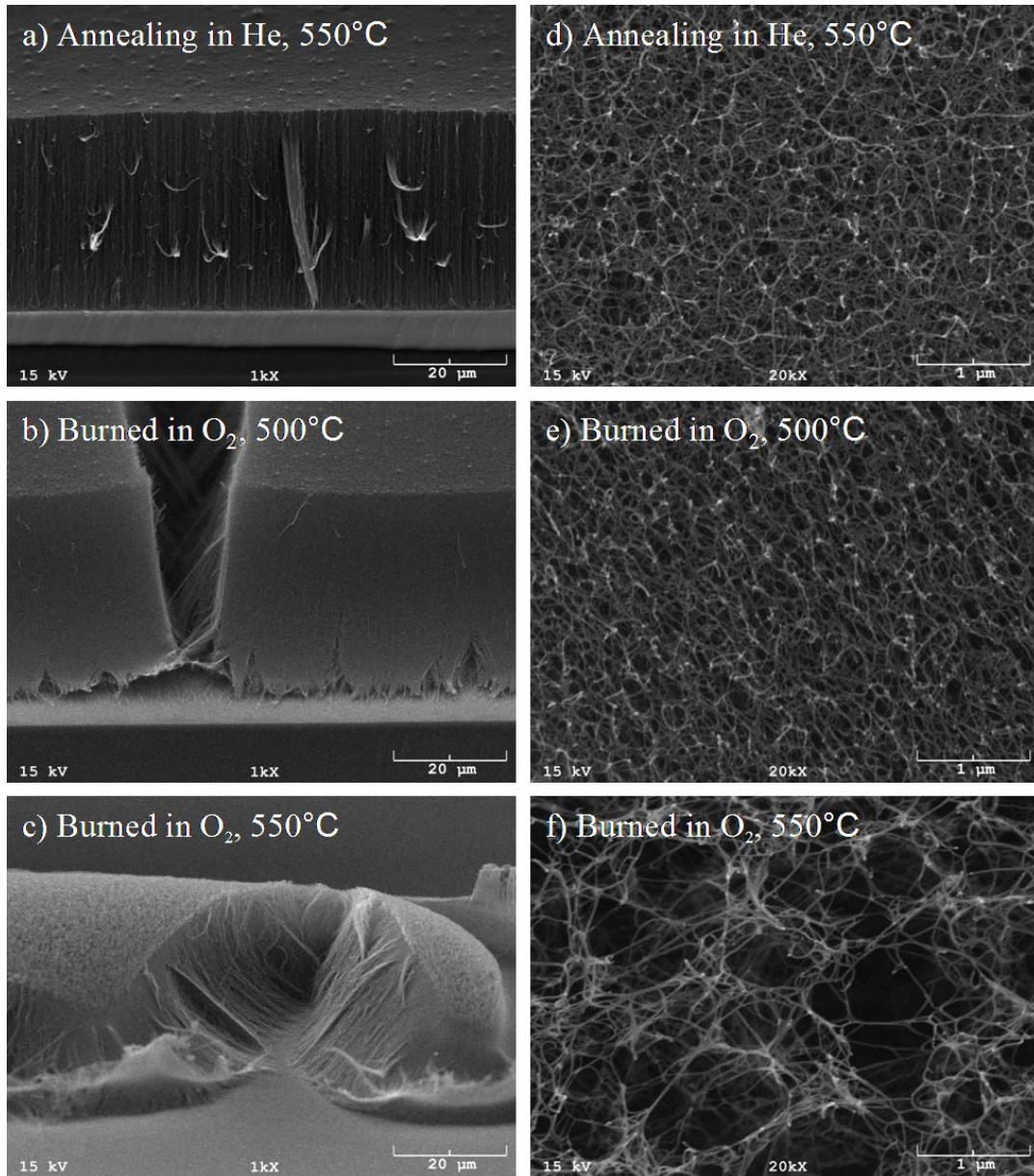
Figure 3.21: morphological change of VSWNT after being selectively oxidized by 5% O2 /He at 500℃ and 550℃. a) and d) are side view and top view of VSWNT annealed in He, b) and e) are VSWNT oxidized at 500℃, c) and f) are VSWNT oxidized at 550℃.

a) VSWNT before oxidation

20 nm

a) VSWNT after oxidation

10nm
x500k
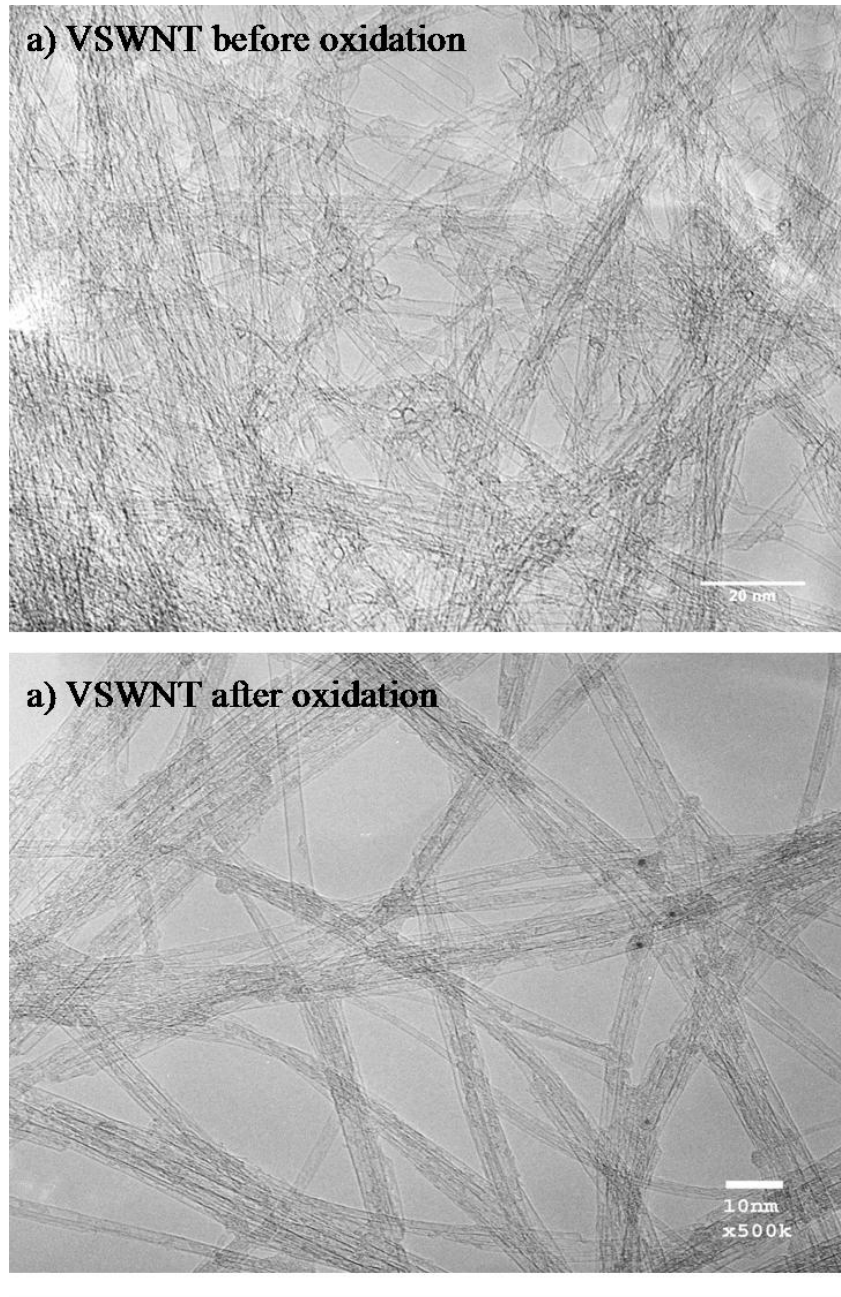
Figure 3.22: *TEM images of VSWNT before (a) and after (b) oxidation*

in O2/He at 550℃.

As what we expected, small tubes are burned first at lower temperature as shown in figure 3.22. The TEM images of VSWNTs before and after oxidation demonstrate a clear difference between them. VSWNTs before oxidation are clean, long, and diverse in diameter. After oxidation, most of small tubes disappear and only large tubes remain. Some tubes are even cut in the middle. A very interesting phenomena we observed is lots of these residual tubes are filled with something inside. It is speculated those fillings are tiny fragments of SWNT left behind oxidation.

3.5.3.2 *Transfer of VSWNT*

We have developed two methods to detach the VSWNT film from Si substrate. One is similar to preparation of thin film for TEM grid. The procedure is as follows: Buffer solution (pH=7) is in a glass beaker. A silicon wafer with VSWNT grown on that is slowly submerged into the buffer at an angle of roughly 20 celsius degree. As the sample is submerged slowly, the VSWNT film starts to depart from the substrate and move laterally onto the water surface. In the end, the detached film floats on the water surface as shown in figure 3.23a. Then one can use any substrate to pick up film from beneath the film. It is worth noticing that the transferred VSWNT remains exactly the same as before transferring.
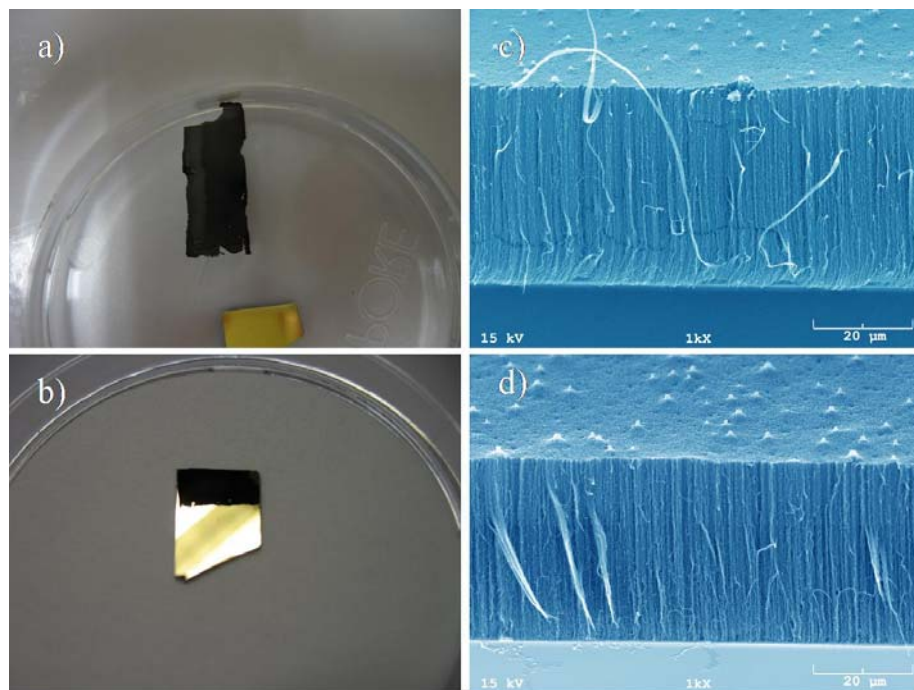
Figure 3.23: VSWNT transferred to Au surface by wet method. a) VSWNT detached from Si wafer and floating on the water, b) VSWNT transferred to Au surface, c) SEM image of original VSWNT, d) SEM image of VSWNT after transfer.

Another method used to transfer VSWNT is similar to wax process for removing hair. A scotch tape or copper tape is first attached on the surface of VSWNT. Push it with a little force and peel the tape off. The VSWNT will come off the Si substrate with tape as shown in figure 3.24. Compared to the first method, the transferred VSWNT was flip over with the spiky top the original bottom of untreated VSWNT. In addition, the VSWNT is deformed to some extent due to pressure imparted on top of VSWNT during process.
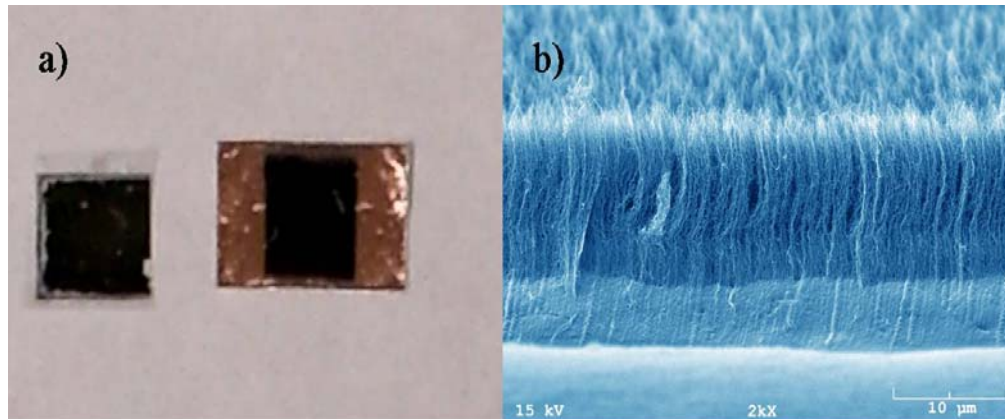
Figure 3.24: *VSWNT transferred to sticky tape surface*

3.5.4 CONCLUSION TO PROCESSING OF VSWNT

We have demonstrated that VSWNT can be selectively oxidized to remove small tubes. During oxidation process, some fragment of SWNT or other things diffuse into large nanotubes. We have also developed two methods to transfer VSWNT onto other substrates without damaging its structure. In the wet method involving using buffer solution, the transferred VSWNT remains exactly the same as before transferring. On the other hand, the transferred VSWNT is deformed to some extent due to pressure imparted on top of VSWNT during process and the VSWNT was flip over with the spiky top the original bottom of untreated VSWNT.

3.6 REFERENCES

1. Ruoff, R. S.; Lorents, D. C., Mechanical and Thermal-Properties of Carbon Nanotubes. *Carbon* **1995,** 33, (7), 925-930.

2. Lu, J. P., Elastic properties of single and multilayered nanotubes. *Journal of Physics and Chemistry of Solids* **1997,** 58, (11), 1649-1652.

3. Kataura, H.; Kumazawa, Y.; Maniwa, Y.; Umezu, I.; Suzuki, S.; Ohtsuka, Y.; Achiba, Y., Optical properties of single-wall carbon nanotubes. *Synthetic Metals* **1999,** 103, (1-3), 2555-2558.

4. Salvetat, J. P.; Bonard, J. M.; Thomson, N. H.; Kulik, A. J.; Forro, L.; Benoit, W.; Zuppiroli, L., Mechanical properties of carbon nanotubes. *Applied Physics a-Materials Science & Processing* **1999,** 69, (3), 255-260.

5. Odom, T. W.; Huang, J. L.; Kim, P.; Lieber, C. M., Structure and electronic properties of carbon nanotubes. *Journal of Physical Chemistry B* **2000,** 104, (13), 2794-2809.

6. Maslov, L., Concept of nonvolatile memory based on multiwall carbon nanotubes. *Nanotechnology* **2006,** 17, (10), 2475-2482.

7. Cui, J. B.; Sordan, R.; Burghard, M.; Kern, K., Carbon nanotube memory devices of high charge storage stability. *Applied Physics Letters* **2002,** 81, (17), 3260-3262.

8. Sun, J. P.; Wang, T. H., A carbon nanotube-based novolatile random access memory. *Acta Physica Sinica* **2002,** 51, (9), 2096-2100.

9. Bachtold, A.; Hadley, P.; Nakanishi, T.; Dekker, C., Logic circuits with carbon nanotube transistors. *Science* **2001,** 294, (5545), 1317-1320.

10. Rueckes, T.; Kim, K.; Joselevich, E.; Tseng, G. Y.; Cheung, C. L.; Lieber, C. M., Carbon nanotube-based nonvolatile random access memory for molecular computing. *Science* **2000,** 289, (5476), 94-97.

11. Nieuwoudt, A.; Massoud, Y., Evaluating the impact of resistance in carbon nanotube bundles for VLSI interconnect using diameter-dependent modeling techniques. *Ieee Transactions on Electron Devices* **2006,** 53, (10), 2460-2466.

12. Ngo, Q.; Cassell, A. M.; Austin, A. J.; Li, J.; Krishnan, S.; Meyyappan, M.; Yang, C. Y., Characteristics of aligned carbon nanofibers for interconnect via applications. *Ieee Electron Device Letters* **2006,** 27, (4), 221-224.

13. Raychowdhury, A.; Roy, K., Modeling of metallic carbon-nanotube interconnects for circuit simulations and a comparison with Cu interconnects for scaled technologies. *Ieee Transactions on Computer-Aided Design of Integrated Circuits and Systems* **2006,** 25, (1), 58-65.

14. Naeemi, A.; Meindl, J. D., Impact of electron-phonon scattering on the performance of carbon nanotube interconnects for GSI. *Ieee Electron Device Letters* **2005,** 26, (7), 476-478.

15. Nihei, M.; Kawabata, A.; Kondo, D.; Horibe, M.; Sato, S.; Awano, Y., Electrical properties of carbon nanotube bundles for future via interconnects. *Japanese Journal of Applied Physics Part 1-Regular Papers Short Notes & Review Papers* **2005,** 44, (4A), 1626-1628.

16. Naeemi, A.; Sarvari, R.; Meindl, J. D., Performance comparison between carbon nanotube and copper interconnects for gigascale integration (GSI). *Ieee Electron Device Letters* **2005,** 26, (2), 84-86.

17. [Anon], Transistor nodes along carbon nanotube interconnect pipes. *Solid State Technology* **2004,** 47, (6), 18-18.

18. Kreupl, F.; Graham, A. P.; Duesberg, G. S.; Steinhogl, W.; Liebau, M.; Unger, E.; Honlein, W., Carbon nanotubes in interconnect applications. *Microelectronic Engineering* **2002,** 64, (1-4), 399-408.

19. Jung, H. Y.; Jung, S. M.; Gu, G. H.; Suh, J. S., Anodic aluminum oxide membrane bonded on a silicon wafer for carbon nanotube field emitter arrays. *Applied Physics Letters* **2006,** 89, (1), -.

20. Song, Y. H.; Kim, K. B.; Hwang, C. S.; Park, D. J.; Lee, J. H.; Kang, K. Y.; Hur, J. H.; Jang, J., Active-matrix field-emission display based on a CNT emitter and a-Si TFTs. *Journal of the Society for Information Display* **2005,** 13, (3), 241-244.

21. Kurachi, H.; Uemura, S.; Yotani, J.; Nagasako, T.; Yamada, H.; Ezaki, T.; Maesoba, T.; Nakao, T.; Ito, M.; Sakurai, A.; Saito, Y.; Shinohara, H., Uniform carbon-nanotube

emitter for field-emission displays. *Journal of the Society for Information Display* **2005,** 13, (9), 727-733.

22.   Hahn, J.; Jung, S. M.; Jung, H. Y.; Heo, S. B.; Shin, J. H.; Suh, J. S., Fabrication of clean carbon nanotube field emitters. *Applied Physics Letters* **2006,** 88, (11), -.

23.   Contarino, M. R.; Sergi, M.; Harrington, A. E.; Lazareck, A.; Xu, J.; Chaiken, I., Modular, self-assembling peptide linkers for stable and regenerable carbon nanotube biosensor interfaces. *Journal of Molecular Recognition* **2006,** 19, (4), 363-371.

24.   Gabai, R.; Segev, L.; Joselevich, E., Single polymer chains as specific transducers of molecular recognition in scanning probe microscopy. *Journal of the American Chemical Society* **2005,** 127, (32), 11390-11398.

25.   Herrera, J. E.; Resasco, D. E., Loss of single-walled carbon nanotubes selectivity by disruption of the Co-Mo interaction in the catalyst. *Journal of Catalysis* **2004,** 221, (2), 354-364.

26.   Kitiyanan, B.; Alvarez, W. E.; Harwell, J. H.; Resasco, D. E., Controlled production of single-wall carbon nanotubes by catalytic decomposition of CO on bimetallic Co-Mo catalysts. *Chemical Physics Letters* **2000,** 317, (3-5), 497-503.

27.   Resasco, D. E.; Alvarez, W. E.; Pompeo, F.; Balzano, L.; Herrera, J. E.; Kitiyanan, B.; Borgna, A., A scalable process for production of single-walled carbon nanotubes (SWNTs) by catalytic disproportionation of CO on a solid catalyst. *Journal of Nanoparticle Research* **2002,** 4, (1-2), 131-136.

28.   Resasco, D. E.; Kitiyanan, L.; Alvarez, W. E.; Borgna, A., Effective Co-Mo bimetallic catalysts for the production of single-wall carbon nanotubes by decomposition of Co. *Abstracts of Papers of the American Chemical Society* **2000,** 219, U536-U536.

29.   Nikolaev, P.; Bronikowski, M. J.; Bradley, R. K.; Rohmund, F.; Colbert, D. T.; Smith, K. A.; Smalley, R. E., Gas-phase catalytic growth of single-walled carbon nanotubes from carbon monoxide. *Chemical Physics Letters* **1999,** 313, (1-2), 91-97.

30.   Guo, T.; Nikolaev, P.; Thess, A.; Colbert, D. T.; Smalley, R. E., Catalytic Growth of Single-Walled Nanotubes by Laser Vaporization. *Chemical Physics Letters* **1995,** 243, (1-2), 49-54.

31. Scott, C. D.; Arepalli, S.; Nikolaev, P.; Smalley, R. E., Growth mechanisms for single-wall carbon nanotubes a laser ablation process (vol 72, pg 573, 2001). *Applied Physics a-Materials Science & Processing* **2002,** 74, (1), 11-11.

32. Shin, K. Y.; Su, H. C.; Tsai, C. H., In situ growth of single-walled carbon nanotubes by bimetallic technique with/without dielectric support for nanodevice applications. *Journal of Vacuum Science & Technology B* **2006,** 24, (1), 358-361.

33. Li, Y. M.; Mann, D.; Rolandi, M.; Kim, W.; Ural, A.; Hung, S.; Javey, A.; Cao, J.; Wang, D. W.; Yenilmez, E.; Wang, Q.; Gibbons, J. F.; Nishi, Y.; Dai, H. J., Preferential growth of semiconducting single-walled carbon nanotubes by a plasma enhanced CVD method. *Nano Letters* **2004,** 4, (2), 317-321.

34. Nerushev, O. A.; Dittmar, S.; Morjan, R. E.; Rohmund, F.; Campbell, E. E. B., Particle size dependence and model for iron-catalyzed growth of carbon nanotubes by thermal chemical vapor deposition. *Journal of Applied Physics* **2003,** 93, (7), 4185-4190.

35. Nerushev, O. A.; Morjan, R. E.; Ostrovskii, D. I.; Sveningsson, M.; Jonsson, M.; Rohmund, F.; Campbell, E. E. B., The temperature dependence of Fe-catalysed growth of carbon nanotubes on silicon substrates. *Physica B-Condensed Matter* **2002,** 323, (1-4), 51-59.

36. Yoon, Y. J.; Bae, J. C.; Baik, H. K.; Cho, S. J.; Lee, S. J.; Song, K. M.; Myung, N. S., Nucleation and growth control of carbon nanotubes in CVD process. *Physica B-Condensed Matter* **2002,** 323, (1-4), 318-320.

37. Yoon, Y. J.; Bae, J. C.; Baik, H. K.; Cho, S.; Lee, S. J.; Song, K. M.; Myung, N. S., Growth control of single and multi-walled carbon nanotubes by thin film catalyst. *Chemical Physics Letters* **2002,** 366, (1-2), 109-114.

38. Delzeit, L. D.; Cassel, A.; Stevens, R. M. D.; Nguyen, C.; Meyyappan, M., Novel catalyst deposition technique for the growth of carbon nanotubes. *Abstracts of Papers of the American Chemical Society* **2001,** 221, U628-U628.

39. Zhang, R. Y.; Amlani, L.; Baker, J.; Tresek, J.; Tsui, R. K., Chemical vapor deposition of single-walled carbon nanotubes using ultrathin Ni/Al film as catalyst. *Nano Letters* **2003,** 3, (6), 731-735.

40. Zhang, R.; Tsui, R. K.; Tresek, J.; Rawlett, A. M.; Amlani, I.; Hopson, T.; Fejes, P., Formation of single-walled carbon nanotubes via reduced-pressure thermal chemical vapor deposition. *Journal of Physical Chemistry B* **2003,** 107, (14), 3137-3140.

41. Hongo, H.; Yudasaka, M.; Ichihashi, T.; Nihey, F.; Iijima, S., Chemical vapor deposition of single-wall carbon nanotubes on iron-film-coated sapphire substrates. *Chemical Physics Letters* **2002,** 361, (3-4), 349-354.

42. Hongo, H.; Nihey, F.; Ichihashi, T.; Ochiai, Y.; Yudasaka, M.; Iijima, S., Support materials based on converted aluminum films for chemical vapor deposition growth of single-wall carbon nanotubes. *Chemical Physics Letters* **2003,** 380, (1-2), 158-164.

43. Li, Y. M.; Kim, W.; Zhang, Y. G.; Rolandi, M.; Wang, D. W.; Dai, H. J., Growth of single-walled carbon nanotubes from discrete catalytic nanoparticles of various sizes. *Journal of Physical Chemistry B* **2001,** 105, (46), 11424-11431.

44. Homma, Y.; Kobayashi, Y.; Ogino, T.; Yamashita, T., Growth of suspended carbon nanotube networks on 100-nm-scale silicon pillars. *Applied Physics Letters* **2002,** 81, (12), 2261-2263.

45. Homma, Y.; Yamashita, T.; Finnie, P.; Tomita, M.; Ogino, T., Single-walled carbon nanotube growth on silicon substrates using nanoparticle catalysts. *Japanese Journal of Applied Physics Part 2-Letters* **2002,** 41, (1ab), L89-L91.

46. Amama, P. B.; Ogebule, O.; Maschmann, M. R.; Sands, T. D.; Fisher, T. S., Dendrimer-assisted low-temperature growth of carbon nanotubes by plasma-enhanced chemical vapor deposition. *Chemical Communications* **2006**, (27), 2899-2901.

47. Amama, P. B.; Maschmann, M. R.; Fisher, T. S.; Sands, T. D., Dendrimer-templated Fe nanoparticles for the growth of single-wall carbon nanotubes by plasma-enhanced CVD. *Journal of Physical Chemistry B* **2006,** 110, (22), 10636-10644.

48. Zhang, Y. G.; Chang, A. L.; Cao, J.; Wang, Q.; Kim, W.; Li, Y. M.; Morris, N.; Yenilmez, E.; Kong, J.; Dai, H. J., Electric-field-directed growth of aligned single-walled carbon nanotubes. *Applied Physics Letters* **2001,** 79, (19), 3155-3157.

49. Chen, Z.; Yang, Y. L.; Wu, Z. Y.; Luo, G.; Xie, L. M.; Liu, Z. F.; Ma, S. J.; Guo, W. L., Electric-field-enhanced assembly of single-walled carbon nanotubes on a solid surface. *Journal of Physical Chemistry B* **2005,** 109, (12), 5473-5477.

50. El-Hami, K.; Matsushige, K., Alignment of different lengths of carbon nanotubes using low applied electric field. *Ieice Transactions on Electronics* **2004,** E87c, (12), 2116-2118.

51. Dittmer, S.; Svensson, J.; Campbell, E. E. B., Electric field aligned growth of single-walled carbon nanotubes. *Current Applied Physics* **2004,** 4, (6), 595-598.

52. Jang, Y. T.; Ahn, J. H.; Ju, B. K.; Lee, Y. H., Lateral growth of aligned mutilwalled carbon nanotubes under electric field. *Solid State Communications* **2003,** 126, (6), 305-308.

53. Chen, X. Q.; Saito, T.; Yamada, H.; Matsushige, K., Aligning single-wall carbon nanotubes with an alternating-current electric field. *Applied Physics Letters* **2001,** 78, (23), 3714-3716.

54. Avigal, Y.; Kalish, R., Growth of aligned carbon nanotubes by biasing during growth. *Applied Physics Letters* **2001,** 78, (16), 2291-2293.

55. Srivastava, A.; Srivastava, A. K.; Srivastava, O. N., Curious aligned growth of carbon nanotubes under applied electric field. *Carbon* **2001,** 39, (2), 201-206.

56. Fischer, J. E.; Zhou, W.; Vavro, J.; Llaguno, M. C.; Guthy, C.; Haggenmueller, R.; Casavant, M. J.; Walters, D. E.; Smalley, R. E., Magnetically aligned single wall carbon nanotube films: Preferred orientation and anisotropic transport properties. *Journal of Applied Physics* **2003,** 93, (4), 2157-2163.

57. Huang, S. M.; Woodson, M.; Smalley, R.; Liu, J., Growth mechanism of oriented long single walled carbon nanotubes using "fast-heating" chemical vapor deposition process. *Nano Letters* **2004,** 4, (6), 1025-1028.

58. Zheng, L. X.; O'Connell, M. J.; Doorn, S. K.; Liao, X. Z.; Zhao, Y. H.; Akhadov, E. A.; Hoffbauer, M. A.; Roop, B. J.; Jia, Q. X.; Dye, R. C.; Peterson, D. E.; Huang, S. M.; Liu, J.; Zhu, Y. T., Ultralong single-wall carbon nanotubes. *Nature Materials* **2004,** 3, (10), 673-676.

59. Huang, S. M.; Maynor, B.; Cai, X. Y.; Liu, J., Ultralong, well-aligned single-walled carbon nanotube architectures on surfaces. *Advanced Materials* **2003,** 15, (19), 1651-+.

60. Huang, S. M.; Cai, X. Y.; Liu, J., Growth of millimeter-long and horizontally aligned single-walled carbon nanotubes on flat substrates. *Journal of the American Chemical Society* **2003,** 125, (19), 5636-5637.

61. Huang, S. M.; Cai, X. Y.; Du, C. S.; Liu, J., Oriented long single walled carbon nanotubes on substrates from floating catalysts. *Journal of Physical Chemistry B* **2003,** 107, (48), 13251-13254.

62. Sato, H.; Tagegawa, H.; Saito, Y., Vertically aligned carbon nanotubes grown by plasma enhanced chemical vapor deposition. *Journal of Vacuum Science & Technology B* **2003,** 21, (6), 2564-2568.

63. Wang, S. G.; Wang, J. H.; Ma, Z. B.; Wang, C. X.; Man, W. D.; Zhang, B. H., Vertically aligned carbon nanotubes grown on geometrically different types of surface. *Diamond and Related Materials* **2003,** 12, (12), 2175-2177.

64. Geohegan, D. B.; Puretzky, A. A.; Ivanov, I. N.; Jesse, S.; Eres, G.; Howe, J. Y., In situ growth rate measurements and length control during chemical vapor deposition of vertically aligned multiwall carbon nanotubes. *Applied Physics Letters* **2003,** 83, (9), 1851-1853.

65. Hiramatsu, M.; Ito, K.; Lau, C. H.; Foord, J. S.; Hori, M., Fabrication of vertically aligned carbon nanostructures by microwave plasma-enhanced chemical vapor deposition. *Diamond and Related Materials* **2003,** 12, (3-7), 786-789.

66. Huh, Y.; Lee, J. Y.; Lee, J. H.; Lee, T. J.; Lyu, S. C.; Lee, C. J., Selective growth and field emission of vertically well-aligned carbon nanotubes on hole-patterned silicon substrates. *Chemical Physics Letters* **2003,** 375, (3-4), 388-392.

67. Kim, N. S.; Lee, Y. T.; Park, J.; Han, J. B.; Choi, Y. S.; Choi, S. Y.; Choo, J.; Lee, G. H., Vertically aligned carbon nanotubes grown by pyrolysis of iron, cobalt, and nickel phthalocyanines. *Journal of Physical Chemistry B* **2003,** 107, (35), 9249-9255.

68. Kumar, M.; Ando, Y., Camphor-a botanical precursor producing garden of carbon nanotubes. *Diamond and Related Materials* **2003,** 12, (3-7), 998-1002.

69. Nihei, M.; Kawabata, A.; Awano, Y., Direct diameter-controlled growth of multiwall carbon nanotubes on nickel-silicide layer. *Japanese Journal of Applied Physics Part 2-Letters* **2003,** 42, (6B), L721-L723.

70.	Pan, Z. W.; Zhu, H. G.; Zhang, Z. T.; Im, H. J.; Dai, S.; Beach, D. B.; Lowndes, D. H., Patterned growth of vertically aligned carbon nanotubes on pre-patterned iron/silica substrates prepared by sol-gel and shadow masking. *Journal of Physical Chemistry B* **2003,** 107, (6), 1338-1344.

71.	Zhang, W. D.; Wen, Y.; Li, J.; Xu, G. Q.; Gan, L. M., Synthesis of vertically aligned carbon nanotubes films on silicon wafers by pyrolysis of ethylenediamine. *Thin Solid Films* **2002,** 422, (1-2), 120-125.

72.	Maruyama, S.; Einarsson, E.; Murakami, Y.; Edamura, T., Growth process of vertically aligned single-walled carbon nanotubes. *Chemical Physics Letters* **2005,** 403, (4-6), 320-323.

73.	Murakami, Y.; Chiashi, S.; Miyauchi, Y.; Hu, M. H.; Ogura, M.; Okubo, T.; Maruyama, S., Growth of vertically aligned single-walled carbon nanotube films on quartz substrates and their optical anisotropy. *Chemical Physics Letters* **2004,** 385, (3-4), 298-303.

74.	Futaba, D. N.; Hata, K.; Namai, T.; Yamada, T.; Mizuno, K.; Hayamizu, Y.; Yumura, M.; Iijima, S., 84% Catalyst activity of water-assisted growth of single walled carbon nanotube forest characterization by a statistical and macroscopic approach. *Journal of Physical Chemistry B* **2006,** 110, (15), 8035-8038.

75.	Futaba, D. N.; Hata, K.; Yamada, T.; Mizuno, K.; Yumura, M.; Iijima, S., Kinetics of water-assisted single-walled carbon nanotube synthesis revealed by a time-evolution analysis. *Physical Review Letters* **2005,** 95, (5), -.

76.	Futaba, D. N.; Hata, K.; Mizuno, K.; Yamada, T.; Yumura, M.; Iijima, S., Growth kinetics of water-assisted single-walled carbon nanotube synthesis. *Abstracts of Papers of the American Chemical Society* **2005,** 229, U1040-U1040.

77.	Hata, K.; Futaba, D. N.; Mizuno, K.; Namai, T.; Yumura, M.; Iijima, S., Water-assisted highly efficient synthesis of impurity-free single-waited carbon nanotubes. *Science* **2004,** 306, (5700), 1362-1364.

78.	Zhang, G. Y.; Mann, D.; Zhang, L.; Javey, A.; Li, Y. M.; Yenilmez, E.; Wang, Q.; McVittie, J. P.; Nishi, Y.; Gibbons, J.; Dai, H. J., Ultra-high-yield growth of vertical single-walled carbon nanotubes: Hidden roles of hydrogen and oxygen. *Proceedings of*

the National Academy of Sciences of the United States of America **2005,** 102, (45), 16141-16145.

79.   Lolli, G.; Zhang, L. A.; Balzano, L.; Sakulchaicharoen, N.; Tan, Y. Q.; Resasco, D. E., Tailoring (n,m) structure of single-walled carbon nanotubes by modifying reaction conditions and the nature of the support of CoMo catalysts. *Journal of Physical Chemistry B* **2006,** 110, (5), 2108-2115.

80.   Resasco, D. E.; Balzano, L.; Lolli, G.; Zhang, L. A., Catalytic synthesis of single-walled carbon nanotubes: Comparison of different production methods and critical analysis of proposed mechanisms (tutorial). *Abstracts of Papers of the American Chemical Society* **2005,** 229, U910-U910.

81.   Resasco, D. E.; Herrera, J. E.; Balzano, L., Controlling the structure of single-walled carbon nanotube with purposely designed heterogeneous catalysts. *Abstracts of Papers of the American Chemical Society* **2004,** 227, U274-U274.

82.   Zhang, L.; Balzano, L.; Resasco, D. E., Single-walled carbon nanotubes of controlled diameter and bundle size and their field emission properties. *Journal of Physical Chemistry B* **2005,** 109, (30), 14375-14381.

83.   Jorio, A.; Pimenta, M. A.; Souza, A. G.; Saito, R.; Dresselhaus, G.; Dresselhaus, M. S., Characterizing carbon nanotube samples with resonance Raman scattering. *New Journal of Physics* **2003,** 5, -.

84.   Dresselhaus, M. S.; Dresselhaus, G.; Saito, R., Physics of Carbon Nanotubes. *Carbon* **1995,** 33, (7), 883-891.

85.   Martel, R.; Schmidt, T.; Shea, H. R.; Hertel, T.; Avouris, P., Single- and multi-wall carbon nanotube field-effect transistors. *Applied Physics Letters* **1998,** 73, (17), 2447-2449.

86.   Chen, Y. C.; Raravikar, N. R.; Schadler, L. S.; Ajayan, P. M.; Zhao, Y. P.; Lu, T. M.; Wang, G. C.; Zhang, X. C., Ultrafast optical switching properties of single-wall carbon nanotube polymer composites at 1.55 mu m. *Applied Physics Letters* **2002,** 81, (6), 975-977.

87.   Sakakibara, Y.; Rozhin, A. G.; Kataura, H.; Achiba, Y.; Tokumoto, M., Carbon nanotube-poly(vinylalcohol) nanocomposite film devices: Applications for femtosecond fiber laser mode lockers and optical amplifier noise suppressors.

Japanese Journal of Applied Physics Part 1-Regular Papers Short Notes & Review Papers **2005,** 44, (4A), 1621-1625.

88.   Ajiki, H.; Ando, T., Aharonov-Bohm Effect in Carbon Nanotubes. *Physica B* **1994,** 201, 349-352.

89.   Shyu, F. L.; Lin, M. F., pi plasmons in two-dimensional arrays of aligned carbon nanotubes. *Physical Review B* **1999,** 60, (20), 14434-14440.

90.   Hwang, J.; Gommans, H. H.; Ugawa, A.; Tashiro, H.; Haggenmueller, R.; Winey, K. I.; Fischer, J. E.; Tanner, D. B.; Rinzler, A. G., Polarized spectroscopy of aligned single-wall carbon nanotubes. *Physical Review B* **2000,** 62, (20), R13310-R13313.

91.   Islam, M. F.; Milkie, D. E.; Kane, C. L.; Yodh, A. G.; Kikkawa, J. M., Direct measurement of the polarized optical absorption cross section of single-wall carbon nanotubes. *Physical Review Letters* **2004,** 93, (3), -.

92.   Anglaret, E.; Righi, A.; Sauvajol, J. L.; Bernier, P.; Vigolo, B.; Poulin, P., Raman resonance and orientational order in fibers of single-wall carbon nanotubes. *Physical Review B* **2002,** 65, (16), -.

93.   Duesberg, G. S.; Loa, I.; Burghard, M.; Syassen, K.; Roth, S., Polarized Raman spectroscopy on isolated single-wall carbon nanotubes. *Physical Review Letters* **2000,** 85, (25), 5436-5439.

94.   Frogley, M. D.; Zhao, Q.; Wagner, H. D., Polarized resonance Raman spectroscopy of single-wall carbon nanotubes within a polymer under strain. *Physical Review B* **2002,** 65, (11), -.

95.   Ichida, M.; Mizuno, S.; Kataura, H.; Achiba, Y.; Nakamura, A., Anisotropic optical properties of mechanically aligned single-walled carbon nanotubes in polymer. *Applied Physics a-Materials Science & Processing* **2004,** 78, (8), 1117-1120.

96.   Jorio, A.; Dresselhaus, G.; Dresselhaus, M. S.; Souza, M.; Dantas, M. S. S.; Pimenta, M. A.; Rao, A. M.; Saito, R.; Liu, C.; Cheng, H. M., Polarized Raman study of single-wall semiconducting carbon nanotubes. *Physical Review Letters* **2000,** 85, (12), 2617-2620.

97.   Jorio, A.; Souza, A. G.; Brar, V. W.; Swan, A. K.; Unlu, M. S.; Goldberg, B. B.; Righi, A.; Hafner, J. H.; Lieber, C. M.; Saito, R.; Dresselhaus, G.; Dresselhaus, M. S., Polarized resonant Raman study of isolated single-wall carbon nanotubes: Symmetry

selection rules, dipolar and multipolar antenna effects. *Physical Review B* **2002,** 65, (12), -.

98. Liu, P. J.; Liu, L. Y.; Zhang, Y. F., Alignment characterization of single-wall carbon nanotubes by Raman scattering. *Physics Letters A* **2003,** 313, (4), 302-306.

99. Rao, A. M.; Jorio, A.; Pimenta, M. A.; Dantas, M. S. S.; Saito, R.; Dresselhaus, G.; Dresselhaus, M. S., Polarized Raman study of aligned multiwalled carbon nanotubes. *Physical Review Letters* **2000,** 84, (8), 1820-1823.

100. Ren, W. C.; Li, F.; Cheng, H. M., Polarized Raman analysis of aligned double-walled carbon nanotubes. *Physical Review B* **2005,** 71, (11), -.

101. Sun, H. D.; Tang, Z. K.; Chen, J.; Li, G., Polarized Raman spectra of single-wall carbon nanotubes mono-dispersed in channels of AlPO4-5 single crystals. *Solid State Communications* **1999,** 109, (6), 365-369.

102. Tan, P. H.; Hu, C. Y.; Dong, J.; Shen, W. C.; Zhang, B. F., Polarization properties, high-order Raman spectra, and frequency asymmetry between Stokes and anti-Stokes scattering of Raman modes in a graphite whisker. *Physical Review B* **2001,** 6421, (21), art. no.-214301.

103. Murakami, Y.; Chiashi, S.; Einarsson, E.; Maruyama, S., Polarization dependence of resonant Raman scattering from vertically aligned single-walled carbon nanotube films. *Physical Review B* **2005,** 71, (8), -.

104. Dresselhaus, M. S.; Eklund, P. C., Phonons in carbon nanotubes. *Advances in Physics* **2000,** 49, (6), 705-814.

105. Heller, D. A.; Barone, P. W.; Swanson, J. P.; Mayrhofer, R. M.; Strano, M. S., Using Raman spectroscopy to elucidate the aggregation state of single-walled carbon nanotubes. *Journal of Physical Chemistry B* **2004,** 108, (22), 6905-6909.

106. Weisman, R. B.; Bachilo, S. M., Dependence of optical transition energies on structure for single-walled carbon nanotubes in aqueous suspension: An empirical Kataura plot. *Nano Letters* **2003,** 3, (9), 1235-1238.

107. Bachilo, S. M.; Balzano, L.; Herrera, J. E.; Pompeo, F.; Resasco, D. E.; Weisman, R. B., Narrow (n,m)-distribution of single-walled carbon nanotubes grown using a solid supported catalyst. *Journal of the American Chemical Society* **2003,** 125, (37), 11186-11187.

108. Dresselhaus, M. S.; Jorio, A.; Pimenta, M. A., Resonance Raman spectroscopy in one-dimensional carbon materials. *Anais Da Academia Brasileira De Ciencias* **2006,** 78, (3), 423-439.

109. Skytt, P.; Glans, P.; Mancini, D. C.; Guo, J. H.; Wassdahl, N.; Nordgren, J.; Ma, Y., Angle-Resolved Soft-X-Ray Fluorescence and Absorption Study of Graphite. *Physical Review B* **1994,** 50, (15), 10457-10461.

110. Banerjee, S.; Hemraj-Benny, T.; Balasubramanian, M.; Fischer, D. A.; Misewich, J. A.; Wong, S. S., Surface chemistry and structure of purified, ozonized, multiwalled carbon nanotubes probed by NEXAFS and vibrational spectroscopies. *Chemphyschem* **2004,** 5, (9), 1416-1422.

111. More, J. J.; Garbow, B. S.; Hillstrom, K. E., Algorithm 566 - Fortran Subroutines for Testing Unconstrained Optimization Software [C5], [E4]. *Acm Transactions on Mathematical Software* **1981,** 7, (1), 136-140.

112. Puretzky, A. A.; Schittenhelm, H.; Fan, X. D.; Lance, M. J.; Allard, L. F.; Geohegan, D. B., Investigations of single-wall carbon nanotube growth by time-restricted laser vaporization. *Physical Review B* **2002,** 65, (24), -.

113. Jost, O.; Gorbunov, A. A.; Pompe, W.; Pichler, T.; Friedlein, R.; Knupfer, M.; Reibold, M.; Bauer, H. D.; Dunsch, L.; Golden, M. S.; Fink, J., Diameter grouping in bulk samples of single-walled carbon nanotubes from optical absorption spectroscopy. *Applied Physics Letters* **1999,** 75, (15), 2217-2219.

114. Scott, C. D.; Arepalli, S.; Nikolaev, P.; Smalley, R. E., Growth mechanisms for single-wall carbon nanotubes in a laser-ablation process. *Applied Physics a-Materials Science & Processing* **2001,** 72, (5), 573-580.

115. Alvarez, W. E.; Kitiyanan, B.; Borgna, A.; Resasco, D. E., Synergism of Co and Mo in the catalytic production of single-wall carbon nanotubes by decomposition of CO. *Carbon* **2001,** 39, (4), 547-558.

116. Alvarez, W. E.; Pompeo, F.; Herrera, J. E.; Balzano, L.; Resasco, D. E., Characterization of single-walled carbon nanotubes (SWNT) produced by CO disproportionation on CO-MO catalysts. *Abstracts of Papers of the American Chemical Society* **2002,** 223, U630-U631.

117. Zhong, G. F.; Iwasaki, T.; Honda, K.; Furukawa, Y.; Ohdomari, I.; Kawarada, H., Very high yield growth of vertically aligned single-walled carbon nanotubes by point-arc microwave plasma CVD. *Chemical Vapor Deposition* **2005,** 11, (3), 127-130.

118. Zhang, L.; Tan, Y. Q.; Resasco, D. E., Controlling the growth of vertically oriented single-walled carbon nanotubes by varying the density of Co-Mo catalyst particles. *Chemical Physics Letters* **2006,** 422, (1-3), 198-203.

CHAPTER 4

SUMMARY OF RESEARCH FOR DISSERTATION

This dissertation is focused on development of controlled methods for synthesis of SWNTs on different substrate, relationship between controlled structures and properties of SWNTs, as well as growth mechanism of SWNTs with ordered structure.

Continuous effort has been made to develop thermal chemical vapor deposition method with Co-Mo bimetallic catalyst system for synthesis of SWNTs of controlled structures in terms of diameter, chirality, aggregation, and alignment. By using the highly selective CoMoCAT$^{®}$ catalytic method, SWNTs have been synthesized with controlled diameter and bundle size on high surface area silica, as characterized by Raman spectroscopy, optical absorption, SEM and TEM. The Vis-NIR optical absorption spectra were used to assign the (n,m) identification parameters to the most abundant nanotubes present on samples synthesized at various temperatures ranging from 750°C to 950°C. (6,5), (7,6), and (8,7) have been found to be the dominant component of semiconducting nanotubes produced respectively at 750°C, 850 ^{o}C, and 950°C. As apposed to the increasing trend of diameter of SWNTs with temperature, the aggregation of SWNTs appeared to decrease with temperature due to thermal effect or stronger aggregation tendency of smaller tubes. The average size

of SWNT bundle produced at 750°C, 850°C, and 950°C has been found to be 20nm, 16nm, and 5nm respectively. Experience and knowledge of production of SWNTs on porous materials has been extended to synthesis of SWNTs on flat substrate. A unique catalyst deposition method and corresponding production process have been invented to grow SWNTs on surface of silicon wafer. This method is advantageous in easy controllability of surface density of catalyst nanoparticles on flat substrate and simple experimental setup and operation of reactions. By varying the surface density of catalyst nanoparticles and patterning method, random network of SWNTs and vertically aligned SWNTs can be selectively synthesized on flat surface. Utilization of similar characterization methods as used in the porous materials case demonstrates SWNTs in vertically aligned SWNTs are extremely clean and pure free of metal impurities. Results from Raman and optical absorption shows these tubes are larger tubes and have broader diameter and chirality distribution than those of conventional CoMoCAT$^{\circledR}$ materials.

In chapter 2, relations of structure of SWNT/silica composites to their field emission properties have been discussed in detail. A simple analysis of the data indicates that the bundle size, rather than the nanotube diameter or differences in work function are more important in determining the field emission properties of SWNT/silica composites. The possibility of tailoring the electrical properties of SWNT emitters by adjusting the synthesis parameters has been demonstrated. In

addition, the present results show that the as-produced SWNT/silica composites have similar or perhaps better field emission properties than the purified nanotube samples, even though the concentration of nanotubes on the emitting surface of the as-produced was much lower than that in the pure SWNT sample. The reason for aggregation variance of SWNTs produced at different temperatures has also been investigated by using SEM, TEM and designing experiments with preheating process. The results show the aggregation of SWNTs is probably affected by thermal effect or larger aggregation tendency of smaller tubes. The above investigations help to obtain better understanding of field emission from SWNT, which is crucial to fabrication of field emission devices consisting SWNTs like flat panel display, microscopy probe and light source.

In chapter 3, investigation of interaction between vertically aligned SWNTs and polarized photon flux has been conducted. The anisotropic optical properties of VSWNT probed by height-resolved polarized Raman and angle-resolved XANES indicate ordered structure and misaligned SWNT coexist in VSWNT and the top layer of VSWNT is dominated by random network of SWNTs as is evidence by SEM images. A series of methods and experiments have been carried out to explore the growth mechanism of VSWNT. XPS characterization on catalyst after calcination and reduction has shown Co-Mo (1:3 in molar ratio) is immobilized on surface as $CoMoO_X$ and Mo oxide. These forms remain unaffected by reduction

pretreatment or only small amount of vacancies are generated. AFM measurement shows a uniform distribution of nanoparticles on surface and correlates that to different forms of SWNT grown from them. Growth of VSWNT with time has been visualized by SEM and simulated by a kinetic model to understand growth mechanism. It is clear that formation of VSWNT involves a two-step process: first formation of random network of SWNTs (crust) and followed growth in alignment. Several examples have been given to illustrate the effect of crust. Interesting results have been observed in oxidation of VSWNT, which is proved to be effective in removing small tubes and leaving behind large tubes. In addition to aggressive processing of VSWNT, non-attacking methods have been developed to transfer VSWNT without losing ordered structure to conductive surface such as gold plated silicon wafer and copper tape by wet process and dry process. The results from these researches provide not only a way to produce ultra-pure SWNTs with ultra-high yield but also deeper insight into the understanding of SWNT growth mechanism with catalyst/flat substrate as research model. Attracting much interest, the vertically aligned structure of SWNT on flat substrate is taken advantage of to fabricate SWNT-based photovoltaic devices, nano-heat sink, interconnects, or field emission devices.

APPENDIX

PATENT

"*Methods for Growing Single-walled Carbon Nanotubes on a Flat Surface and Transferring Them onto a Polymer*", U.S. patent, provisional, No. 60/694,545

"*Methods for Growing and Harvesting Carbon Nanotubes*", U.S. patent, pending, No. 11/450,642

PUBLICATIONS

1. Zhang, Liang; Li, Zhongrui; Tan, Yongqiang; Lolli,Giulio; Nakulchaicharoen, Nataphan; Requejo, Felix; Resasco, Daniel E.. *Influence of a Top Crust of Entangled Nanotubes on the Structure of Vertically Aligned Forests of Single-Walled Carbon Nanotubes.* Chemistry of Materials, in press.

2. Zhang, Liang; Tan, Yongqiang; Resasco, Daniel E.. *Controlling the growth of vertically-oriented single-walled carbon nanotubes by varying the density of Co-Mo catalyst particles.* Chemical Physics Letters (2006) 422, 198-203

3. Zhang, Liang; Balzano, Leandro; Resasco, Daniel E.. *Single-Walled Carbon Nanotubes of Controlled Diameter and Bundle Size and Their Field Emission Properties.* Journal of Physical Chemistry B (2005), 109(30), 14375-14381.

4. Lolli, Giulio; Zhang, Liang; Balzano, Leandro; Sakulchaicharoen, Nataphan; Tan, Yongqiang; Resasco, Daniel E.. *Tailoring (n,m) Structure of Single-Walled Carbon Nanotubes by Modifying Reaction Conditions and the Nature of the Support of CoMo Catalysts.* Journal of Physical Chemistry B (2006), 110(5), 2108-2115

5. Zhang, Liang; Li, Zhongrei, Lolli, Giulio; Balzano, Leandro; Tan, Yongqiang; Resasco, Daniel E. ; Requejo, Félix G.; Mun, Bongjin Simon. *Mechanism of Growth of Vertically-Oriented Single-Walled Carbon Nanotubes on Surface: Topologically Confinement Induced Synchronized Alignment and Growth.* Abstracts of papers, 2006 AICHE Annual Meeting, San Francisco, CA, United States, November 12-17, 2006

6. Zhang, Liang; Resasco, Daniel E.. *Tunable Growth of Vertically Aligned Single-walled Carbon Nanotubes on Flat Surface: from Surface Morphology of Catalyst to Reaction Parameters.* Abstracts of papers, NSTI Nanotech 2006 9th Annual Meeting, Boston, MA, United States, May 7-11, 2006

7. Zhang, Liang; Resasco, Daniel E.. *Various Forms of SWNT Including Vertically Aligned Arrays Grown on Flat Surface by Atmospheric CVD.* 2005 AICHE Annual Meeting, Cincinnati, OH, United States, November 2, 2005

8. Zhang, Liang; Resasco, Daniel E.. *Role of Morphology of Bimetallic Catalyst in the Synthesis of Vertically Aligned Single-walled Carbon Nanotubes.* 2005 OMS Annual Meeting, Oklahoma City, OK, United States, November 5, 2005

9. Resasco, Daniel E.; Balzano, Leandro; Lolli, Giulio; Zhang, Liang. *Catalytic synthesis of single-walled carbon nanotubes: Comparison of different production*

186

methods and critical analysis of proposed mechanisms (Tutorial). Abstracts of Papers, 229th ACS National Meeting, San Diego, CA, United States, March 13-17, 2005

10. Zhang, Liang; Balzano, Leandro; Resasco, Daniel E.. *Field Emission Properties of SWNT Selectively Produced by Catalytic Method.* 2004 AICHE Annual Meeting, Austin, TX, United States, November 7-12, 2004

11. Resasco, Daniel E.; Balzano, Leandro; Herrera, Jose E.; Matarredona, Olga; Zhang, Liang. *Controlled growth of SWCNT on solid catalysts with narrow (n,m) distribution.* AIP Conference Proceedings (2004), 723(Electronic Properties of Synthetic Nanostructures), 27-31.

PRESENTATIONS

SPEAKER

1. 2006 AICHE Annual Meeting, San Francisco, CA, USA, November 12-17, 2006

2. NSTI Nanotech 2006, Boston, MA, USA, May 7-11, 2006

3. 2005 AICHE Annual Meeting, Cincinnati, OH, USA, November 2, 2005

4. 2005 OMS Annual Meeting, Oklahoma City, OK, USA, November 5, 2005

5. 2004 AICHE Annual Meeting, Austin, TX, USA, November 7-12, 2004

POSTER

1. 2006 Cargese International School NanosciencesTech, Cargese, Corsica, France
   Transparent SWNT Thin Films: High Conductivity and Doping

2. 2006 NSF Oklahoma EPSCoR Annual Meeting, Norman, OK, USA
   Synchronized Growth and Alignment of SWNT on Surface: Effect of Topological Confinement

3. 2005 NSF Oklahoma EPSCoR Annual Meeting, Stillwater, OK, USA
   Growth of SWNT on Si Wafer by APCVD with Co-Mo Catalyst